NAG2-723

# Automated Finite Element Modeling Of Wing Structures For Shape Optimization

by

Michael Stephen Harvey

A thesis submitted in partial fulfillment
of the requirements for the degree of

Master of Science

in

Aeronautics and Astronautics

University of Washington

1993

Approved by_____
(Chairperson of Supervisory Committee)

Program Authorized
to Offer Degree Department of Aeronautics and Astronautics

Date November 12, 1993

**Master's Thesis**

In presenting this thesis in partial fulfillment of the requirements for a Master's degree at the University of Washington, I agree that the Library shall make its copies freely available for inspection. I further agree that extensive copying of this thesis is allowable only for scholarly purposes, consistent with "fair use" as prescribed in the U.S. Copyright Law. Any other reproduction for any purposes or by any means shall not be allowed without my written permission.

Signature_____

Date_____

## TABLE OF CONTENTS

## LIST OF FIGURES

## LIST OF TABLES

# GLOSSARY

Notation:

| | |
|---|---|
| CST | 3 - noded Constant Strain Triangle membrane element |
| LST | 6 - noded Linear Strain Triangle membrane element |
| $x_i, y_i, z_i$ | general global location of node 'i' |
| [K] | system global stiffness matrix |
| [M] | system global mass matrix |
| {U} | system global displacement vector |
| {F} | system global force vector |
| E | Modulus of Elasticity |
| $\nu$ | poisson's ratio |
| $\rho$ | density |

---

| | |
|---|---|
| $\sigma$ | rod element axial stress |
| $\sigma_{xx}, \sigma_{yy}$ | membrane element normal stresses |
| $\sigma_{xy}$ | membrane element shear stress |
| $\varepsilon_{xx}, \varepsilon_{yy}$ | membrane element normal strains |
| $\varepsilon_{xy}$ | membrane element shear strain |

---

| | |
|---|---|
| {X} | element coordinate vector: |
| | Rod: $\{x_1, y_1, z_1, x_2, y_2, z_2\}$, |
| | CST: $\{x_1, y_1, z_1, x_2, y_2, z_2, x_3, y_3, z_3\}$, |
| | LST: $\{x_1, y_1, z_1, x_2, y_2, z_2, x_3, y_3, z_3, x_4, y_4, z_4, x_5, y_5, z_5, x_6, y_6, z_6\}$ |

| | |
|---|---|
| $[k_L]$ | element stiffness matrix in local coordinates |
| | Rod: 2x2 matrix; |
| | CST: 6x6 matrix; |
| | LST: 12x12 matrix |
| $[k_G]$ | element stiffness matrix in global coordinates |
| | Rod: 6x6 matrix; |
| | CST: 9x9 matrix. |
| | LST: 18x18 matrix |
| $\{U_L\}$ | element displacement vector in local coordinates |
| | Rod: $\{u_1, u_2\}^T$, |
| | CST: $\{u_1, v_1, u_2, v_2, u_3, v_3\}^T$, |
| | LST: $\{u_1, v_1, u_2, v_2, u_3, v_3, u_4, v_4, u_5, v_5, u_6, v_6\}^T$ |
| $\{U_G\}$ | element displacement vector in global coordinates |
| | Rod: $\{u_1, v_1, w_1, u_2, v_2, w_2\}^T$, |
| | CST: $\{u_1, v_1, w_1, u_2, v_2, w_2, u_3, v_3, w_3\}^T$, |
| | LST: $\{u_1, v_1, w_1, u_2, v_2, w_2, u_3, v_3, w_3, u_4, v_4, w_4, u_5, v_5, w_5, u_6, v_6, w_6\}^T$ |
| $[M_{ROD}]$ | 6x6 rod element mass matrix in global coordinates |
| $[M_{CST}]$ | 9x9 CST element mass matrix in global coordinates |
| - ---------- | |
| S | stress smoothing polynomial |
| $\{q\}$ | stress smoothing polynomial coefficients |
| $[A_S],\{b_S\}$ | least squares approximation variables ($[A_S]\{q\}=\{b_S\}$) |
| $[A_{new}]$ | normal equations technique matrix ($[A_{new}]=[A_S]^T[A_S]$) |
| $\{b_{new}\}$ | normal equations tecnique vector ($\{b_{new}\}=[A_S]^T\{b_S\}$) |

---

| | |
|---|---|
| $\lambda,\Phi$ | eigenvalue/eigenvector solution to $[K-\lambda M]\{\Phi\}=\{0\}$ |
| $\lambda,\Psi'$ | eigenvalue/eigenvector solution to $[A-\lambda I]\{\Psi\}=\{0\}$ |
| [A] | square symmetric matrix where $A = (\sqrt{M})^{-1} K (\sqrt{M})^{-1}$ |
| [I] | identity matrix |
| $\omega$ | undamped circular natural frequency (radians/second) |
| f | undamped natural frequency (cycles/second, Hertz) |

---

| | |
|---|---|
| L | rod element length |
| [T] | 2x6 rod element transformation matrix |
| cx, cy, cz | rod element directional cosines of the local x-axis to the global x,y,z-axis |
| $l_1, m_1, n_1$ | CST/LST directional cosines of the local x-axis to the global x-axis |
| $l_2, m_2, n_2$ | CST/LST directional cosines of the local y-axis to the global y-axis |
| [B] | 3x6 CST element geometry matrix |
| [D] | 3x3 CST element material property matrix |
| $[\bar{k}_n]$ | CST element local normal stiffness |
| $[\bar{k}_s]$ | CST element local shear stiffness |
| $[\lambda]$ | 2x3 membrane directional cosines matrix |
| $[\Lambda]$ | 6x9 CST element transformation matrix |
| P, Q, R | node numbers of membrane element 'i' |
| $l_1, l_2, l_3$ | side lengths of membrane element 'i' |
| {L} | membrane element side length vector = $\{l_1, l_2, l_3\}$ |
| b, s, h, a | membrane element local geometry properties |
| {G} | membrane element local geometry vector = {b, s, h, a} |
| $a_1, a_2, a_3$ | LST element global geometry properties (x-direction) |
| $b_1, b_2, b_3$ | LST element global geometry properties (y-direction) |

| | |
|---|---|
| $\{B\}$ | LST element global geometry vector = $\{a_1, a_2, a_3, b_1, b_2, b_3\}$ |
| $[M]$ | 9x12 LST element geometry matrix |
| $[N]$ | 9x9 LST element material property/geometry matrix |
| $[C]$ | 3x3 LST element material property matrix |
| $[\tilde{C}]$ | 9x9 LST element material property matrix |
| $[\tilde{\Lambda}]$ | 12x18 LST element transformation matrix |

---

| | |
|---|---|
| $p_s$ | percent span ratio of any point 'i' in spanwise direction |
| $p_{rc}$ | percent chord ratio of any point 'i' along root rib in chordwise direction |
| $p_{tc}$ | percent chord ratio of any point 'i' along wingtip rib in chordwise direction |

---

| | |
|---|---|
| $\beta$ | generic shape design variable |
| $\kappa$ | generic sizing design variable |

Shape Variables:

| | |
|---|---|
| $x_{FL}$ | x-position of forward/left corner of wing |
| $x_{AL}$ | x-position of aft/left corner of wing |
| $x_{FR}$ | x-position of forward/right corner of wing |
| $x_{AR}$ | x-position of aft/right corner of wing |
| $y_L$ | y-position of left side of wing |
| $y_R$ | y-position of right side of wing |
| $\alpha$ | wing sweep (degrees) |

Size Variables:

| | |
|---|---|
| $A_i$ | rod element 'i' cross-sectional area |
| $t_i$ | membrane element 'i' thickness |

## ACKNOWLEDGEMENTS

The author wishes to express his deepest gratitude to his advisor, Professor Eli Livne, for his support and encouragement throughout the duration of this project and his vast knowledge on the subjects of this thesis.

Additionally, the author would like to express his special appreciation to his wife, Christina, for her complete support and patience during this study.

# CHAPTER 1

# INTRODUCTION

The displacement formulation of the finite element method is the most general and most widely used technique for structural analysis of airplane configurations. Modern structural synthesis techniques based on the finite element method have reached a certain maturity in recent years, and large airplane structures can now be optimized with respect to sizing type design variables for many load cases subject to a rich variety of constraints including stress, buckling, frequency, stiffness and aeroelastic constraints (Refs. 1-3). These structural synthesis capabilities use gradient based nonlinear programming techniques to search for improved designs. For these techniques to be practical a major improvement was required in computational cost of finite element analyses (needed repeatedly in the optimization process). Thus, associated with the progress in structural optimization, a new perspective of structural analysis has emerged, namely, structural analysis specialized for design optimization application, or what is known as "design oriented structural analysis" (Ref. 4). This discipline includes approximation concepts and methods for obtaining behavior sensitivity information (Ref. 1), all needed to make the optimization of large structural systems (modeled by thousands of degrees of freedom and thousands of design variables) practical and cost effective.

In the airplane conceptual and preliminary design stages configuration shape optimization is essential. Wings should be allowed to change in planform and airfoil shape. Fuselage structures should be allowed to be shaped simultaneously, and the position of wings and control surfaces should be determined as part of the optimization process. While a substantial amount of work in the context of structural optimization has been devoted to structural shape synthesis of solid and machine parts, very little has been done to date in the area of airplane structures. Moreover, even with the availability of computer graphics

and computer aided design tools, the preparation of a new finite element model for a new configuration is still too time consuming. It is estimated in Ref. 5 that it would take about 12 months to complete a single structural, loads and aeroelastic design cycle for a high speed civil transport. A major part of this effort is dedicated to the generation and updates of the finite element model.

This thesis focuses on techniques for modeling airplane wings for the conceptual and preliminary design stages using finite elements. The emphasis is on shape optimization. An automatic mesh generator is developed to efficiently handle planform and airfoil shape variations. Simple bar and triangular membrane elements are used to represent spar / rib caps as well as skins and internal webs. Analytic deformation, stress and natural frequency behavior sensitivities are obtained with respect to shape design variables in addition to the sizing type design variables. Extensive numerical tests of the resulting modeling technique are conducted to evaluate its accuracy and economy. The new technique combines advantages of equivalent plate wing modeling (Ref. 6) (ease of model generation and shape sensitivity calculations) with those of finite element models which are general and can handle local effects and structural discontinuities in real wing structures.

The outline of this work is as follows: in Chapter 2 the two finite element modeling approaches are discussed. In Chapter 3 wing behavior sensitivities with respect to both shape and sizing type design variables are derived. Chapter 4 will focus on aspects of automatic mesh generation while Chapter 5 will deal with issues of finite element modeling implementation. In Chapter 6 the three wing models to be analyzed are introduced and described. Chapter 7 details all results pertaining to wing displacements, stresses and natural frequencies while Chapter 8 concludes with sensitivity and computational cost results. Detailed mathematical derivations are given in the appendices.

# CHAPTER 2

# MODELING CONSIDERATIONS

## 2.1 Introduction

Two modeling approaches for built up wing structures are described in this chapter. Both are based on truss (rod) elements for spar and rib caps. Membrane (plane stress) elements are used for cover skins and spar/rib webs. The motivation for using these simple models is not only in their simplicity and speed of computation, but mainly because it is possible to obtain closed form explicit analytic sensitivity of their stiffness and mass matrices with respect to shape design variables. In the first approach linear rod elements and constant strain triangular membranes (CST's) are used. In the second approach linear rod elements and linear strain triangular membranes (LST's) are used. Discussion of these two approaches and guidelines to follow are included in this chapter. In both cases there are no rotational degrees of freedom in the model.

## 2.2 CST modeling

The simplest of the two techniques is the one employing the three-noded CST membrane element with a linear rod element. The CST is used to represent all wing cover skin panels and rib and spar shear webs. The rod element is used to model all rib and spar cap areas. These are low order elements. Stresses in these elements are constant throughout their interior and for convergence a large number of elements may be needed.

A finite element capability, then, must include grid refinements that are quick and easy to perform, and a study of modeling accuracy to establish modeling guidelines as to the degree of grid refinement required. The possibilities to be investigated include refinement

in the spanwise direction, refinement in the chordwise direction or a combination of the two. For grid refinement in one direction only, more nodes are created along the spars for refining spanwise, while more nodes are added along the ribs for chordwise refining (Figure 2.1). As one can see, all newly created nodes still lie on a rib or spar, and thus they are supported by the internal structure of the wing. For a combination of the two, grid refinement introduces a "floating node," or a node that has no vertical support (Figure 2.2). As a result, the stiffness matrix becomes singular, and a special procedure must be used to eliminate this singularity. One way of overcoming this difficulty (Ref. 7) is by linking the displacement at a floating node via multi-point constraints to the displacements of it's neighboring nodes. Since the equations of constraint depend on wing geometry, though, analytic differentiation of stiffness and mass terms with respect to shape becomes quite complicated.

Our solution is to add either "dummy" rib or "dummy" spar elements whose thickness is substantially lower than the real ribs or spars (say, 1% thick) so as to not influence the stiffness or mass of the wing but provide support for the floating nodes. The advantage here is that all nodes and elements (whether real or dummy) are treated in the same way in the course of analytic differentiation and no special treatment has to de devised for the floating nodes. It must be remembered, however, that floating nodes can not have any vertical loads applied to them. Thus when aerodynamic loads are distributed over the wing they can only be applied to nodes supported by the actual internal structure of the wing.

Using CST webs for the spars and ribs creates another problem. Since only one row of CST elements is used in the depth direction of the wing due to a wing's small depth/chord ratio, this leads to finite element models that are too stiff (Ref. 7). This comes as no surprise since the constant stresses in a CST cannot capture the linear distribution of stresses in a typical beam web. To correct for this the CST web membrane elements are modified to only carry shear stresses by using just the shear stiffness portion of a CST's stiffness

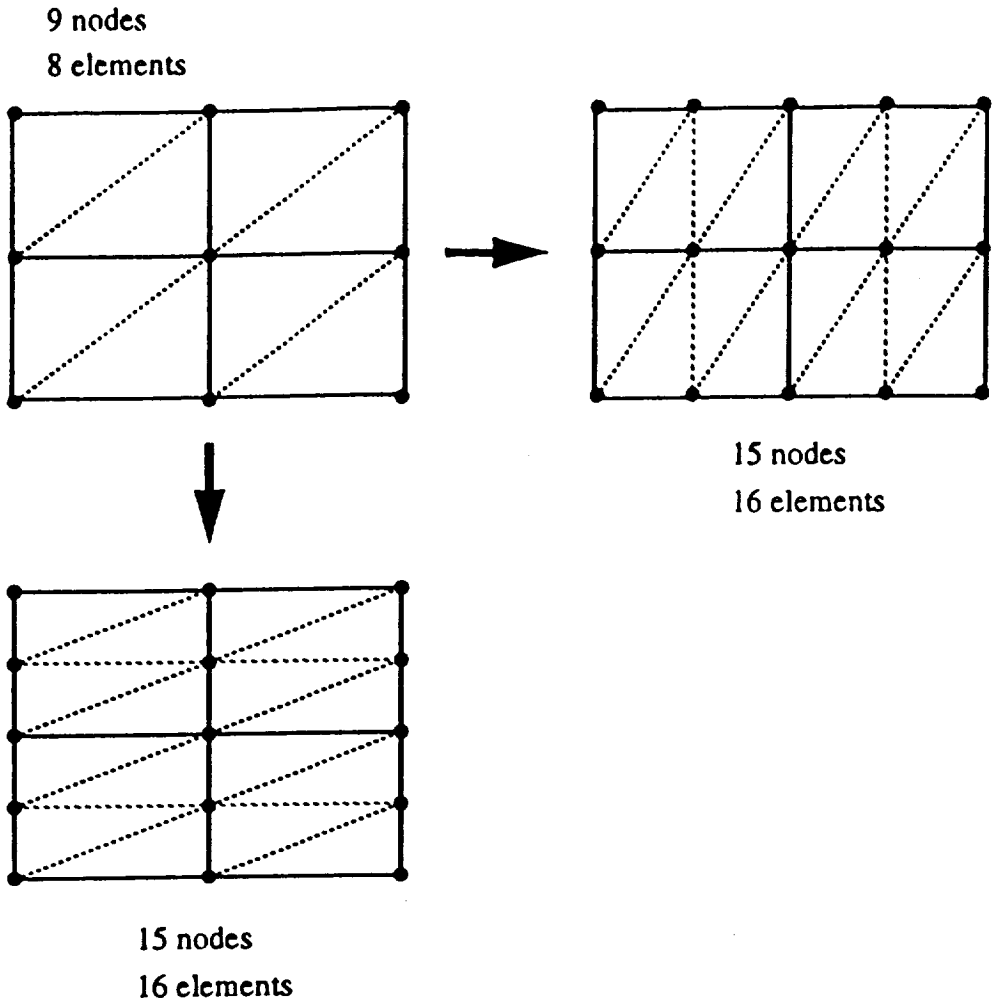


Figure 2.1 - CST spanwise or chordwise refinement

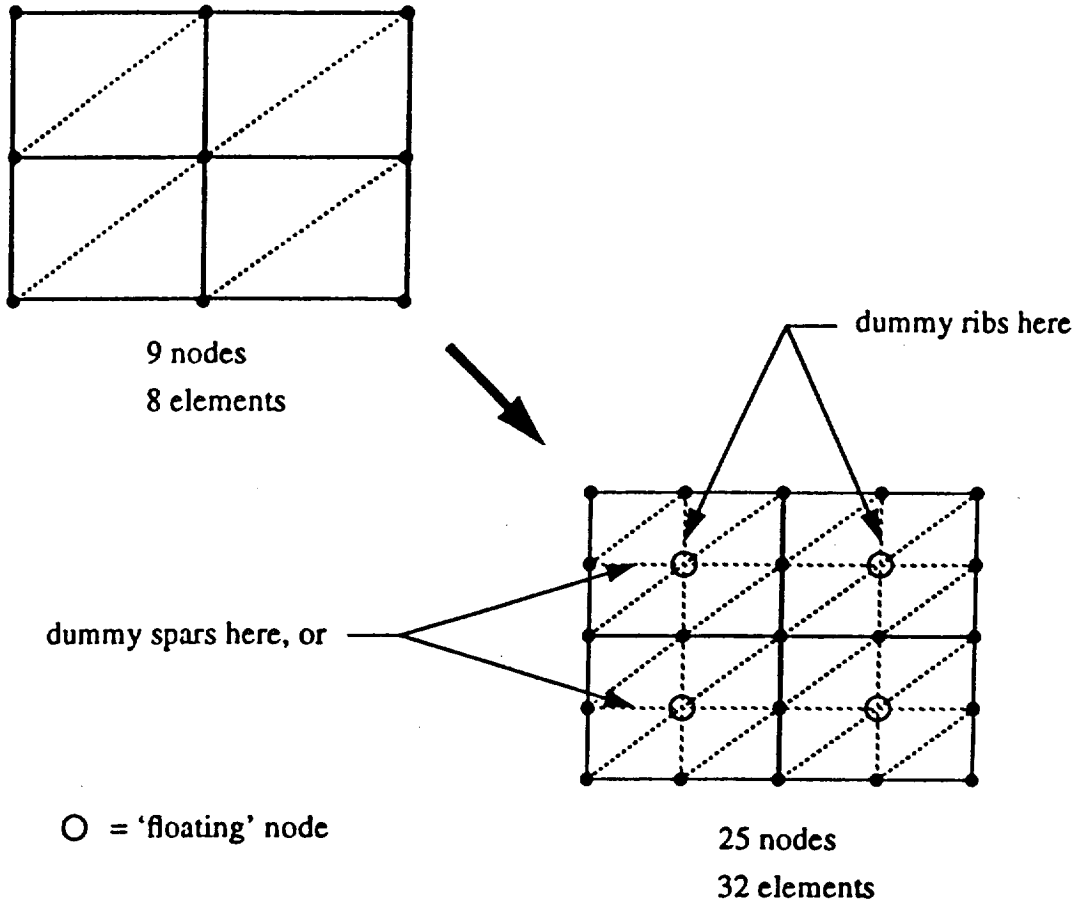


Figure 2.2 - CST spanwise and chordwise refinement

matrix. They act as pure shear webs, and vertical rod spacers connecting the upper wingskin to the lower wingskin replace the normal stiffness of the web elements in the transverse direction to keep upper and lower skins separated.

## 2.3 LST modeling

Using LST elements in place of the CST elements leads to better convergence of finite element results because of the higher order of the LST. The problems with floating nodes, however, are still present. The LST is a 6-noded element whose three additional nodes are located along the midpoint of its sides. Because of these midside nodes, floating nodes now appear not only in the wing skin planes, but also in the rib and spar planes (Figure 2.3).Thus, in the spirit of our approach to CST modeling, a combination of two of the following techniques is necessary to provide support for these nodes and eliminate singularity: dummy ribs, dummy spars, and/or dummy layers. The dummy layers are added to support the mid-depth nodes of the spar and rib webs. They are similar to the other dummy elements in that their thickness is very low (1% of the actual wing skin thicknesses).

Since the LST's lead to better convergence of the finite element solution, the most basic mesh possible (the one defined by the location of real spars and ribs in the wing) is usually quite accurate. The stress output for a LST element consists of a pair of normal stresses $\sigma_{xx}$, $\sigma_{yy}$ and a shear stress $\sigma_{xy}$ at the corner nodes where each stress varies linearly across the element's interior.

Due to the higher order of the LST, shear stresses through the wing thickness are better represented. Thus, no pure shear LST is necessary when using LST models.

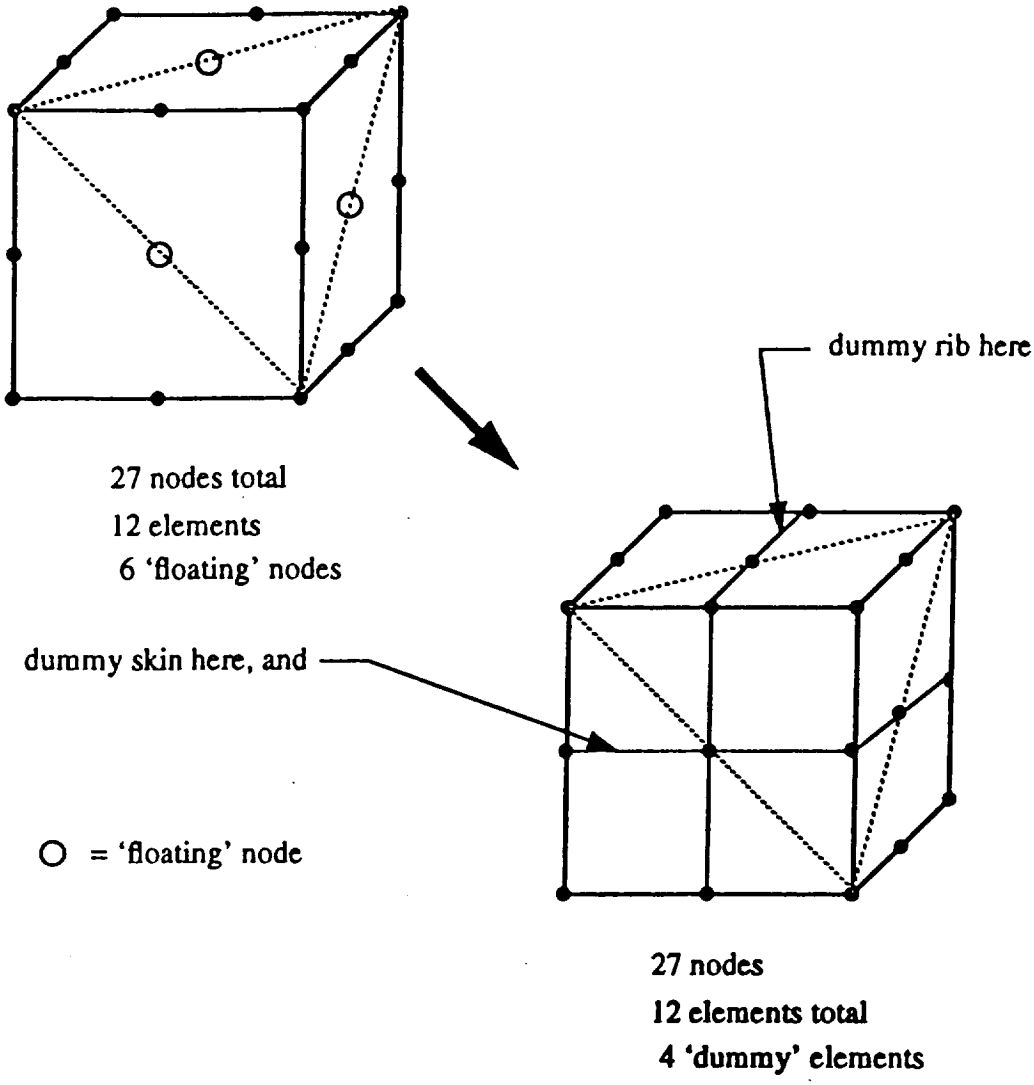


Figure 2.3 - LST dummy element selection

## 2.4 Wing lumped mass modeling

For natural frequency calculations, a lumped mass matrix modeling technique is used. The mass of each finite element is distributed evenly to it's nodes and then merged to the global lumped mass matrix whose structure is strictly diagonal. Since floating nodes can not support any load or force, inaccuracies in the calculation of higher natural frequencies and mode shapes will arise. It will be seen in Chapter 7 that natural frequency accuracy is a direct function of dummy element thickness and guidelines for the selection of this thickness will be provided.

## 2.5 Finite element derivations

For complete details of the finite elements used and their respective stiffness, stress and mass matrices, consult Appendix A.

# CHAPTER 3

# BEHAVIOR SENSITIVITIES

## 3.1 Introduction

Accurate and computationally efficient derivatives of behavior functions (such as displacements, stresses or natural frequencies) with respect to design variables are important in the context of gradient based optimization not only for calculation of the gradients themselves but also as a basis for constructing constraint and objective function approximations (Refs. 1, 8 and 9). When structural shape optimization is involved, it is difficult to obtain these sensitivities in a closed, explicit analytic form (without any numerical integration, as is usually used for evaluating mass and stiffness terms of general elements). One popular way for obtaining structural behavior sensitivities is by finite differences (Ref. 1). This technique, however, can be time consuming when the computational cost of a single analysis is high. In addition, and especially in the case of shape variations, finite difference derivatives are sensitive to the step size used, and can lead to erroneous results (Ref. 1).

In the present finite element modeling capability developed, simple finite elements such as truss rod and plane stress CST's and LST's are used not only because of computational efficiency in formulating the stiffness and mass matrices, but also because of the explicit algebraic nature of these matrices (Refs. 10, 11 and Appendix A). This makes it possible to obtain behavior sensitivities in an analytic, explicit manner, thus avoiding numerical problems associated with finite differences and significantly reducing computing time.

The wing structural design variables are divided into two categories: shape and sizing. The wing planform is divided into trapezoids. The shape of each trapezoid is defined by

six shape design variables. The variables $y_L$, $y_R$ are the left and right spanwise coordinates of the trapezoid, while $x_{FL}$, $x_{AL}$, $x_{FR}$, $x_{AR}$ are the longitudinal locations of its four vertices (Figure 3.1). The sizing variables include the cross-sectional area $A_i$ of any rod element 'i' and the thickness $t_j$ of any CST or LST membrane element 'j.' Based on the formulations in Appendix A, analytic expressions for the sensitivity of element stiffness and mass matrices can be derived with respect to the location of an element's nodes. This is done here in a manner similar to Ref. 12. The position of each element's nodes can be linked to the overall shape of an individual wing trapezoid knowing the rules used for generating the mesh for that trapezoid. Chain rule differentiation is then used for obtaining stiffness and mass sensitivities of individual elements with respect to overall wing planform shape design variables. Details of these derivations can be found in the appendices.

## 3.2 Sensitivities with respect to shape variables

### 3.2.1 Global displacements

The linear static structural equation serving as a basis for static analysis is

$$[K]\{U\} = \{F\} \tag{3-1}$$

The equation for displacement sensitivity with respect to any design variable in the case where external loads do not change is (Ref. 1)

$$\frac{\partial\{U\}}{\partial\beta} = -\left([K]^{-1}\right)\frac{\partial[K]}{\partial\beta}\{U\} \tag{3-2}$$

where $[K]$ is the stiffness matrix, $\{U\}$ is the displacement vector and $\beta$ is a typical

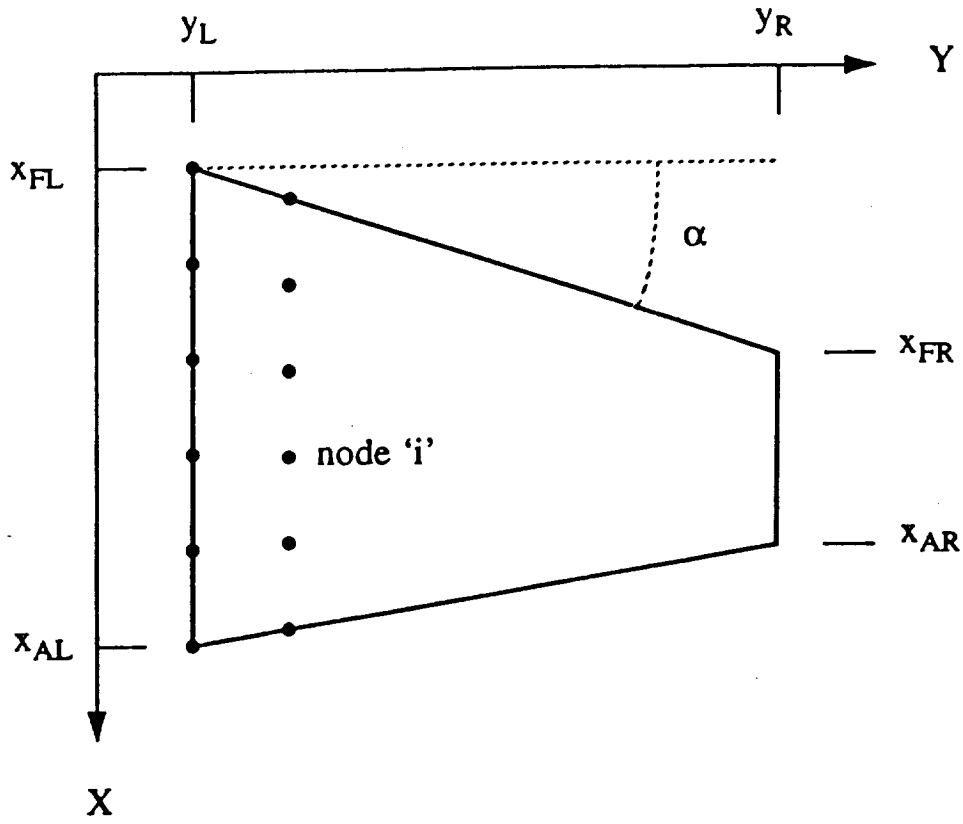


Figure 3.1 - Wing shape variable designation

design variable.

Once displacements and displacement sensitivities are known, it is possible to obtain derivatives of stresses within elements. The stiffness matrix [K] is nonlinear in the shape design variables. However, explicit expressions for stiffness terms in rod and plane stress elements are available (see Appendix A) and can be used for differentiation.

### 3.2.2 Stress in the i'th rod element

As shown in Section A.1.2, the stress in a truss element depends on the shape design variables both explicitly (through a location vector $\{X\}$) and implicitly (through an elastic deformation vector $\{U_G\}$). Therefore

$$\frac{\partial \sigma_i}{\partial \beta} = \frac{\partial \sigma_i}{\partial \{X\}_i} \frac{\partial \{X\}_i}{\partial \beta} + \frac{\partial \sigma_i}{\partial \{U_G\}_i} \frac{\partial \{U_G\}_i}{\partial \beta} \tag{3-3}$$

where $\{X\}_i$ and $\{U_G\}_i$ are the location and displacement vectors in global coordinates associated with a rod element, respectively.

### 3.2.3 Stress in the i'th CST element

Stress sensitivities for the CST with respect to planform shape design variables are obtained by differentiation of the stress equations in Section A.2.2 giving

$$\frac{\partial}{\partial\beta}\begin{Bmatrix}\sigma_{xx}\\ \sigma_{yy}\\ \sigma_{xy}\end{Bmatrix}_i = [D]_i[R]_i[\Lambda]_i\frac{\partial\{U_G\}_i}{\partial\beta} + [D]_i[R]_i\frac{\partial[\Lambda]_i}{\partial\beta}\{U_G\}_i + [D]_i\frac{\partial[R]_i}{\partial\beta}[\Lambda]_i\{U_G\}_i \tag{3-4}$$

where $\{U_G\}_i$ is the vector containing CST element i's nodal displacements in global coordinates. The material matrix $[D]_i$ does not depend on the shape of the element, therefore it's derivative with respect to planform shape is zero.

### 3.2.4 Stress in the i'th LST element

The equations of Sections A.3.1 and A.3.2 are now differentiated analytically to obtain sensitivities of stresses at the three vertices of an LST with respect to shape design variables. Chain rule differentiation is used to link variations in element node locations to the global planform shape changes of the wing to give

$$\frac{\partial}{\partial\beta}\left\{\begin{Bmatrix}\sigma_{xx}\\ \sigma_{yy}\\ \sigma_{xy}\end{Bmatrix}_1 \begin{Bmatrix}\sigma_{xx}\\ \sigma_{yy}\\ \sigma_{xy}\end{Bmatrix}_2 \begin{Bmatrix}\sigma_{xx}\\ \sigma_{yy}\\ \sigma_{xy}\end{Bmatrix}_3\right\}_i = [\bar{C}]_i[M]_i[\bar{\Lambda}]_i\frac{\partial\{U_G\}_i}{\partial\beta} + [\bar{C}]_i[M]_i\frac{\partial[\bar{\Lambda}]_i}{\partial\beta}\{U_G\}_i + [\bar{C}]_i\frac{\partial[M]_i}{\partial\beta}[\bar{\Lambda}]_i\{U_G\}_i \tag{3-5}$$

The matrix $[\tilde{C}]$ is a material constitutive matrix and does not depend on the shape of the element. $\{U_G\}$ is the vector of element nodal displacements in global coordinates.

### 3.2.5 Natural frequencies

The governing equation of motion for an undamped structure in free vibration is

$$[K - \omega^2 M]\ \{\Phi\} = \{0\} \tag{3-6}$$

where $\lambda = \omega^2$ is an eigenvector, $\{\Phi\}$ is it's respective mode shape and $\omega$ is a circular natural frequency (radians/second). Implicit differentiation of $\lambda$ with respect to any shape variable $\beta$ yields

$$\frac{\partial \lambda_i}{\partial \beta} = \frac{\phi_i^T \left[ \frac{\partial [K]}{\partial \beta} - \lambda_i \frac{\partial [M]}{\partial \beta} \right] \phi_i}{\phi_i^T [M]\, \phi_i} \tag{3-7}$$

for eigenvalue and mode shape 'i'. Since the natural frequency (in Hertz) is given by

$$f_i = \frac{\sqrt{\lambda_i}}{2\pi} \tag{3-8}$$

the natural frequency sensitivity after differentiation is

$$\frac{\partial f_i}{\partial \beta} = \frac{1}{4\pi\sqrt{\lambda_i}} \frac{\partial \lambda_i}{\partial \beta} \tag{3-9}$$

### 3.3 Sensitivities with respect to sizing variables

In this case the stiffness and mass matrices depend linearly on the design variables. In the case of truss elements and CST's or LST's, these design variables are cross sectional area and membrane thickness, respectively.

#### 3.3.1 Global Displacements

With $\kappa$ as a sizing type design variable, the matrix equations for sensitivities of the displacement vector in global coordinates are (Ref. 1)

$$\frac{\partial \{U\}}{\partial \kappa} = -\left(\left[K\right]^{-1}\right) \frac{\partial [K]}{\partial \kappa} \{U\} \tag{3-10}$$

Again, it is assumed that external loads do not change with changes in the sizing design variables.

#### 3.3.2 Stress in the i'th rod element

If the design variable is a rod cross sectional area $A_j$:

$$\frac{\partial \sigma_i}{\partial A_j} = \frac{\partial \sigma_i}{\partial \{U_G\}_i} \frac{\partial \{U_G\}_i}{\partial A_j} \tag{3-11}$$

If the design variable is a membrane thickness $t_j$:

$$\frac{\partial \sigma_i}{\partial t_j} = \frac{\partial \sigma_i}{\partial \{U_G\}_i} \frac{\partial \{U_G\}_i}{\partial t_j} \tag{3-12}$$

where $\{U_G\}_i$ for both stress sensitivities is a 6x1 vector containing nodal displacements in global coordinates for rod element i.

### 3.3.3 Stress in the i'th CST element

If the design variable is a rod area $A_j$:

$$\frac{\partial}{\partial A_j} \begin{Bmatrix} \sigma_x \\ \sigma_y \\ \tau_{xt} \end{Bmatrix}_i = [D]_i [B]_i [\Lambda]_i \frac{\partial \{U_G\}_i}{\partial A_j} \tag{3-13}$$

If the design variable is a membrane thickness $t_j$:

$$\frac{\partial}{\partial t_j} \begin{Bmatrix} \sigma_x \\ \sigma_y \\ \tau_{xt} \end{Bmatrix}_i = [D]_i [B]_i [\Lambda]_i \frac{\partial \{U_G\}_i}{\partial t_j} \tag{3-14}$$

where $\{U_G\}_i$ for both stress sensitivities is a 9x1 vector containing nodal displacements in global coordinates for CST element 'i.'

### 3.3.4 Stress in the i'th LST element

If the design variable is a rod area $A_j$:

$$\frac{\partial}{\partial A_j}\left\{\begin{array}{c}\left\{\begin{array}{c}\sigma_x\\ \sigma_y\\ \tau_{xy}\end{array}\right\}_1\\ \left\{\begin{array}{c}\sigma_x\\ \sigma_y\\ \tau_{xy}\end{array}\right\}_2\\ \left\{\begin{array}{c}\sigma_x\\ \sigma_y\\ \tau_{xy}\end{array}\right\}_3\end{array}\right\}_i = [\bar{C}]_i[M]_i[\bar{\Lambda}]_i\frac{\partial\{U_G\}_i}{\partial A_j} \tag{3-15}$$

If the design variable is a membrane thickness $t_j$:

$$\frac{\partial}{\partial t_j}\left\{\begin{array}{c}\left\{\begin{array}{c}\sigma_x\\ \sigma_y\\ \tau_{xy}\end{array}\right\}_1\\ \left\{\begin{array}{c}\sigma_x\\ \sigma_y\\ \tau_{xy}\end{array}\right\}_2\\ \left\{\begin{array}{c}\sigma_x\\ \sigma_y\\ \tau_{xy}\end{array}\right\}_3\end{array}\right\}_i = [\bar{C}]_i[M]_i[\bar{\Lambda}]_i\frac{\partial\{U_G\}_i}{\partial t_j} \tag{3-16}$$

where $\{U_G\}_i$ for both stress sensitivities is a 18x1 vector containing nodal displacements in global coordinates for LST element i.

### 3.3.5 Natural frequencies

With $\kappa$ again as a sizing type variable $A_j$ or $t_j$, the eigenvalue sensitivity is

$$\frac{\partial \lambda_i}{\partial \kappa} = \frac{\phi_i^T \left[ \frac{\partial [K]}{\partial \kappa} - \lambda_i \frac{\partial [M]}{\partial \kappa} \right] \phi_i}{\phi_i^T [M] \phi_i} \tag{3-17}$$

and the natural frequency sensitivity is

$$\frac{\partial f_i}{\partial \kappa} = \frac{1}{4\pi\sqrt{\lambda_i}} \frac{\partial \lambda_i}{\partial \kappa} \tag{3-18}$$

Derivatives of nodal displacements with respect to shape type design variables are obtained from Section 3.2.1 while derivatives of nodal displacements with respect to sizing type design variables are obtained from Section 3.3.1. Sizing derivatives of the stiffness and mass terms are straight forward because of the linear dependency (see Appendix A). Thus, stress sensitivities with respect to sizing type design variables require sensitivities of deformations only. Additionally, all other matrix and vector transformations used to move from local to global coordinates and from deformation (displacement) to stresses are fixed in this case.

# CHAPTER 4

# AUTOMATIC MESH GENERATION

## 4.1 Introduction

The desire to circumvent the creation of finite element input files by hand and to automate model generation for wing shape synthesis makes it necessary to combine a mesh generation capability with the finite element analysis and sensitivity techniques (Ref. 13). At this stage of the present work this capability is limited to wings with ribs parallel to the root rib, spars beginning at the root rib and terminating at the wing tip and a thickness distribution symmetric about the wing's mid-plane (Figure 4.1). This modeling is sufficient for the studies conducted in this work. The limitations are minor and can be removed by making the mesh generator more general for other wing layouts and also for fuselage structures. For the structural wing model the elements used include constant stress rods (to model cap areas) and either CST membranes or LST membranes (to model wing skins and webs). The mesh generator and finite element capabilities are linked together so that when combined with an optimization package, the shape of the wing (in addition to cap areas and skin thicknesses) can be optimized.

## 4.2 Wing design variables and design rules

Figure 4.2 shows a sample mesh created by the mesh generator, and will be used to define key parameters needed. The structure shown is a single wing trapezoid containing five structural spars and six ribs including a root rib. In order to refine the mesh it is possible to add "dummy" ribs and spars between structural ribs and spars, as shown. The parameters "adrib" and "adspar" define the number of added dummy ribs or dummy spars

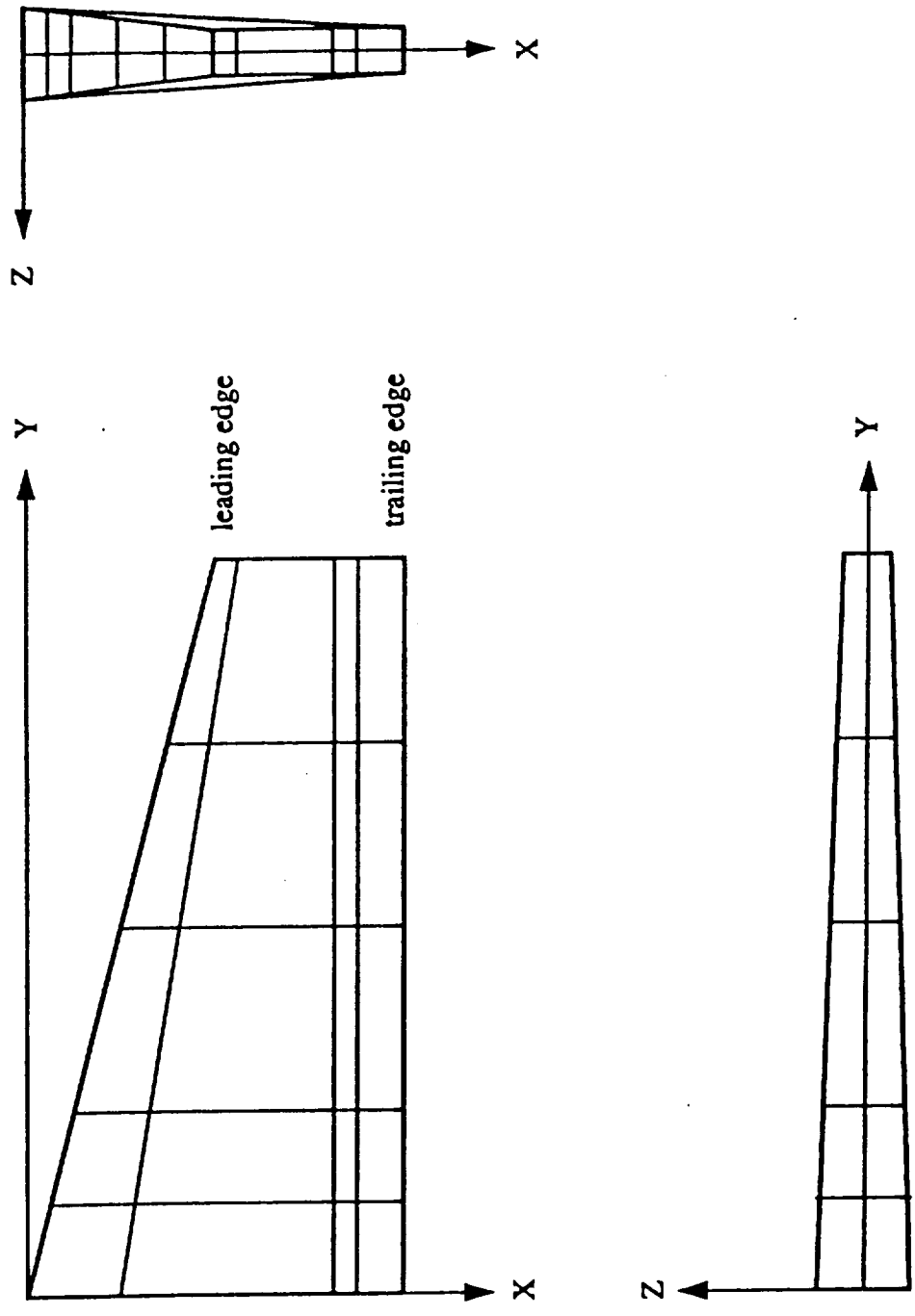


Figure 4.1 - Mesh generator example

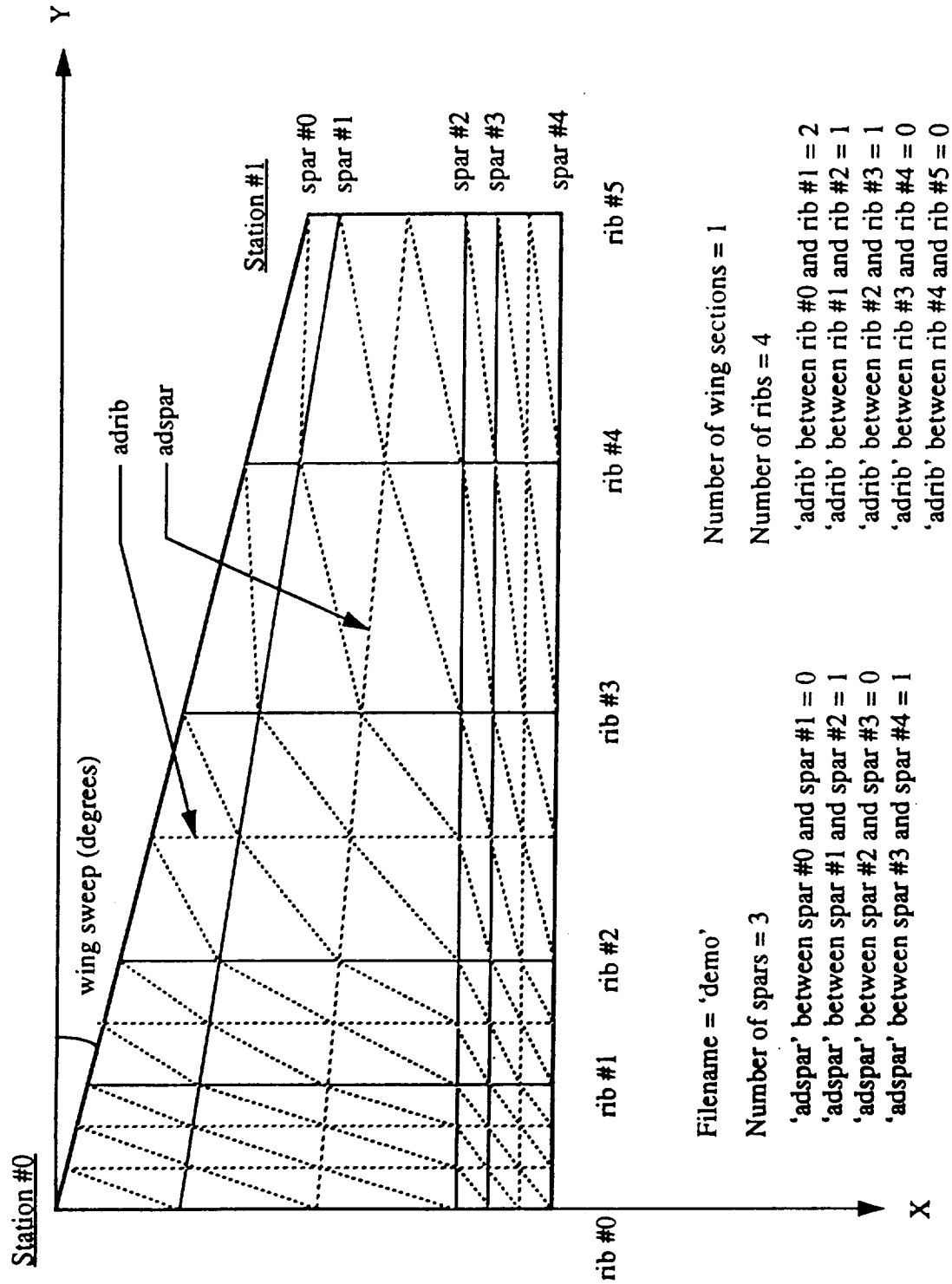


Figure 4.2 - Mesh generator data input requirements

between adjacent structural ribs or spars. These dummy ribs and spars, whose stiffness is negligibly low compared with the actual structure, are needed to support the added "floating" nodes on cover skin surfaces modeled by triangular membrane elements. This is necessary since there are only displacements and no rotations associated with each node, and since the skin cover elements have no bending stiffness.

The x-y coordinates of the vertices of the wing trapezoid and spanwise and chordwise locations of ribs and spars serve as shape design variables for the planform. All dummy spars or ribs are assumed to be evenly spaced between real spars or ribs. Wing depth definition is also used based on associated shape design variables. Finally, all spar and rib cap areas and all wing skin, spar web and rib web membrane thicknesses are used as sizing type design variables. It should be mentioned again that at this stage of the present work rib generation is limited to ribs that are parallel to the root rib, and spars have all to originate at the root chord and end on the tip chord of a trapezoidal section.

### 4.3 Planform expansion to three dimensions

With wing depth specified by the proper shape (depth) design variables, an explicit equation for depth distribution as a function of x and y is established over the wingspan. The planar mesh described in the previous section is now projected upward and downwards to generate the meshes for the upper and lower cover skins. Realistic thickness and camber distributions can be modeled by proper selection of depth shape functions and construction of a series in those functions whose coefficients serve as shape design variables.

### 4.4 Shape variable coordinate linking matrix

With the 3-D grid complete, the linking of each node's x-, y- and z- coordinates to the six planform shape design variables of a wing trapezoidal section $x_{FL}$, $x_{AL}$, $x_{FR}$, $x_{AR}$, $y_L$ and $y_R$ (Fig. 3.1) and its depth design variables is straightforward, as detailed in Appendix B. Derivatives of each nodal location with respect to each shape design variable can easily be obtained. These derivatives, used in the finite element program for shape sensitivity analysis, are the same as the coefficients that link each node to the shape variables since the linking equations are linear.

### 4.5 Finite element placement

Individual finite elements are placed and connected to the proper nodes according to the following rules: spar and rib caps (for the real structural spars and ribs only) are represented by rod elements connecting nodes on the upper skin or lower skin along the spar or rib lines. Intersections of spar lines and rib lines (including dummy spars and ribs) define quadrilateral cells on the upper and lower skins. Each of these cells is divided into two triangular elements. For the webs of all ribs and spars, each quadrilateral cell (defined by the end nodes of the upper and lower rod elements associated with the cell) is divided into two triangular elements.

As discussed earlier, mesh refinement involves the need for dummy ribs or dummy spars if a floating node is present. For CST models, dummy ribs are sufficient. For LST models, dummy ribs and dummy layers are necessary to support both vertical and horizontal floating degrees of freedom. The dummy layer (of negligibly thin material) connecting the mid-side nodes of LST used in spar and rib webs is covered by triangular elements in a manner similar to the cover skins.

Following the rules described above, it is possible to generate explicit relations between each element, its end nodes and the global shape design variables defining the shape of the whole wing. These relations are then used for obtaining analytic sensitivities of stiffness and mass sensitivities using chain rule differentiation (as described in the appendices).

# CHAPTER 5

# FINITE ELEMENT IMPLEMENTATION ISSUES

## 5.1 Introduction

Implementation issues concerning the finite element modeling technique described in Chapters 2-4 are discussed in this chapter. A standard displacement approach is followed (Refs. 14, 15). The finite element code of Ref. 14 for three dimensional trusses serves as a basis upon which the new capability is developed. Constant strain triangular elements (CST's) and linear strain triangular elements (LST's) are added to the library of elements. A banded matrix solution solver (Ref. 16) is used for static analysis. A QR eigenvalue solution technique is used for the natural modes analysis. Analytic sensitivities of stiffness and mass matrices are generated and used to obtain sensitivities of displacements, stresses and natural frequencies.

## 5.2 Global displacement solution

The governing equation for a static structural system is given by

$$[K]\{U\} = \{F\} \tag{5-1}$$

where K is the banded global stiffness matrix, U is the vector of global displacements to be solved for and F is the vector of nodal loads. The decomposition technique of Ref. 16 is used for solution.

### 5.3 Natural frequency solution

The governing equation for a dynamic structural system undergoing undamped free vibration is given by

$$[K - \omega^2 M]\ \{\phi\} = \{0\} \tag{5-2}$$

where K is the global stiffness matrix, $\omega$ is a natural frequency in radians/second, M is the lumped global mass matrix and $\phi$ is a mode shape. For a non-trivial solution of natural frequencies and mode shapes to exist, the determinant of $[K - \omega^2 M]$ must equal zero. The method of solution will be to use a QR decomposition algorithm (Ref. 18) that solves the standard eigenvalue problem

$$[A - \lambda I]\ \{\psi\} = \{0\} \tag{5-3}$$

where A is a square symmetric matrix, $\lambda$ is an eigenvalue, I is the identity matrix and $\psi$ is the corresponding eigenvector. The original equation is converted into the standard form by using the fact that since M is diagonal and positive definite, it's square root is easily calculated. Thus, pre- and post-multiplying eqn. 5-2 by $(\sqrt{M})^{-1}$ gives

$$\left[ (\sqrt{M})^{-1} K (\sqrt{M})^{-1} - \omega^2 (\sqrt{M})^{-1} M (\sqrt{M})^{-1} \right] \{\psi\} = \{0\} \tag{5-4}$$

or

$$[A - \lambda I]\ \{\psi\} = \{0\} \tag{5-5}$$

where $A = (\sqrt{M})^{-1} K (\sqrt{M})^{-1}$ is square symmetric and $\lambda = \omega^2$.

Since $\psi$ solves the standard eigenvalue problem (eqn. 5-3), to find $\phi$ which solves the original eigenvalue problem (eqn. 5-2) it is necessary to use the formula

$$\phi = (\sqrt{M})^{-1} \psi \quad . \tag{5-6}$$

## 5.4 Element stress solution

All individual finite element stresses are calculated using the previously found global displacements. Equations for axial stresses in rod elements are given in Appendix A.1.2. Similarly, for CST elements, stress equations are given in Appendix A.2.2. For LST elements stress equations are given in Appendix A.3.2.

### 5.4.1 Stress smoothing

Since stresses throughout a CST element are constant, stress differences can be found between neighboring CST's and an averaging process (Ref. 17) is needed in order to obtain a smooth stress distribution over the skin in areas where no discontinuities are expected.

As an option in the present capability, a least squares fitting procedure is used to fit an $N^{th}$ order polynomial for each skin stress ($\sigma_{xx}$, $\sigma_{yy}$, $\sigma_{xy}$) over each wing skin trapezoid. Thus if S(x,y) is any component of the plane stress in the skin, then

$$S(x, y) = q_1 + q_2 x + q_3 y + \ldots + q_k y^N \tag{5-7}$$

or in matrix form:

$$S(x,y) = \{\ 1\ x\ y\ \dots\ \} \begin{Bmatrix} q_1 \\ q_2 \\ q_3 \\ \dots \end{Bmatrix} \tag{5-8}$$

where polynomial terms are picked based on Pascal's triangle in Table 5.1. In the present capability polynomial order can range from 2 to 5.

For least squares fitting, stresses in each CST are taken at the centroid of the element. Thus, for each CST element 'i', '$x_i$' and '$y_i$' refer to the element's centroid position. Writing polynomial equations for the stress $\sigma$ in 'k' elements leads to 'k' equations of the form $[A_S]\{q\} = \{b_S\}$ where

$$[A_S] = \begin{bmatrix} 1 & x_1 & y_1 & \dots & y_1^N \\ 1 & x_2 & y_2 & \dots & y_2^N \\ 1 & x_3 & y_3 & \dots & y_3^N \\ \dots & \dots & \dots & \dots & \dots \\ 1 & x_k & y_k & \dots & y_k^N \end{bmatrix} \tag{5-9}$$

and

Table 5.1 - Choice of stress smoothing polynomial

| | |
|---|---|
| $1$ | |
| $x \quad y$ | N = 1 |
| $x^2 \quad xy \quad y^2$ | N = 2 |
| $x^3 \quad x^2y \quad xy^2 \quad y^3$ | N = 3 |
| $x^4 \quad x^3y \quad x^2y^2 \quad xy^3 \quad y^4$ | N = 4 |
| $x^5 \quad x^4y \quad x^3y^2 \quad x^2y^3 \quad xy^4 \quad y^5$ | N = 5 |

$$\{b_S\} = \begin{Bmatrix} \sigma_1 \\ \sigma_2 \\ \sigma_3 \\ \cdots \\ \sigma_K \end{Bmatrix} \tag{5-10}$$

To solve for {q}, the normal equations approach is used (Ref. 18) to yield

$$[A_S]^T [A_S] \{q\} = [A_S]^T \{b_S\} \tag{5-11}$$

or

$$[A_{new}] \{q\} = \{b_{new}\} \tag{5-12}$$

which can be directly solved using Ref. 16.

### 5.4.2 Stress smoothing sensitivities

Differentiating the previous equations for smoothed stresses with respect to a shape design variable $\beta$ leads to

$$\frac{\partial S(x, y)}{\partial \beta} = \{1, x, y, \ldots\}^T \frac{\partial \{q\}}{\partial \beta} + \{0, \frac{\partial x}{\partial \beta}, \frac{\partial y}{\partial \beta}, \ldots\}^T \{q\} \tag{5-13}$$

where the vector $\{ (\partial q) / (\partial \beta) \}$ is obtained from

$$[A_{new}]\frac{\partial\{q\}}{\partial\beta} = \frac{\partial\{b_{new}\}}{\partial\beta} - \frac{\partial[A_{new}]}{\partial\beta}\{q\} \tag{5-14}$$

Now

$$\frac{\partial[A_{new}]}{\partial\beta} = \frac{\partial[A_S]}{\partial\beta}^T[A_S] + [A_S]^T\frac{\partial[A_S]}{\partial\beta} \tag{5-15}$$

and

$$\frac{\partial[b_{new}]}{\partial\beta} = \frac{\partial[A_S]}{\partial\beta}^T[b_S] + [A_S]^T\frac{\partial[b_S]}{\partial\beta} \tag{5-16}$$

where

$$\frac{\partial[A_S]}{\partial\beta} = \begin{bmatrix} 0 & \frac{\partial x_1}{\partial\beta} & \frac{\partial y_1}{\partial\beta} & \cdots & N\frac{\partial y_1^{N-1}}{\partial\beta} \\ 0 & \cdots & \cdots & \cdots & \cdots \\ 0 & \cdots & \cdots & \cdots & \cdots \\ \cdots & \cdots & \cdots & \cdots & \cdots \\ 0 & \cdots & \cdots & \cdots & N\frac{\partial y_k^{N-1}}{\partial\beta} \end{bmatrix} \tag{5-17}$$

and

$$\frac{\partial \{b_S\}}{\partial \beta} = \begin{Bmatrix} \frac{\partial \sigma_1}{\partial \beta} \\ \cdots \\ \cdots \\ \cdots \\ \frac{\partial \sigma_k}{\partial \beta} \end{Bmatrix} \tag{5-18}$$

For shape sensitivities, the expressions above take care of the motion of the $(x_i,y_i)$ points used for least squares fitting as well as the motion of the point where the stress is calculated. For sizing sensitivities, all points used for least squares fitting and stress output calculations are fixed and their derivatives are zero. Therefore, all derivatives of $[A_S]$ with respect to any size variable $\kappa$ are zero, resulting in

$$[A_{new}] \frac{\partial \{q\}}{\partial \kappa} = \frac{\partial \{b_{new}\}}{\partial \kappa} \tag{5-19}$$

where

$$\frac{\partial [b_{new}]}{\partial \kappa} = [A_S]^T \frac{\partial [b_S]}{\partial \kappa} \tag{5-20}$$

and

$$\frac{\partial \{b_S\}}{\partial \kappa} = \begin{Bmatrix} \frac{\partial \sigma_1}{\partial \kappa} \\ \cdots \\ \cdots \\ \cdots \\ \frac{\partial \sigma_k}{\partial \kappa} \end{Bmatrix}. \tag{5-21}$$

# CHAPTER 6

# WING MODEL TEST CASES

## 6.1 Introduction

Three wing models are described here for later use as test cases. For each, a brief physical description is given along with all load cases to be examined.

## 6.2 Gallagher wing

The Gallagher model 1 wing (Ref. 19) is an unswept, untapered cantilever wing as shown in Figure 6.1. The aspect ratio is 4 and the depth-to-chord ratio is 0.075. All internal members, being formed channels, are modeled as shear webs using membrane elements. The channel flanges are modeled as rod elements whose cross-sectional area matches that of the flange area. Additionally, the skins are modeled with membrane elements only. The material used is 6061-T6 aluminum and its properties are:

$$E = 10.0 \times 10^{6} \text{ psi} \qquad \nu = 0.3 \qquad \rho = 0.000259 \text{ lbm/in}^3$$

The load case analyzed is a 100 lbf. point load at each rib / spar intersection, first applied one at a time to derive the wings influence coefficients and then applied simultaneously (representing a continuous load over the wing) to examine its deformed shape. All wing skin thicknesses are 0.063" , web thicknesses are 0.040" and cap areas are modelled as being 0.02 square inches. Numerical tests include evaluation of the difference between modeling the spar / rib webs as plane stress elements carrying normal and shear stresses and spar / rib webs modeled by shear webs only. The effect of mesh refinement is exam-

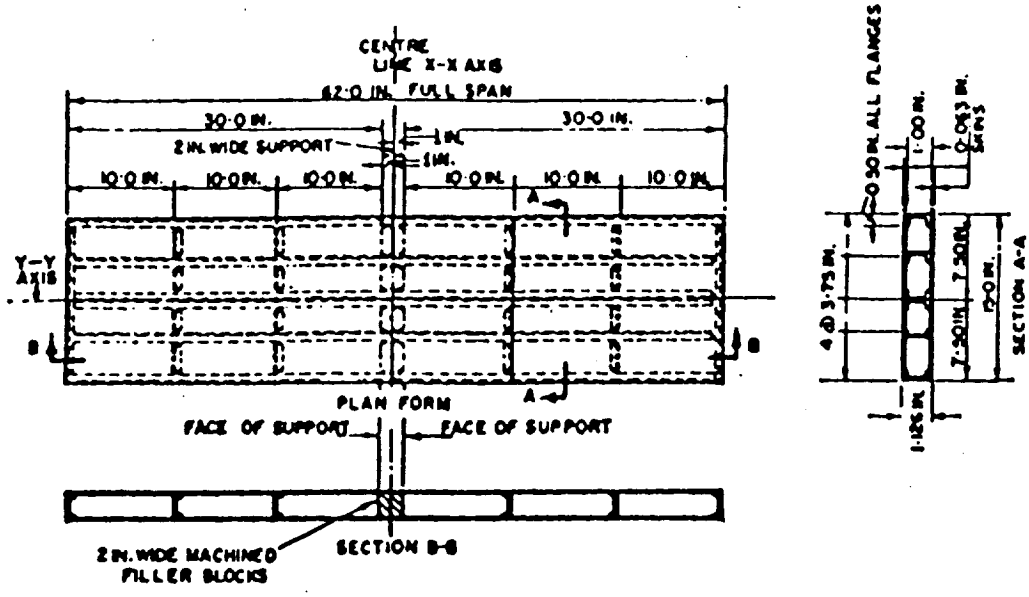


Figure 6.1 - Gallagher model 1 wing - physical description

ined. The results from finite element models based on CST membranes are compared to those with LST membranes.

### 6.3 Denke wing

The Denke wing (Ref. 20) is a 45 degree swept back wing with an aspect ratio of 10, a depth-to-chord ratio of 0.35 and can be seen in Figure 6.2. Only four internal ribs are present along with the front and rear spars. Two load cases are considered. Load case 1 involves a 1 lbf. point load applied vertically at the tip trailing edge, while load case 2 involves a 1 lbf. point load applied vertically at the leading edge at 60% span. The material properties used are:

$$E = 10.0 \times 10^{6} \text{ psi} \qquad \nu = 0.3 \qquad \rho = 0.000259 \text{ lbm/in}^3$$

All wing skin thicknesses are 0.032", web thicknesses are 0.051" and stringer areas are 0.371 square inches for the leading and trailing edge elements, and 0.061 square inches for all remaining stringers.

Again, effects of using plane stress and pure shear elements for spar and rib webs are studied as well as comparisons between the performance of CST's and LST's. This wing is an example of a thick, high aspect ratio wing typical in transonic transport airplane construction. Displacements and experimentally measured stresses in spar caps are used to assess accuracy of the present capability.

### 6.4 Turner/Martin/Weikel wing

The Turner wing (Ref. 21), originally studied by Eggwertz and Noton, can be seen

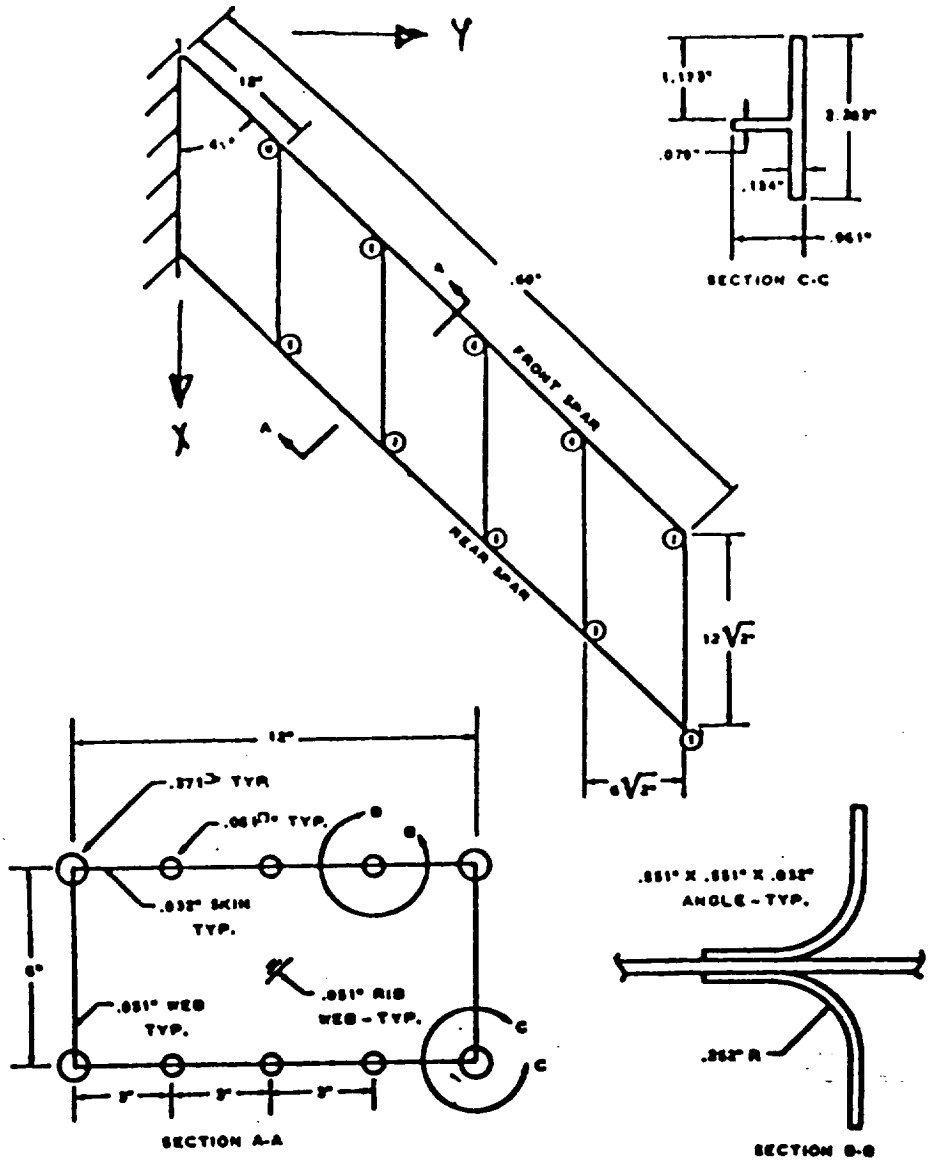


Figure 6.2 - Denke wing - physical description

in Figure 6.3. It has a 30 degree sweep, aspect ratio of 5 and a depth-to-chord ratio of 0.21. Five spars and three ribs are assumed to be perfectly attached to the upper and lower wing-skins and to each other. Cover skins are modeled as plane stress elements and a comparison is made between modeling the spar and rib webs as plane stress or pure shear elements. The material used is aluminum with the following properties:

$$E = 10.0 \times 10^{6} \text{ psi} \qquad \nu = 0.3 \qquad \rho = 0.000259 \text{ lbm/in}^3$$

All wing skin thicknesses are 0.118", web thicknesses are 0.059" and cap areas are 0.0619 square inches.

Measured displacements and skin stresses in the root area are used for evaluation. It should be mentioned (Ref. 21) that while measured skin stresses $\sigma_{yy}$ along the span (in the direction of the spars) are quite accurate, there is a reason to believe that normal stresses perpendicular to the spars $\sigma_{xx}$ and skin shear stresses $\sigma_{xy}$ are inaccurate. Since they are very small compared to $\sigma_{yy}$, there would be no significant effect on failure estimation for the wing.

For the Turner wing, in addition to the experimental data, finite element results, in particular wing skin stresses and model natural frequencies, from a commercially available code (ELFINI, Ref. 22), were generated and used to compare to results from the present capability.

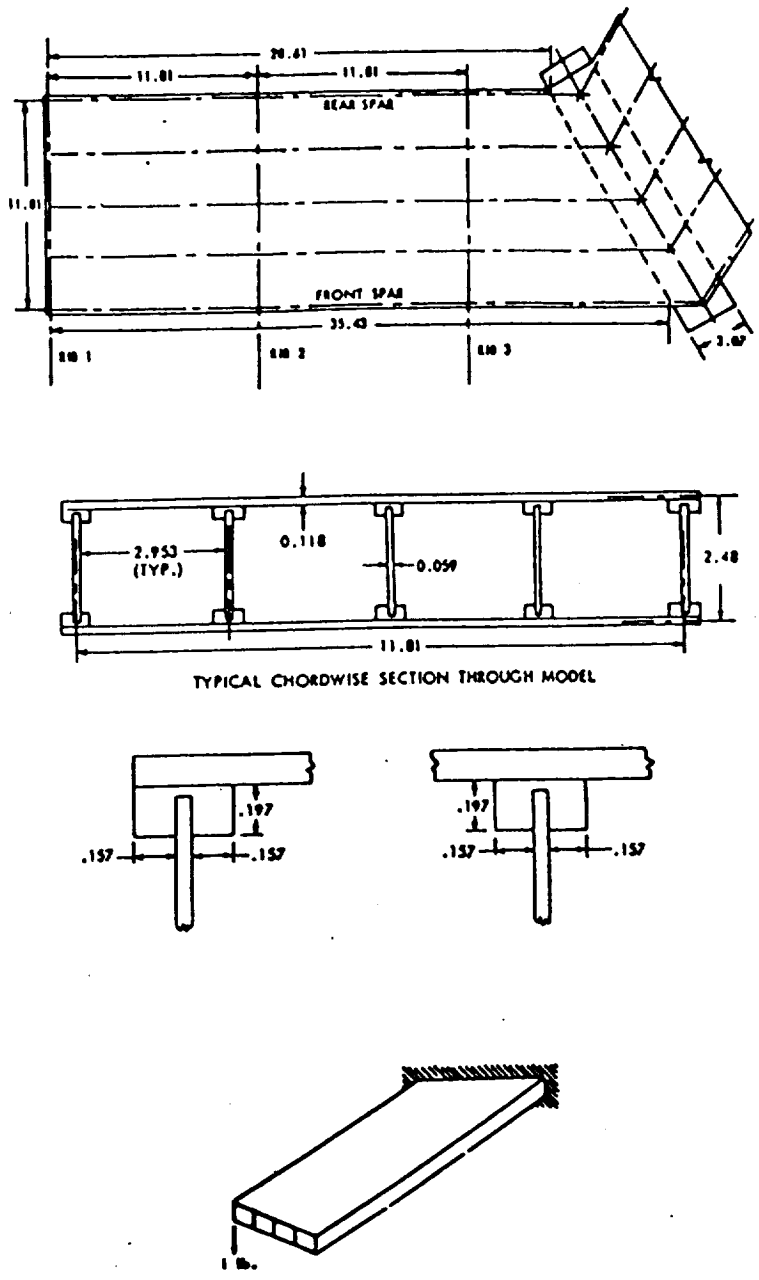


Figure 6.3 - Turner wing - physical description

# CHAPTER 7

# NUMERICAL RESULTS

## 7.1 Introduction

Three wing models are used to assess the present capability. First, accuracy of the finite element results needs to be evaluated, since the present capability is based on very basic, low order elements (in an effort to gain computational speed and obtain analytic sensitivities). This is done by comparing results obtained by the present capability to results by commercially available codes and to experimental results wherever possible.

## 7.2 Gallagher wing

Figure 7.1 shows both the original wing skin mesh (based on existing ribs and spars) and a refined wing skin mesh employing four dummy ribs between each primary rib. When CST's are used for cover skins and rib / spar webs, the effect of increasing the number of spanwise divisions on the tip displacement using shear webs versus regular CST's in the vertical webs is shown in Figure 7.2. Natural frequency convergence under mesh refinement is seen in Figure 7.3. As the number of divisions increase, the finite element displacement solution approaches that found experimentally (Ref. 19). It is interesting to note that the effect of modeling the spar and rib webs with shear webs becomes more important as the mesh is refined. The refined finite element model with shear webs is about 5% stiffer than the experimental model.

A comparison of a refined CST model prediction (adrib = 5) and the LST model is shown in Figure 7.4. The LST model uses a mesh based on the existing ribs and spars as in the coarser CST model. Mid-chord deflections along the entire span for both models are

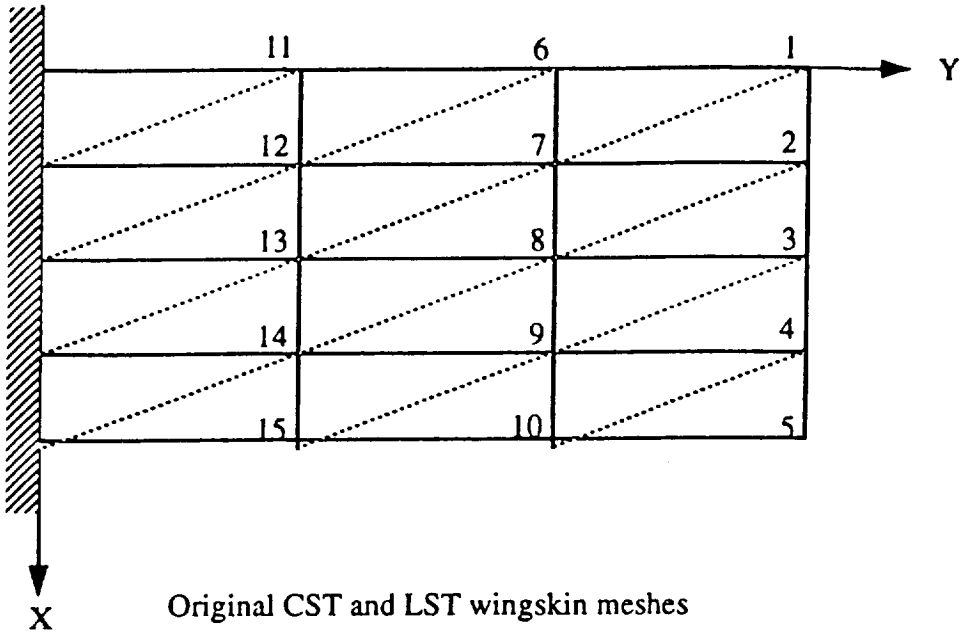


Original CST and LST wingskin meshes

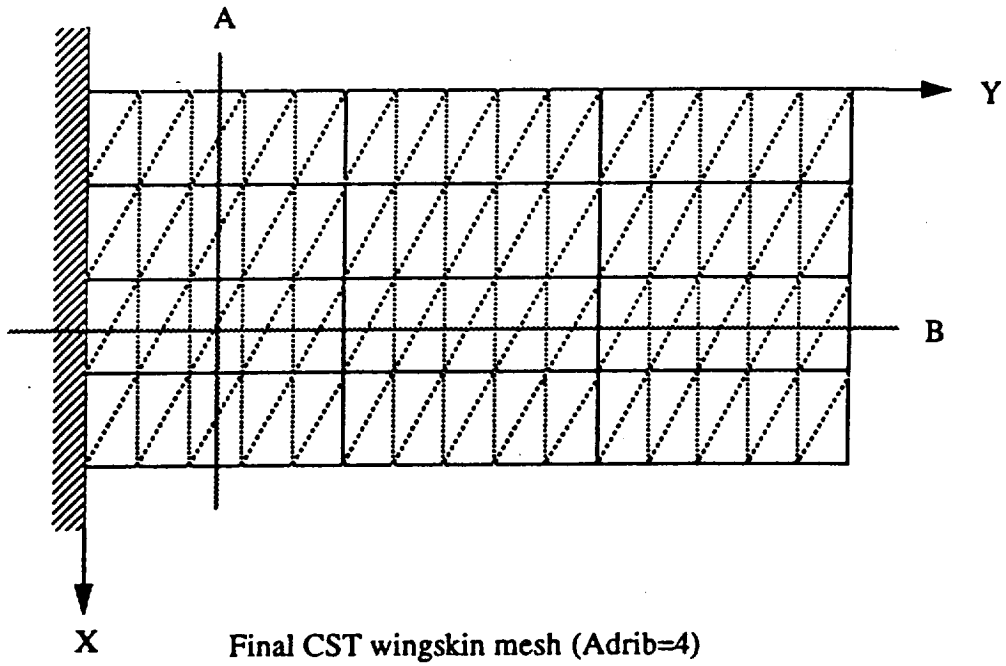


Final CST wingskin mesh (Adrib=4)

Figure 7.1 - Gallagher model 1 wing skin meshes

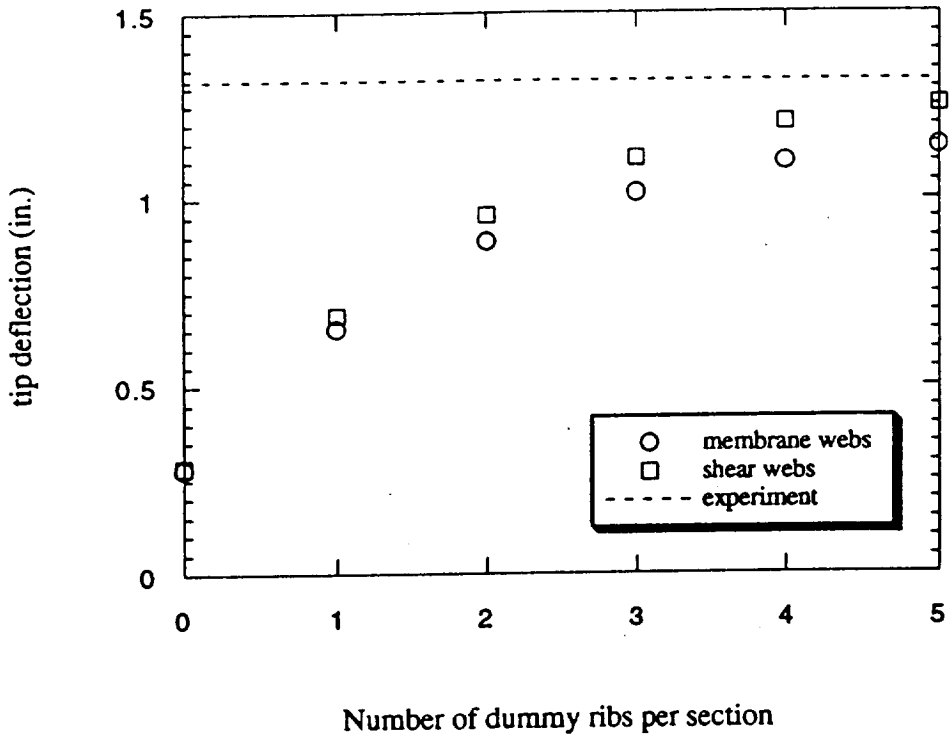


Figure 7.2 - Mid-spar tip deflection convergence with spanwise mesh refinement - Gallagher wing

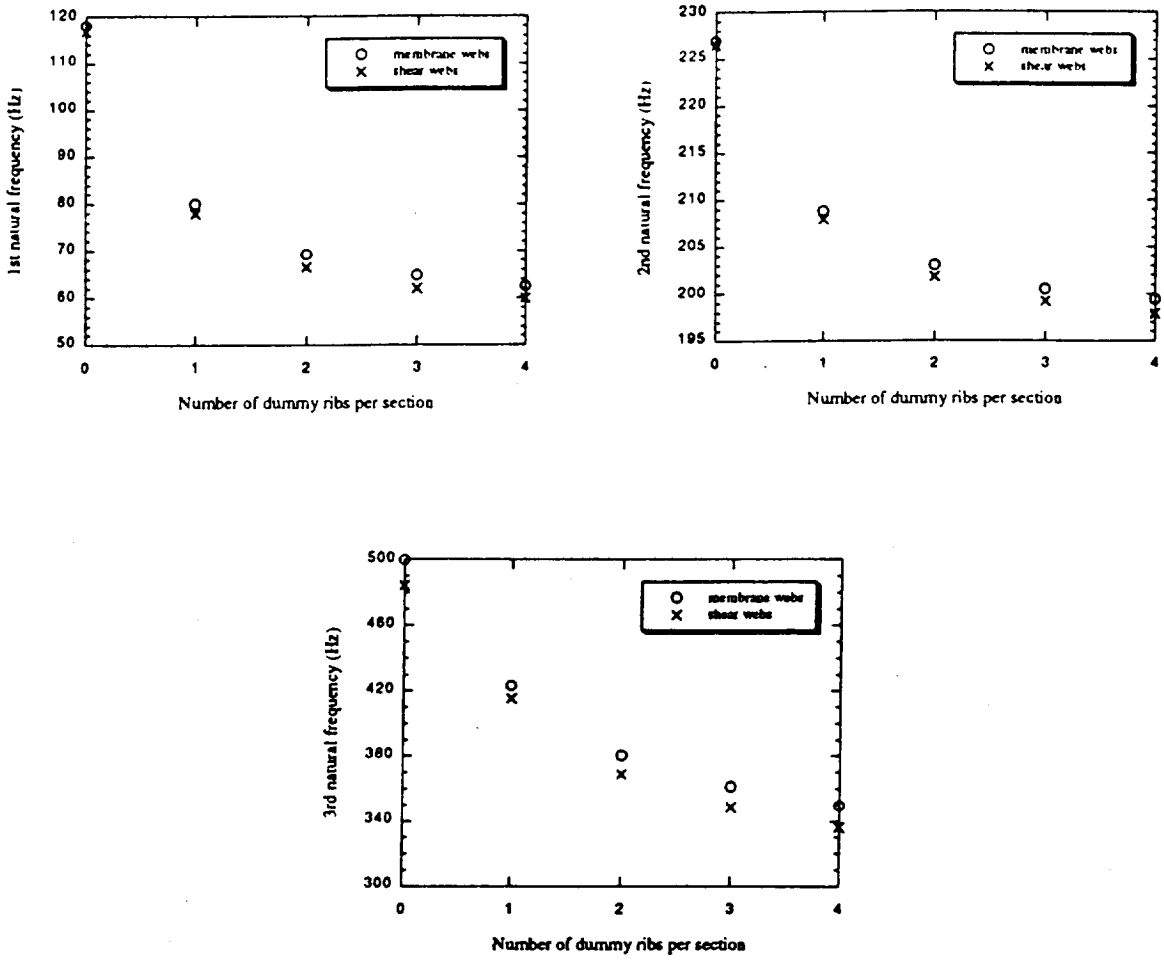


Figure 7.3 - Natural frequency convergence with spanwise mesh refinement - Gallagher wing

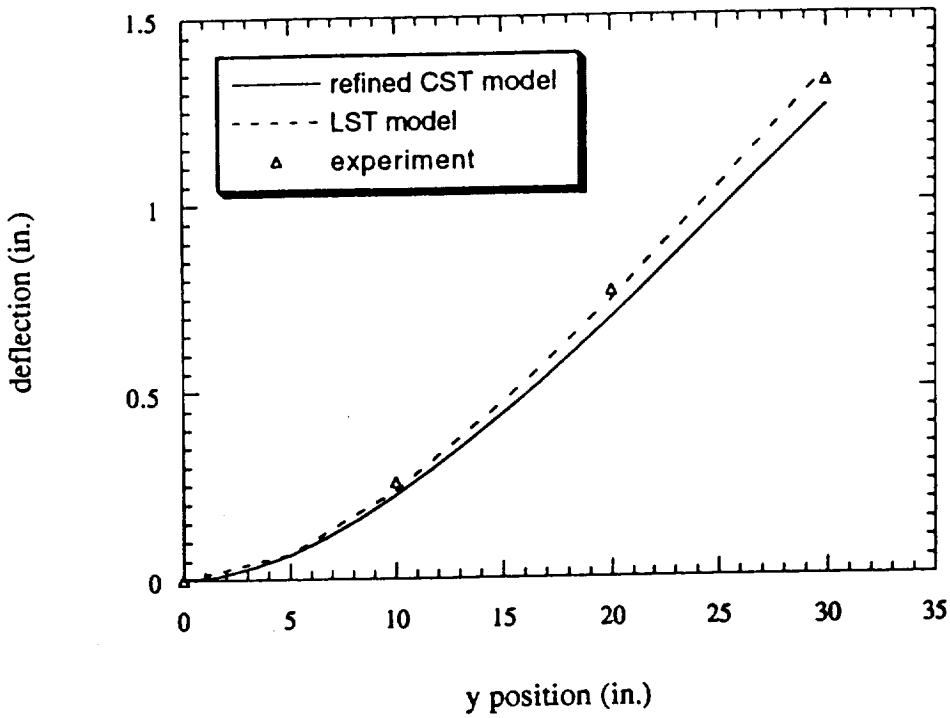


Figure 7.4 - Mid-spar deflection under a uniform load - Gallagher wing

compared to experimental data. Both models are in close agreement with only a 5.07% and a 2.05% wingtip deflection deviation from experiment, respectively (Table 7.1).

Gallagher's experimental influence coefficient matrix (Ref. 19) is reproduced in Table 7.2 along with the resulting approximate influence matrix for the refined CST model (adrib=5) and the LST model. It can be seen that displacement results are good for the LST model while the CST model is slightly stiffer.

No experimental data is available for stresses on the Gallagher wing. As expected stresses in skin CST's fluctuate and change discontinuously from element to element. Performance of the stress smoothing technique (Chapter 5) was evaluated by using polynomials of order two through five along with the adrib=4 mesh. The resulting polynomial fits are presented in Table 7.3, and plots along cuts A and B (Figure 7.1) are shown for each stress in Figures 7.5 through 7.10. It is found that a polynomial of order N=4 captures CST stress variations well over the wing in this case.

### 7.3 Denke wing

Figure 7.11 shows both the original wing skin mesh (based on existing spars and ribs) and a refined wing skin mesh employing two dummy ribs between each pair of primary ribs. Deflection results for the Denke wing (in the case of CST elements) with an increasing number of spanwise divisions are compared in Figures 7.12 and 7.13. Results of using shear webs and CST membranes (including normal stresses) for spar and rib webs are shown for both load cases. Natural frequency convergence results are shown in Figure 7.14.

Excellent correlation between experiment and finite element modeling using CST's is shown in Figures 7.15 and 7.16 for load cases 1 and 2, respectively. The CST model used for these and all subsequent results has adrib=2. Comparison of results from the LST

Table 7.1 - Displacements of the Gallagher model 1 wing

Mid-chord deflection (in.)

| Node | experiment | CST model | % error | LST model | % error |
|---|---|---|---|---|---|
| 3.0 | 1.319 | 1.252 | 5.07 | 1.346 | 2.05 |
| 8.0 | 0.765 | 0.691 | 9.65 | 0.740 | 3.24 |
| 13.0 | 0.258 | 0.221 | 14.17 | 0.233 | 9.51 |

Table 7.2 - Gallagher model 1 influence coefficients

Points on Model 1

| | 1 | 2 | 3 | 4 | 5 | 6 | 7 | 8 | 9 | 10 | 11 | 12 | 13 | 14 | 15 |
|---|---|---|---|---|---|---|---|---|---|---|---|---|---|---|---|
| 1 | 0.1746 | 0.1621 | 0.151 | 0.1415 | 0.1296 | 0.0987 | 0.0902 | 0.0827 | 0.075 | 0.066 | 0.0312 | 0.0285 | 0.0252 | 0.0216 | 0.0175 |
| 2 | | 0.1631 | 0.1554 | 0.1494 | 0.1428 | 0.0914 | 0.088 | 0.0846 | 0.0802 | 0.0747 | 0.028 | 0.0279 | 0.0257 | 0.0238 | 0.0212 |
| 3 | | | 0.1572 | 0.1566 | 0.1546 | 0.0832 | 0.0836 | 0.0854 | 0.0844 | 0.0823 | 0.0244 | 0.0257 | 0.0254 | 0.0255 | 0.0242 |
| 4 | | | | 0.1645 | 0.1664 | 0.0772 | 0.0804 | 0.0854 | 0.0895 | 0.0914 | 0.0216 | 0.0248 | 0.0264 | 0.0276 | 0.0284 |
| 5 | | | | | 0.1804 | 0.0706 | 0.0766 | 0.0847 | 0.093 | 0.1014 | 0.0184 | 0.0234 | 0.0262 | 0.0292 | 0.0318 |
| 6 | | | | | | 0.0687 | 0.0591 | 0.0502 | 0.0444 | 0.0379 | 0.025 | 0.0216 | 0.0173 | 0.0136 | 0.0106 |
| 7 | | | | | | | 0.0573 | 0.0512 | 0.0468 | 0.0426 | 0.0208 | 0.0178 | 0.0173 | 0.0151 | 0.013 |
| 8 | | | | | | | | 0.054 | 0.0515 | 0.0492 | 0.0168 | 0.0174 | 0.018 | 0.0172 | 0.0165 |
| 9 | | | | | | | | | 0.058 | 0.0583 | 0.0139 | 0.0158 | 0.0178 | 0.0196 | 0.0209 |
| 10 | | | | | | | | | | 0.0714 | 0.0105 | 0.0142 | 0.017 | 0.0205 | 0.025 |
| 11 | | | | | | | | | | | 0.0174 | 0.0124 | 0.0071 | 0.0048 | 0.0028 |
| 12 | | | | | | | | | | | | 0.0137 | 0.0082 | 0.0064 | 0.0052 |
| 13 | | | | | | | | | | | | | 0.0105 | 0.0081 | 0.0073 |
| 14 | | | | | | | | | | | | | | 0.0125 | 0.0118 |
| 15 | | | | | | | | | | | | | | | 0.0169 |

Experimental

Points on Model 1

| | 1 | 2 | 3 | 4 | 5 | 6 | 7 | 8 | 9 | 10 | 11 | 12 | 13 | 14 | 15 |
|---|---|---|---|---|---|---|---|---|---|---|---|---|---|---|---|
| 1 | 0.1745 | 0.1612 | 0.1488 | 0.1376 | 0.1272 | 0.0923 | 0.0854 | 0.0782 | 0.0708 | 0.0631 | 0.0279 | 0.0258 | 0.0231 | 0.0198 | 0.0158 |
| 2 | | 0.157 | 0.1503 | 0.1438 | 0.1377 | 0.0846 | 0.0819 | 0.0785 | 0.0745 | 0.07 | 0.0248 | 0.0243 | 0.0231 | 0.0214 | 0.0188 |
| 3 | | | 0.1516 | 0.1504 | 0.149 | 0.0771 | 0.0782 | 0.0787 | 0.0783 | 0.0773 | 0.0217 | 0.0228 | 0.0232 | 0.0229 | 0.0219 |
| 4 | | | | 0.1572 | 0.1614 | 0.0699 | 0.0745 | 0.0786 | 0.0821 | 0.0848 | 0.0187 | 0.0213 | 0.0231 | 0.0244 | 0.025 |
| 5 | | | | | 0.1748 | 0.0629 | 0.0708 | 0.0782 | 0.0855 | 0.0925 | 0.0156 | 0.0198 | 0.0231 | 0.0259 | 0.0281 |
| 6 | | | | | | 0.0597 | 0.0516 | 0.0446 | 0.0383 | 0.0324 | 0.0205 | 0.0176 | 0.0145 | 0.0115 | 0.0082 |
| 7 | | | | | | | 0.0495 | 0.0455 | 0.0418 | 0.0384 | 0.0172 | 0.0162 | 0.0148 | 0.0131 | 0.0111 |
| 8 | | | | | | | | 0.0465 | 0.0455 | 0.0447 | 0.0139 | 0.0146 | 0.0149 | 0.0147 | 0.014 |
| 9 | | | | | | | | | 0.0496 | 0.0519 | 0.011 | 0.013 | 0.0148 | 0.0163 | 0.0173 |
| 10 | | | | | | | | | | 0.0599 | 0.0081 | 0.0115 | 0.0146 | 0.0176 | 0.0206 |
| 11 | | | | | | | | | | | 0.0125 | 0.0086 | 0.0058 | 0.0037 | 0.0019 |
| 12 | | | | | | | | | | | | 0.0084 | 0.0064 | 0.005 | 0.0038 |
| 13 | | | | | | | | | | | | | 0.0072 | 0.0064 | 0.0058 |
| 14 | | | | | | | | | | | | | | 0.0084 | 0.0086 |
| 15 | | | | | | | | | | | | | | | 0.0125 |

CST model

Points on Model 1

| | 1 | 2 | 3 | 4 | 5 | 6 | 7 | 8 | 9 | 10 | 11 | 12 | 13 | 14 | 15 |
|---|---|---|---|---|---|---|---|---|---|---|---|---|---|---|---|
| 1 | 0.1863 | 0.1726 | 0.1601 | 0.1489 | 0.1383 | 0.0982 | 0.0913 | 0.084 | 0.0764 | 0.0683 | 0.0293 | 0.0274 | 0.0247 | 0.0213 | 0.0169 |
| 2 | | 0.169 | 0.1621 | 0.1553 | 0.1488 | 0.0903 | 0.0879 | 0.0845 | 0.0802 | 0.0753 | 0.0262 | 0.0259 | 0.0247 | 0.0229 | 0.0199 |
| 3 | | | 0.1637 | 0.162 | 0.16 | 0.0827 | 0.0842 | 0.0848 | 0.0841 | 0.0826 | 0.0231 | 0.0244 | 0.0248 | 0.0244 | 0.023 |
| 4 | | | | 0.169 | 0.1726 | 0.0753 | 0.0806 | 0.0845 | 0.0879 | 0.0903 | 0.0199 | 0.0229 | 0.0247 | 0.0259 | 0.0262 |
| 5 | | | | | 0.1863 | 0.0683 | 0.0764 | 0.084 | 0.0913 | 0.0982 | 0.0169 | 0.0213 | 0.0247 | 0.0274 | 0.0293 |
| 6 | | | | | | 0.0631 | 0.0548 | 0.0475 | 0.0411 | 0.035 | 0.0215 | 0.0185 | 0.0153 | 0.0123 | 0.0098 |
| 7 | | | | | | | 0.0528 | 0.0486 | 0.0448 | 0.0411 | 0.018 | 0.0172 | 0.0156 | 0.0139 | 0.0116 |
| 8 | | | | | | | | 0.0497 | 0.0486 | 0.0475 | 0.0147 | 0.0155 | 0.0158 | 0.0155 | 0.0146 |
| 9 | | | | | | | | | 0.0528 | 0.0548 | 0.0126 | 0.0139 | 0.0156 | 0.0172 | 0.018 |
| 10 | | | | | | | | | | 0.0631 | 0.0088 | 0.0123 | 0.0153 | 0.0185 | 0.0215 |
| 11 | | | | | | | | | | | 0.0125 | 0.0086 | 0.0058 | 0.0038 | 0.002 |
| 12 | | | | | | | | | | | | 0.0085 | 0.0065 | 0.0051 | 0.0038 |
| 13 | | | | | | | | | | | | | 0.0074 | 0.0065 | 0.0058 |
| 14 | | | | | | | | | | | | | | 0.0085 | 0.0086 |
| 15 | | | | | | | | | | | | | | | 0.0125 |

LST model

Table 7.3 - Gallagher model 1 stress smoothing polynomials

Sigma X:

N=2 $S = 4144 + 163.1x - 434.5y - 11.72x^2 + 0.85xy + 9.85y^2$

N=3 $S = 4600 + 523.8x - 870y - 38.9x^2 - 17.7xy + 49.1y^2 + 0.145x^3 + 1.51x^2y - 0.137xy^2 - 0.85y^3$

N=4 $S = 6279 - 116.6x - 1564y + 130.8x^2 - 20.62xy + 153.8y^2 - 15.35x^3 + 0.382x^2y + 0.195xy^2 - 6.255y^3 + 0.447x^4 + 0.139x^3y - 0.067x^2y^2 + 0.0149xy^3 + 0.088y^4$

N=5 $S = 8613 - 968.9x - 2890y + 229.6x^2 + 168.9xy + 406.5y^2 - 5.66x^3 - 34.15x^2y - 6.05xy^2 - 27.6y^3 - 1.52x^4 + 2.56x^3y + 0.6x^2y^2 + 0.116xy^3 + 0.87y^4 + 0.075x^5 - 0.06x^4y - 0.025x^3y^2 - 0.0024x^2y^3 - 0.001xy^4 - 0.01y^5$

Sigma Y:

N=2 $S = 25500 + 54.36x - 1478y - 2.72x^2 - 0.43xy + 21.2y^2$

N=3 $S = 24890 + 396.3x - 1467y - 44.6x^2 - 10.4xy + 22.5y^2 + 1.45x^3 + 0.61x^2y + 0.028xy^2 - 0.034y^3$

N=4 $S = 24460 + 323.4x - 1245y + 18.06x^2 - 51.6xy + 2.16y^2 - 6.38x^3 + 0.33x^2y + 1.53xy^2 + 0.789y^3 + 0.271x^4 - 0.02x^3y - 0.076x^2y^2 - 0.008xy^3 - 0.013y^4$

N=5 $S = 24160 + 998.5x - 1334y - 389.7x^2 + 37xy + 4.16y^2 + 81.75x^3 - 20.4x^2y + 1.92xy^2 + 0.387y^3 - 7.39x^4 + 2.13x^3y + 0.065x^2y^2 - 0.072xy^3 + 0.012y^4 + 0.23x^5 - 0.066x^4y - 0.0062x^3y^2 - 0.0x^2y^3 + 0.0011xy^4 - 0.00044y^5$

Tau XY:

N=2 $S = -1149 + 144.2x + 86.33y - 0.0584x^2 - 10.45xy - 0.19y^2$

N=3 $S = -2435 + 36.5x + 446y + 54.9x^2 - 56.4xy - 13y^2 - 2.4x^3 + 0x^2y + 1.53xy^2 - 0.03y^3$

N=4 $S = -3819 + 78.6x + 1085y + 94.8x^2 - 134.2xy - 69.7y^2 - 6.3x^3 - 0.186x^2y + 8.13xy^2 + 1.5y^3 + 0.128x^4 + 0.0026x^3y + 0.0043x^2y^2 - 0.148xy^3 - 0.006y^4$

N=5 $S = -6531 + 1865x + 2029y - 473.4x^2 - 309.5xy - 207y^2 + 84.1x^3 + 9.8x^2y + 26.1xy^2 + 9.27y^3 - 6.66x^4 - 0.0013x^3y - 0.577x^2y^2 - 0.9xy^3 - 0.18y^4 + 0.19x^5 + 0.028x^4y + 0.028x^3y^2 - 0.0012x^2y^3 + 0.013xy^4 + 0.001y^5$

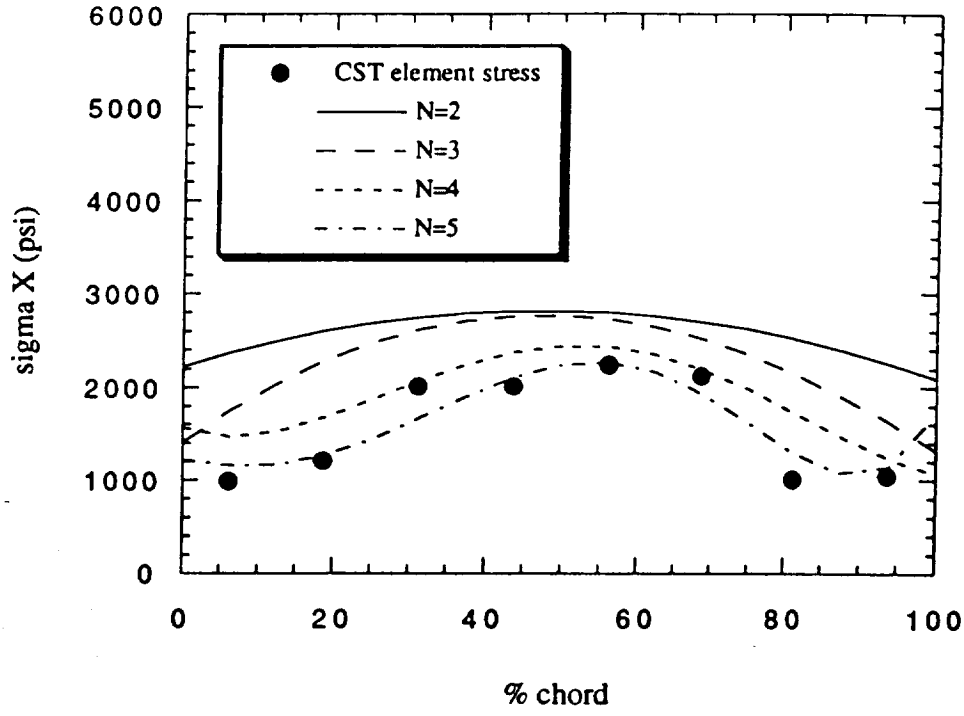


Figure 7.5 - $\sigma_{xx}$ stress smoothing along line A - Gallagher wing

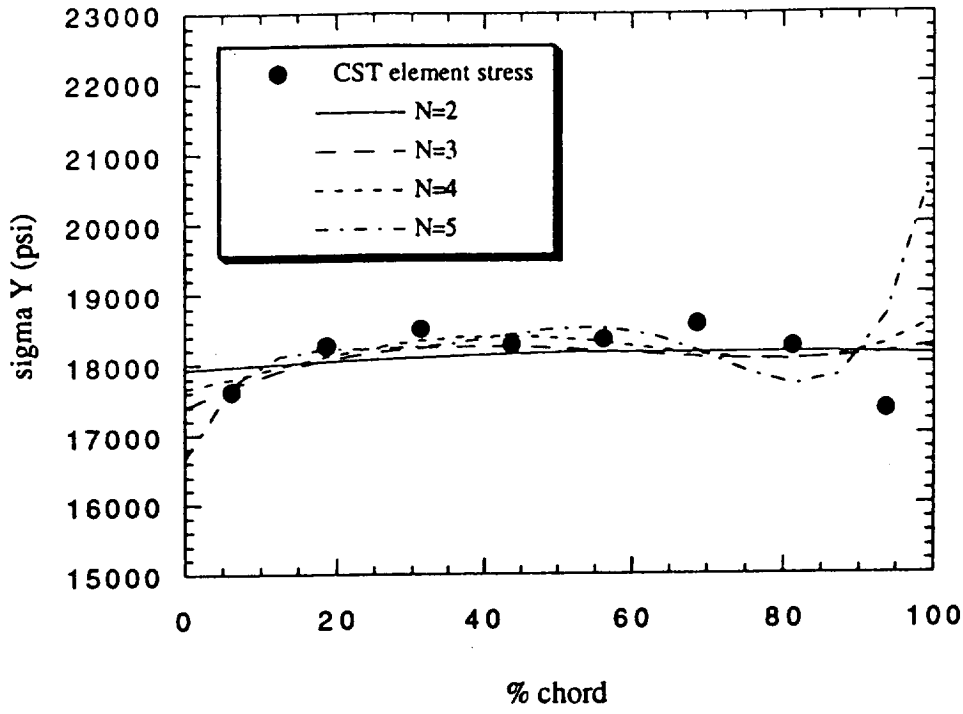


Figure 7.6 - $\sigma_{yy}$ stress smoothing along line A - Gallagher wing

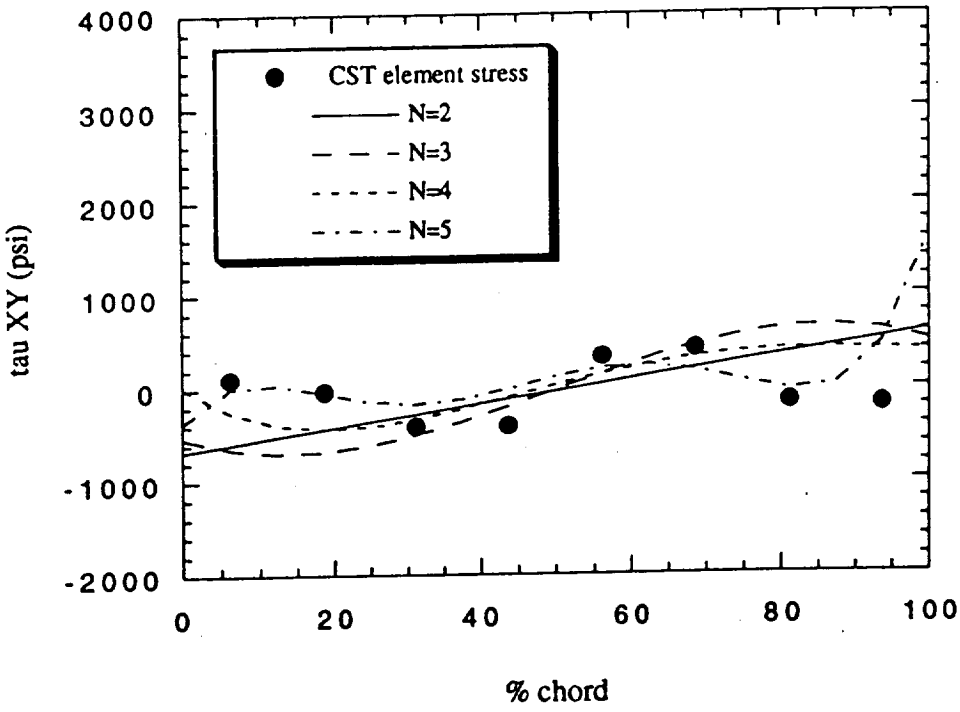


Figure 7.7 - $\sigma_{xy}$ stress smoothing along line A - Gallagher wing

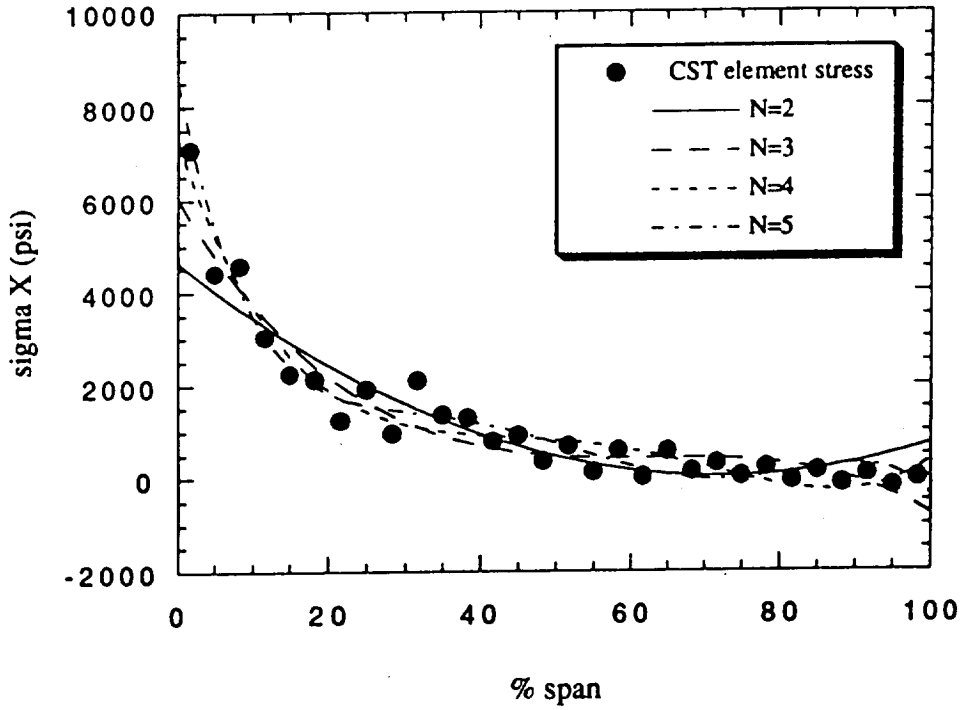


Figure 7.8 - $\sigma_{xx}$ stress smoothing along line B - Gallagher wing

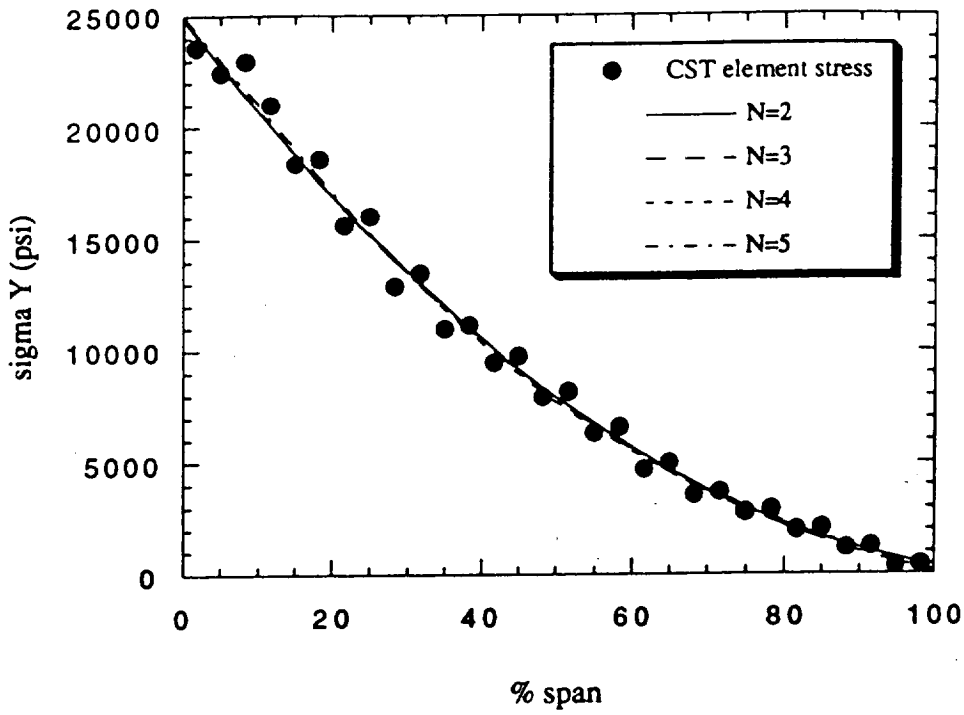


Figure 7.9 - $\sigma_{yy}$ stress smoothing along line B - Gallagher wing

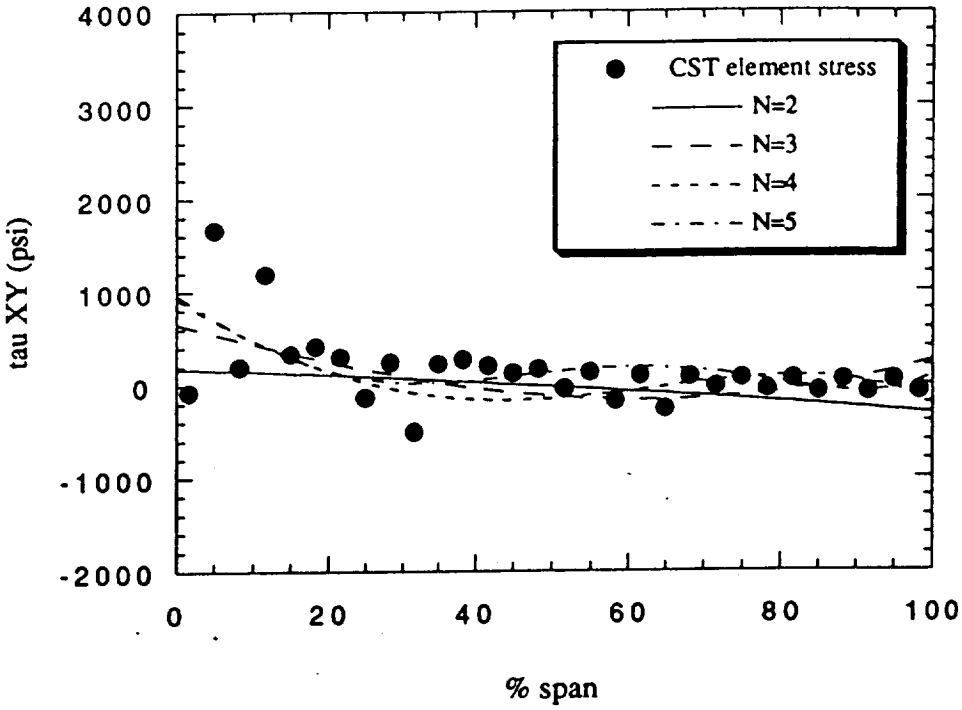


Figure 7.10 - $\sigma_{xy}$ stress smoothing along line B - Gallagher wing

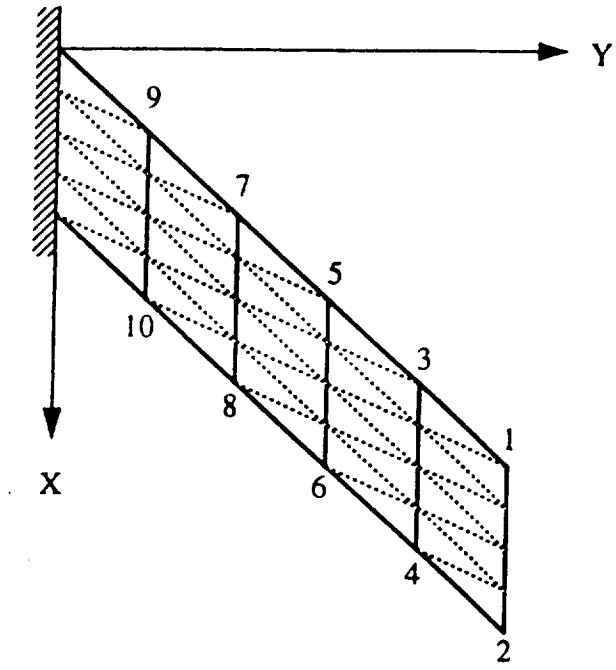


Original CST and LST wingskin meshes

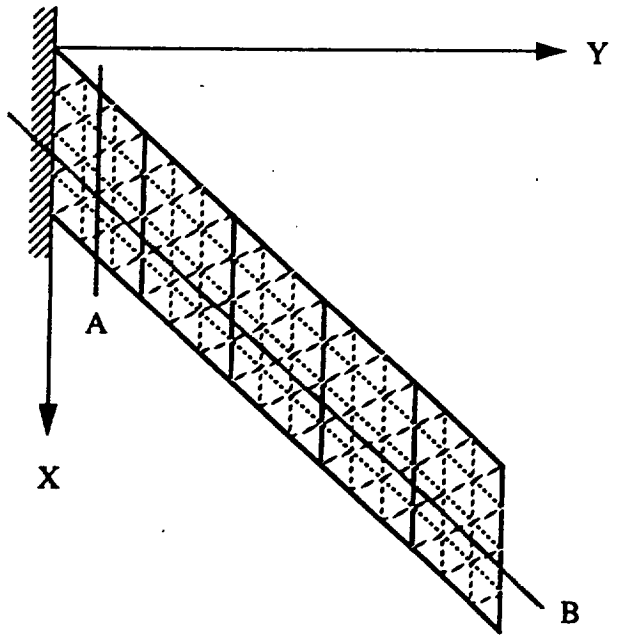


Final CST wingskin mesh (Adrib=2)

Figure 7.11 - Denke wing skin meshes

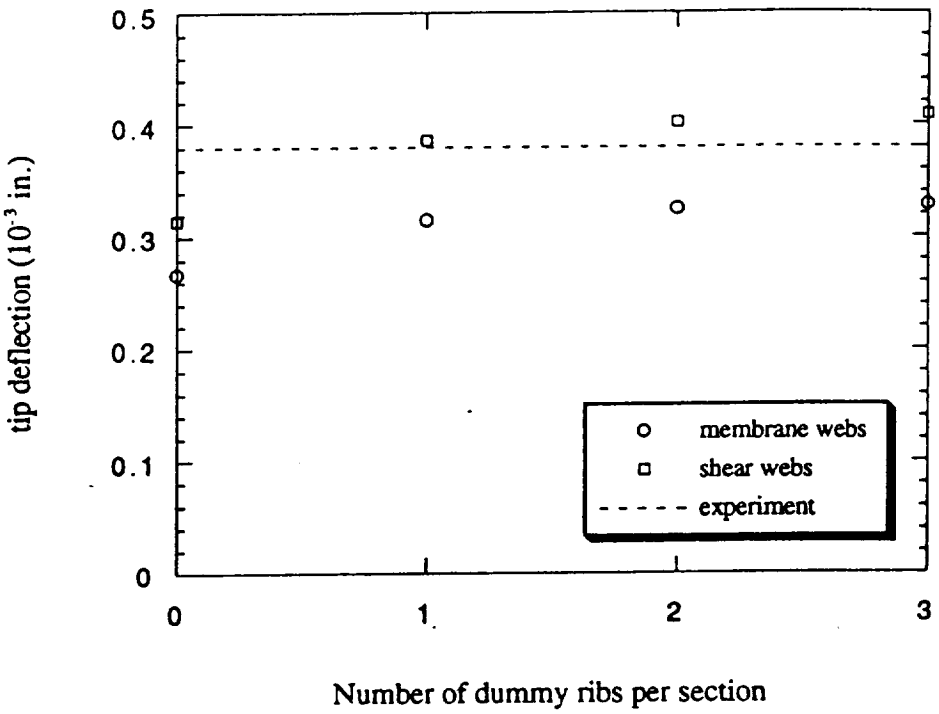


Figure 7.12 - Trailing edge tip deflection convergence with spanwise mesh refinement - Denke wing (load case 1)

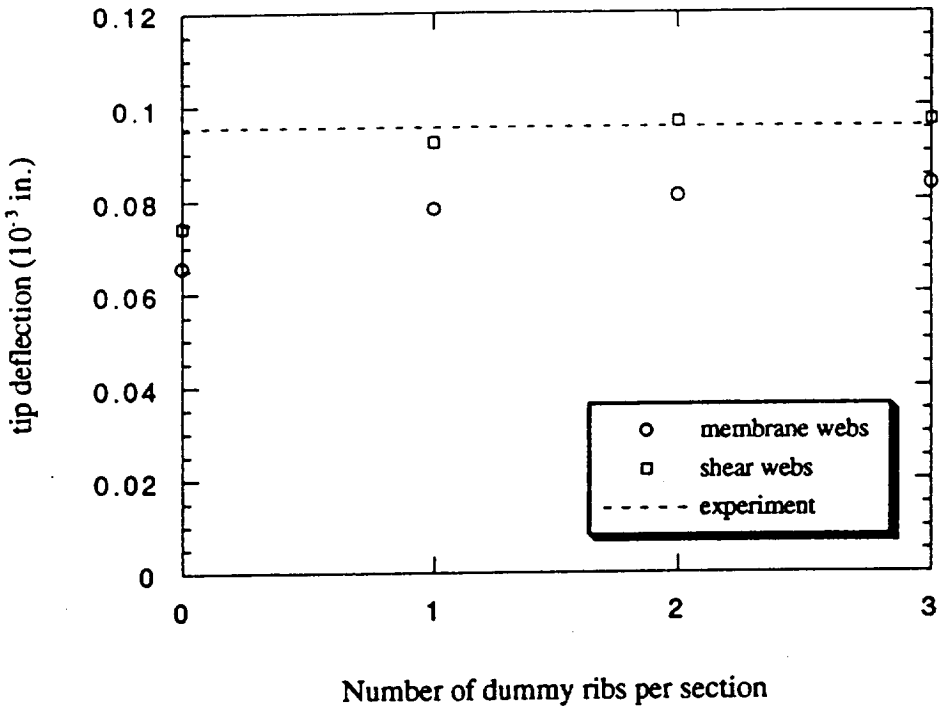


Figure 7.13 - Trailing edge tip deflection convergence with spanwise mesh refinement - Denke wing (load case 2)

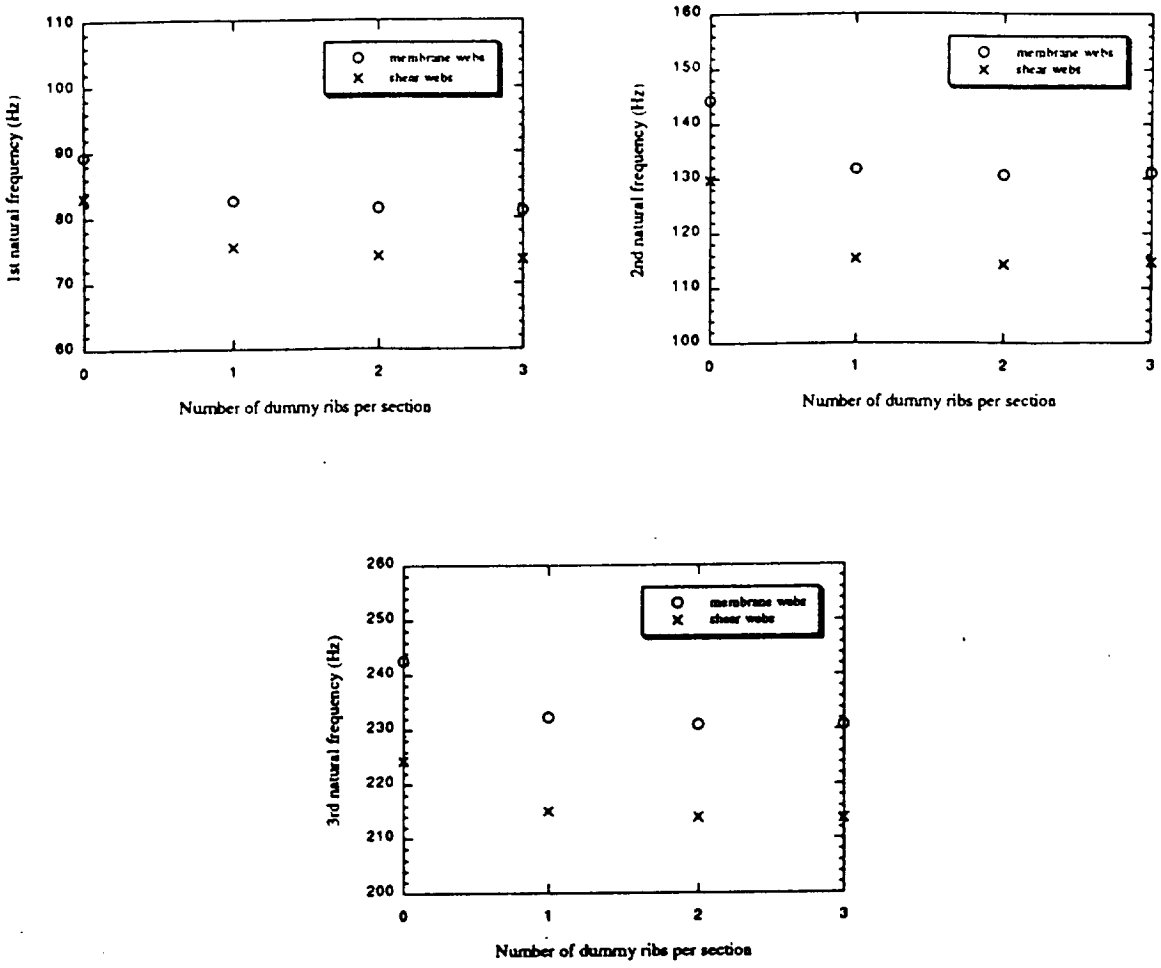


Figure 7.14 - Natural frequency convergence with spanwise mesh refinement - Denke wing

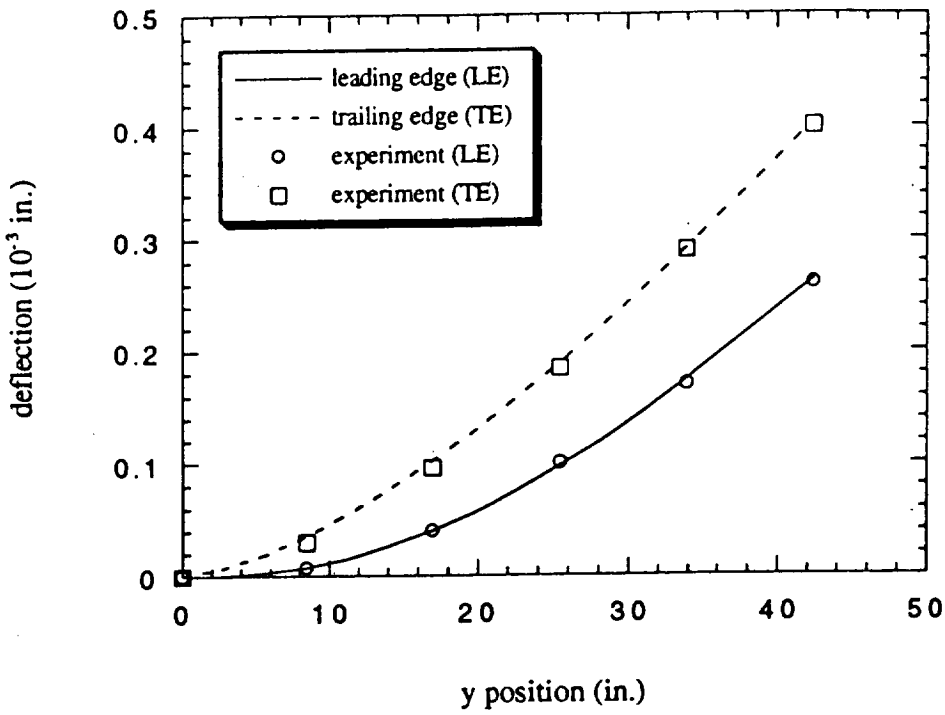


Figure 7.15 - CST model leading and trailing edge deflection - Denke wing (load case 1)

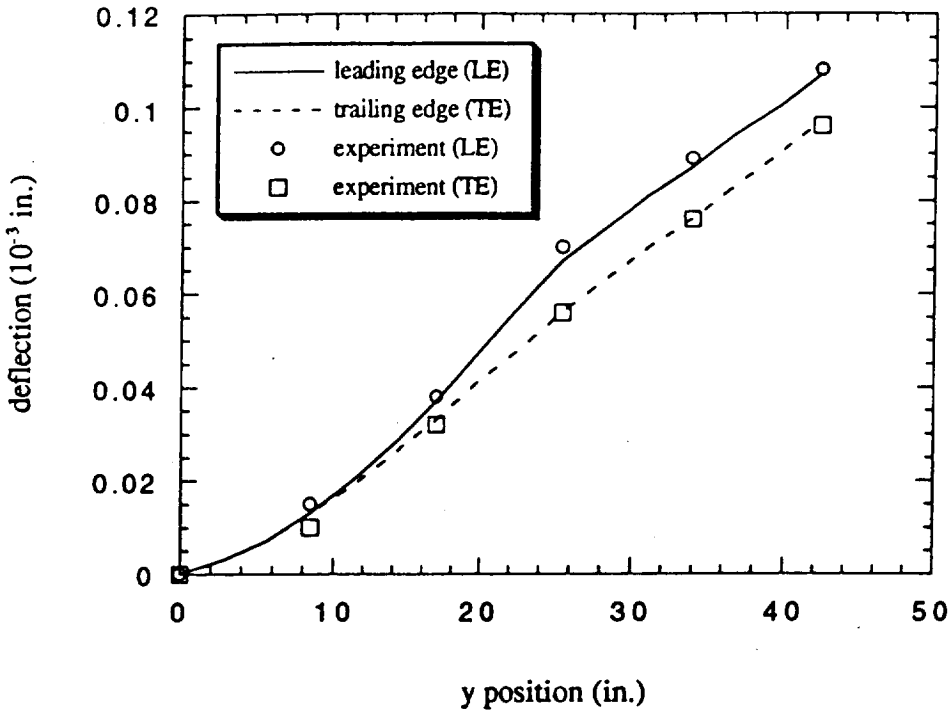


Figure 7.16 - CST model leading and trailing edge deflection - Denke wing (load case 2)

model (basic mesh) with experimental results are shown in Figures 7.17 and 7.18. The correlation is good. It is slightly stiffer than the best case CST model results along the leading edge in load case 2 (Figure 7.16). Numerical results are listed in Table 7.4 and are seen to be reasonably close to experiment.

Stress behavior is first analyzed in the spar caps along the wing root. Figure 7.19 shows the comparison for each model with respect to published values (Ref. 20). As can be seen, finite element stress magnitudes are lower than experiment towards the root trailing edge, and a rather large discrepancy exists in the CST model at 80% of the chord. One reason for this is that the Ref. 20 results were taken at the wing root while the finite element results were taken from the mid-point of the root rod element (the axial stress is assumed constant throughout its length). In addition, the well known root trailing edge stress singularity in swept back wings appears, and accuracy of all calculated results deteriorates in that region.

A comparison of cap stresses along the leading and trailing edge spar caps for each model (CST and LST) for load case 2 is seen in Figures 7.20 and 7.21. Good correlation with experiment exists. The stress values plotted for each spar cap element were taken at its geometric midpoint as mentioned previously.

No experimental wing skin stress data is available for the Denke wing. Skin stress curve fits were again attempted for each stress along both a chordwise and a spanwise cut (Fig. 7.11) in the CST model. Numerical details of the various curve fitting polynomials are given in Table 7.5. Figures 7.22 through 7.27 show the resulting plots. As with the Gallagher wing, a polynomial of order N=4 gives the best representation for the fluctuating CST element stresses with $\sigma_{yy}$ showing the best behavior.

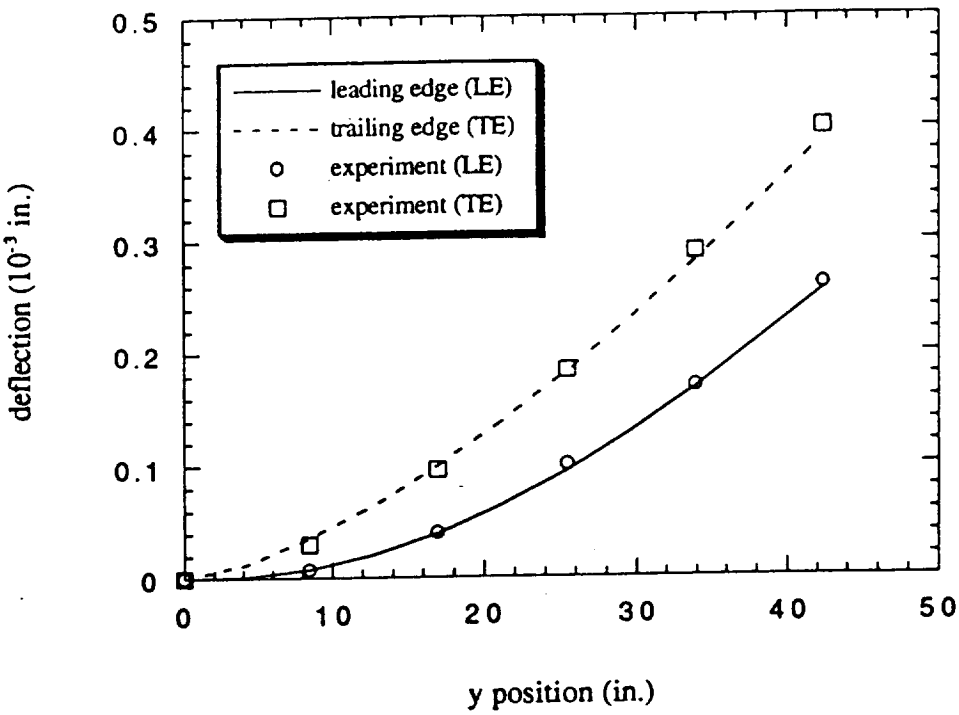


Figure 7.17 - LST model leading and trailing edge deflection - Denke wing (load case 1)

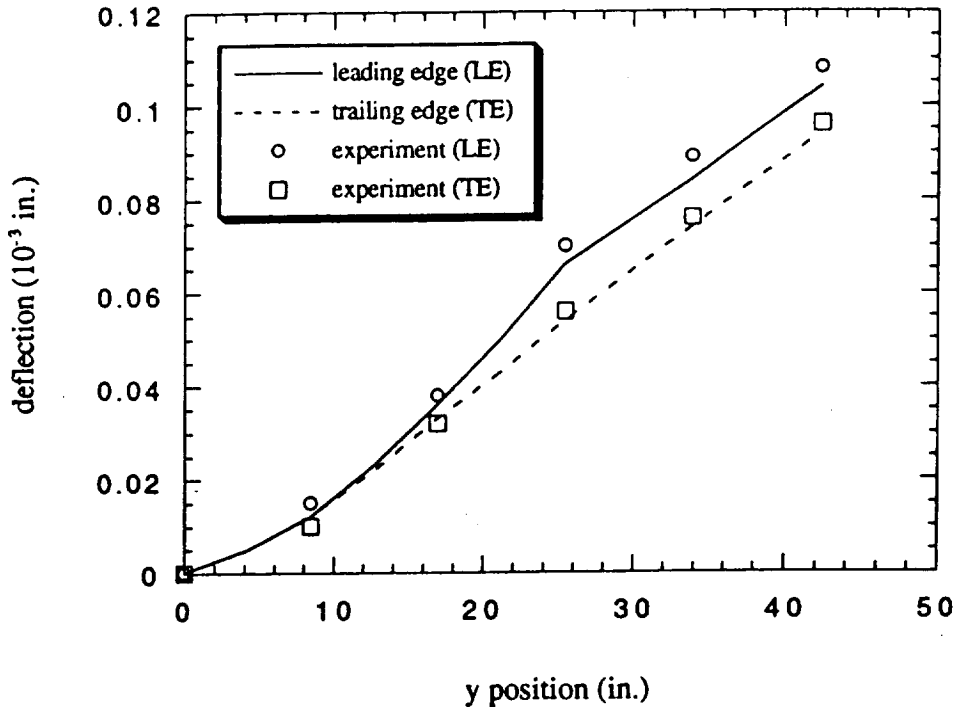


Figure 7.18 - LST model leading and trailing edge deflection - Denke wing (load case 2)

Table 7.4 - Displacements of the Denke wing

| Load case 1 | Deflection (x10-3 in.) | | | | |
|---|---|---|---|---|---|
| Node | experiment | CST model | % error | LST model | % error |
| 1 | 0.007 | 0.007 | 0.00 | 0.007 | 0.00 |
| 2 | 0.033 | 0.035 | 6.06 | 0.035 | 6.06 |
| 3 | 0.040 | 0.040 | 0.00 | 0.039 | 2.50 |
| 4 | 0.096 | 0.102 | 6.25 | 0.099 | 3.13 |
| 5 | 0.100 | 0.097 | 3.00 | 0.094 | 6.00 |
| 6 | 0.185 | 0.189 | 2.16 | 0.183 | 1.08 |
| 7 | 0.170 | 0.174 | 2.35 | 0.168 | 1.18 |
| 8 | 0.290 | 0.291 | 0.34 | 0.281 | 3.10 |
| 9 | 0.260 | 0.263 | 1.15 | 0.255 | 1.92 |
| 10 | 0.400 | 0.403 | 0.75 | 0.389 | 2.75 |

| Load case 2 | Deflection (x10-3 in.) | | | | |
|---|---|---|---|---|---|
| Node | experiment | CST model | % error | LST model | % error |
| 1 | 0.014 | 0.013 | 7.14 | 0.012 | 14.29 |
| 2 | 0.011 | 0.013 | 18.18 | 0.012 | 9.09 |
| 3 | 0.038 | 0.037 | 2.63 | 0.036 | 5.26 |
| 4 | 0.032 | 0.033 | 3.13 | 0.033 | 3.13 |
| 5 | 0.070 | 0.067 | 4.29 | 0.066 | 5.71 |
| 6 | 0.056 | 0.056 | 0.00 | 0.054 | 3.57 |
| 7 | 0.089 | 0.087 | 2.25 | 0.084 | 5.62 |
| 8 | 0.076 | 0.076 | 0.00 | 0.074 | 2.63 |
| 9 | 0.108 | 0.107 | 0.93 | 0.104 | 3.70 |
| 10 | 0.096 | 0.097 | 1.04 | 0.094 | 2.08 |

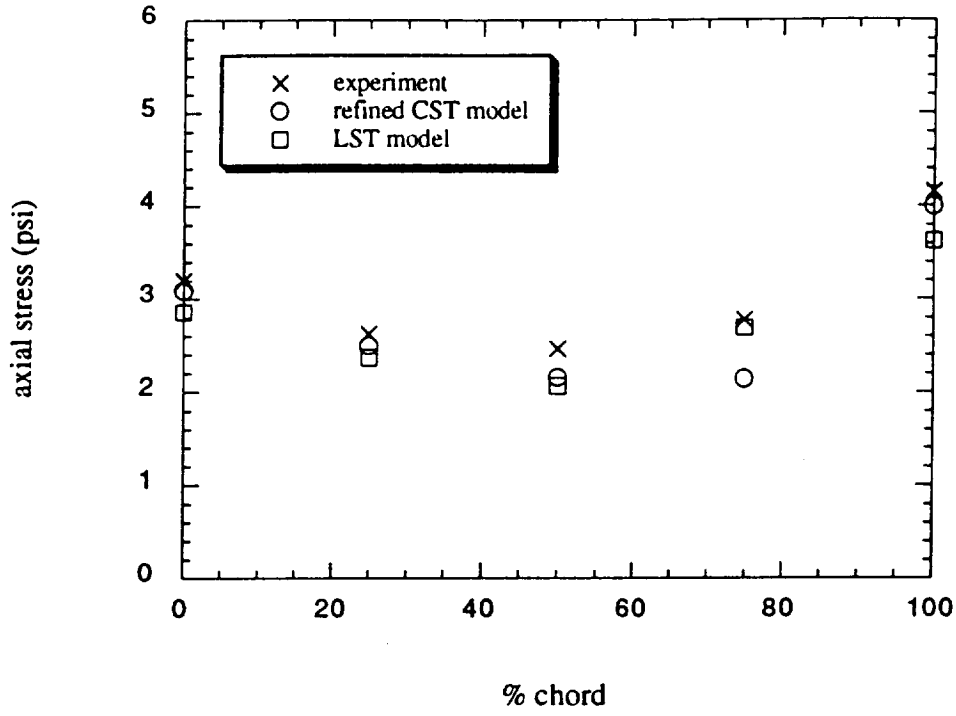


Figure 7.19 - Root chord cap stresses - Denke wing (load case 2)

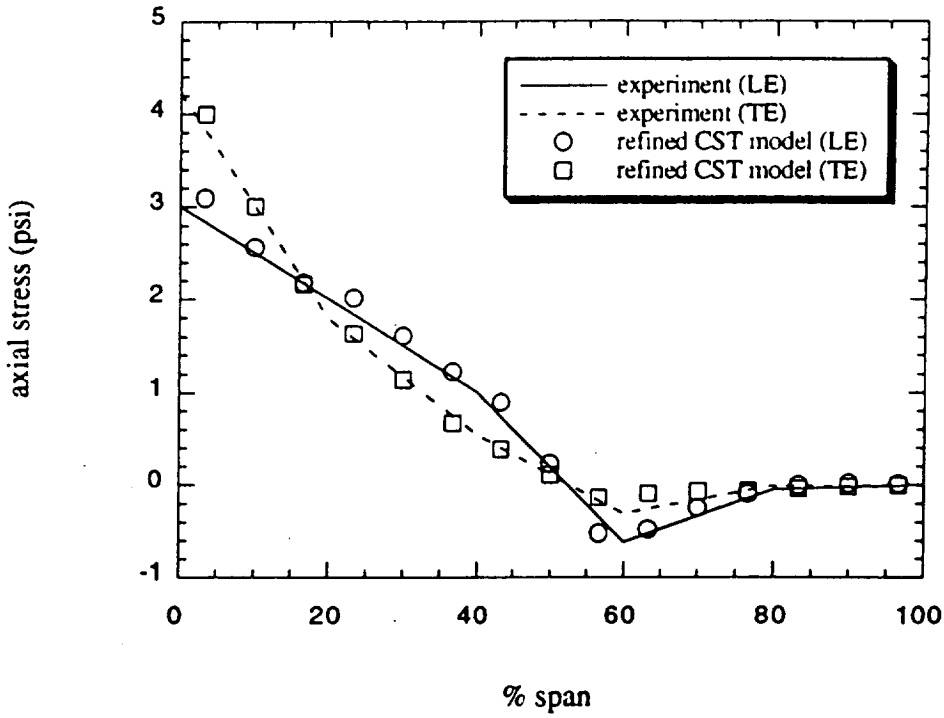


Figure 7.20 - CST model spar cap stresses - Denke wing (load case 2)

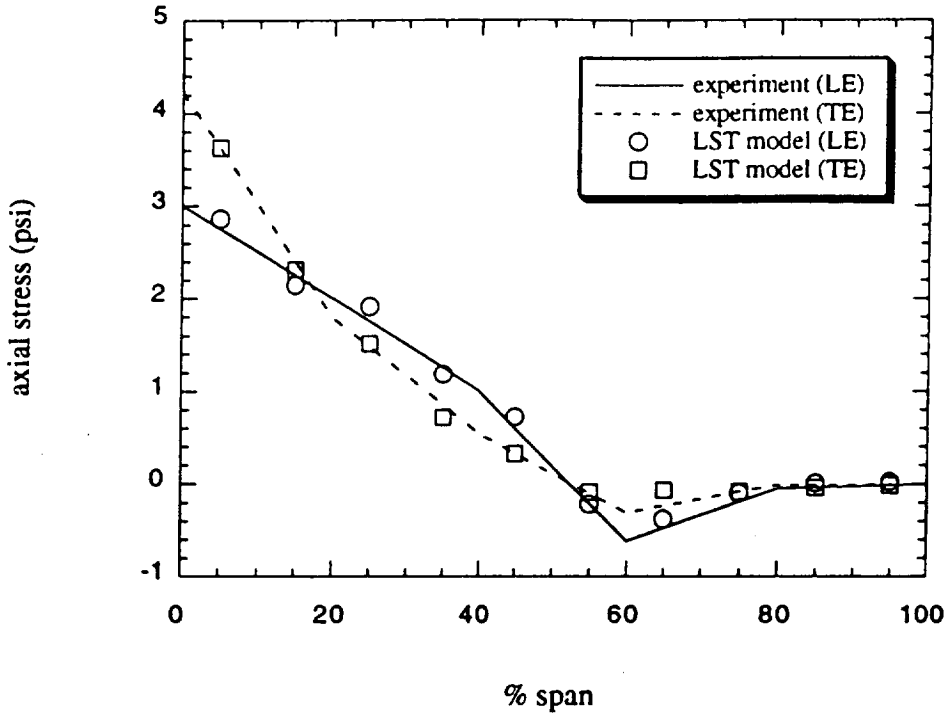


Figure 7.21 - LST model spar cap stresses - Denke wing (load case 2)

Table 7.5 - Denke stress smoothing polynomials

Sigma X:

N=2 $S = -0.5732 + 0.133x - 0.2246y - 0.0005606x^2 - 0.0009817xy + 0.004109y^2$

N=3 $S = 0.9131 - 0.05502x - 0.2869y + 0.007494x^2 - 0.00063xy + 0.005896y^2 - 0.0001728x^3 + 0.000346x^2y - 0.0004927xy^2 + 0.0002019y^3$

N=4 $S = 1.616 - 0.2591x - 0.2163y + 0.02552x^2 - 0.00929xy + 0.002164y^2 - 0.0009427x^3 + 0.001616x^2y - 0.0018xy^2 + 0.000973y^3 + 0.0000117x^4 - 0.00002935x^3y + 0.0000317x^2y^2 - 0.000009087xy^3 - 0.000005911y^4$

N=5 $S = 2.127 - 0.98x + 0.5835y + 0.251x^2 - 0.467xy + 0.228y^2 - 0.028x^3 + 0.07816x^2y - 0.07174xy^2 + 0.0213y^3 + 0.0014x^4 - 0.005123x^3y + 0.00692x^2y^2 - 0.004126xy^3 + 0.000937y^4 - 0.0000258x^5 + 0.000115x^4y - 0.0002024x^3y^2 + 0.000175x^2y^3 - 0.000074xy^4 + 0.00001185y^5$

Sigma Y:

N=2 $S = 4.56 - 0.0895x - 0.08107y - 0.0004309x^2 + 0.001836xy + 0.0001947y^2$

N=3 $S = 2.713 + 0.1171x + 0.0265y - 0.008532x^2 - 0.003825xy + 0.002099y^2 + 0.0003573x^3 - 0.001119x^2y + 0.0017xy^2 - 0.0008231y^3$

N=4 $S = 1.683 + 0.1255x + 0.3875y + 0.00897x^2 - 0.06642xy + 0.02704y^2 - 0.00097x^3 + 0.002349x^2y + 0.0007279xy^2 - 0.001396y^3 + 0.00004581x^4 - 0.000194x^3y + 0.0003256x^2y^2 - 0.0002886xy^3 + 0.0001078y^4$

N=5 $S = 2.161 - 0.098x + 0.539y - 0.0287x^2 + 0.077xy - 0.0864y^2 + 0.01676x^3 - 0.06263x^2y + 0.07636xy^2 - 0.02968y^3 - 0.001712x^4 + 0.00766x^3y - 0.01253x^2y^2 + 0.008884xy^3 - 0.002301y^4 + 0.0000539x^5 - 0.0002943x^4y + 0.0006389x^3y^2 - 0.0006924x^2y^3 + 0.0003766xy^4 - 0.00008273y^5$

Tau XY:

N=2 $S = -1.191 + 0.00433x + 0.05274y - 0.0002078x^2 + 0.000339xy - 0.000801y^2$

N=3 $S = -1.368 + 0.1041x - 0.07157y - 0.004549x^2 + 0.002929xy + 0.00359y^2 - 0.0000683x^3 + 0.0004915x^2y - 0.0007492xy^2 + 0.0002806y^3$

N=4 $S = -1.556 + 0.1912x - 0.1758y - 0.002212x^2 - 0.02199xy + 0.03325y^2 - 0.0006887x^3 + 0.003224x^2y - 0.003743xy^2 + 0.0008293y^3 + 0.00001036x^4 - 0.00002879x^3y - 0.000003943x^2y^2 + 0.00005072xy^3 - 0.00002422y^4$

N=5 $S = -1.63 + 0.086x + 0.03225y + 0.0284x^2 - 0.08423xy + 0.05124y^2 - 0.0043x^3 + 0.0126x^2y - 0.01077xy^2 + 0.002693y^3 + 0.0002488x^4 - 0.00095x^3y + 0.00137x^2y^2 - 0.0009256xy^3 + 0.00025y^4 - 0.0000067x^5 + 0.0000356x^4y - 0.000078x^3y^2 + 0.00009x^2y^3 - 0.00005xy^4 + 0.000011y^5$

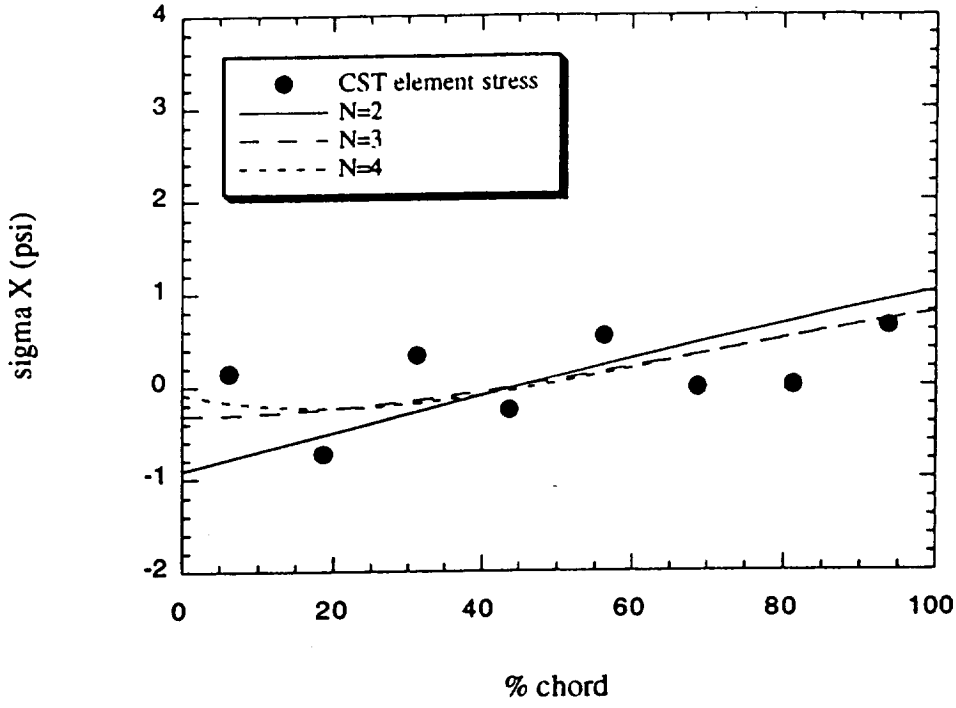


Figure 7.22 - $\sigma_{xx}$ stress smoothing along line A - Denke wing (load case 2)

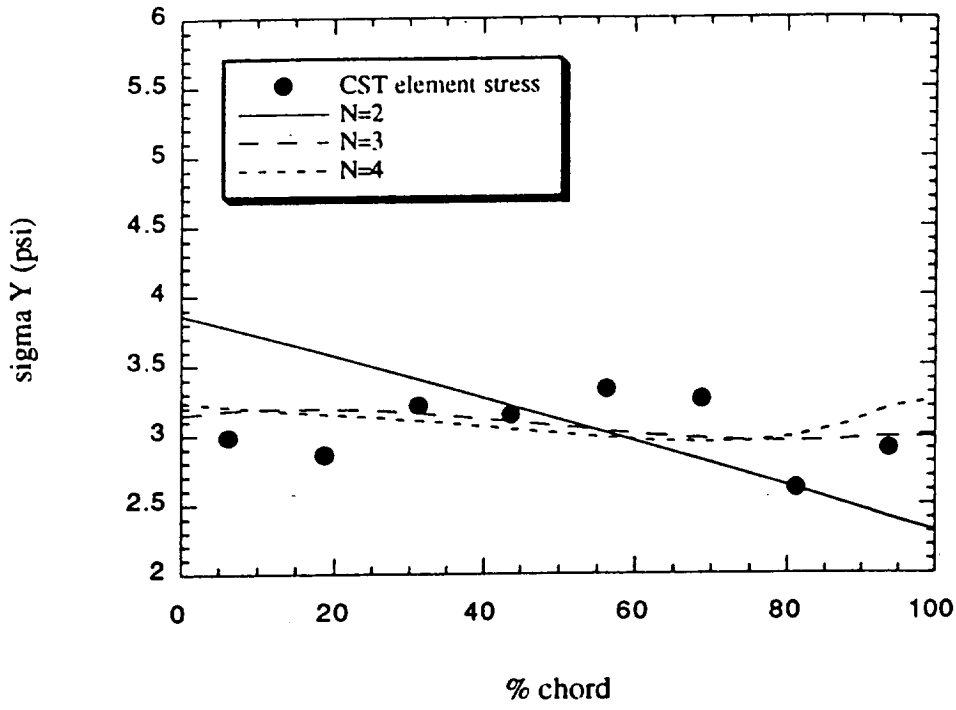


Figure 7.23 - $\sigma_{yy}$ stress smoothing along line A - Denke wing (load case 2)

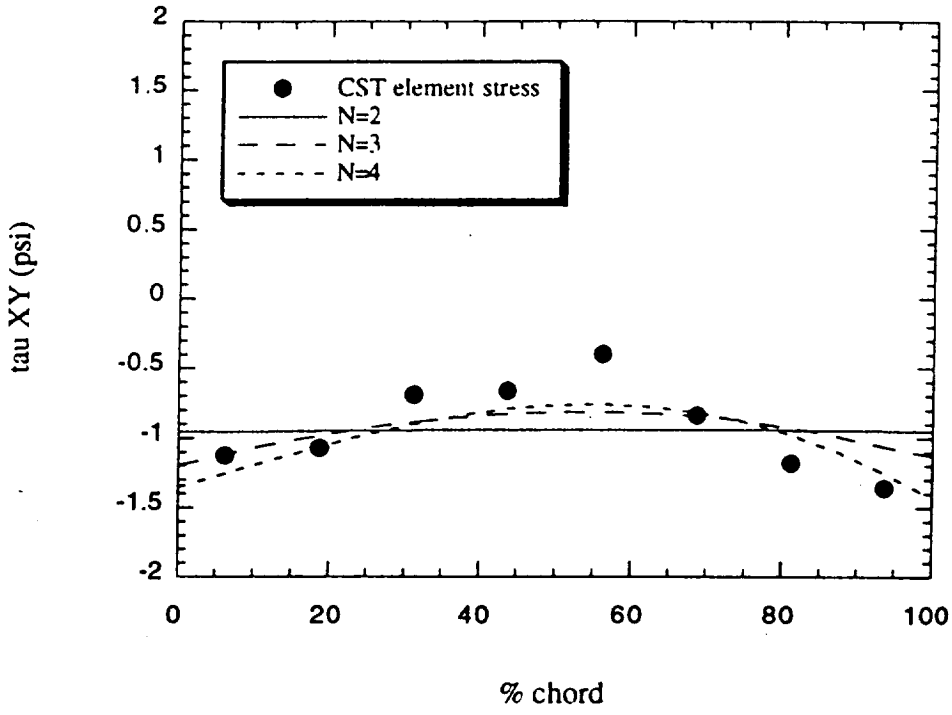


Figure 7.24 - $\sigma_{xy}$ stress smoothing along line A - Denke wing (load case 2)

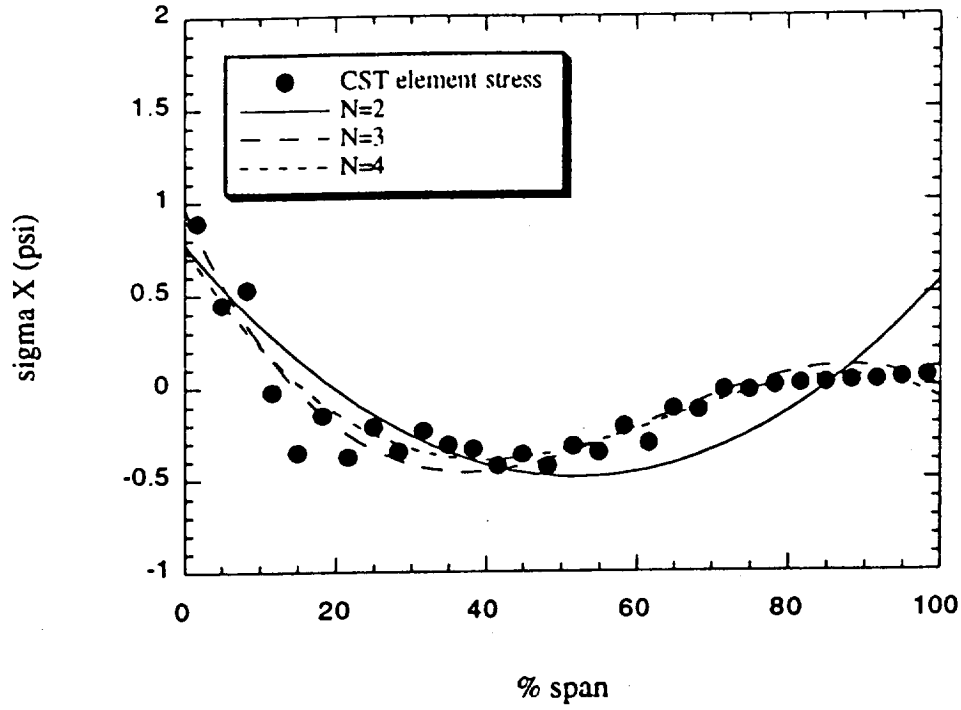


Figure 7.25 - $\sigma_{xx}$ stress smoothing along line B - Denke wing (load case 2)

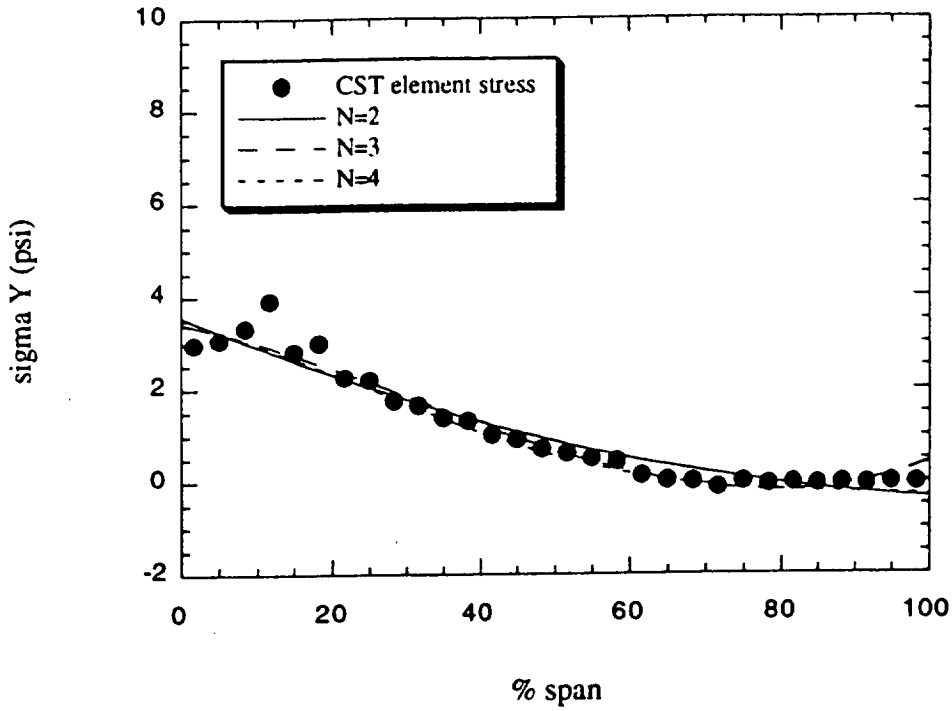


Figure 7.26 - $\sigma_{yy}$ stress smoothing along line B - Denke wing (load case 2)

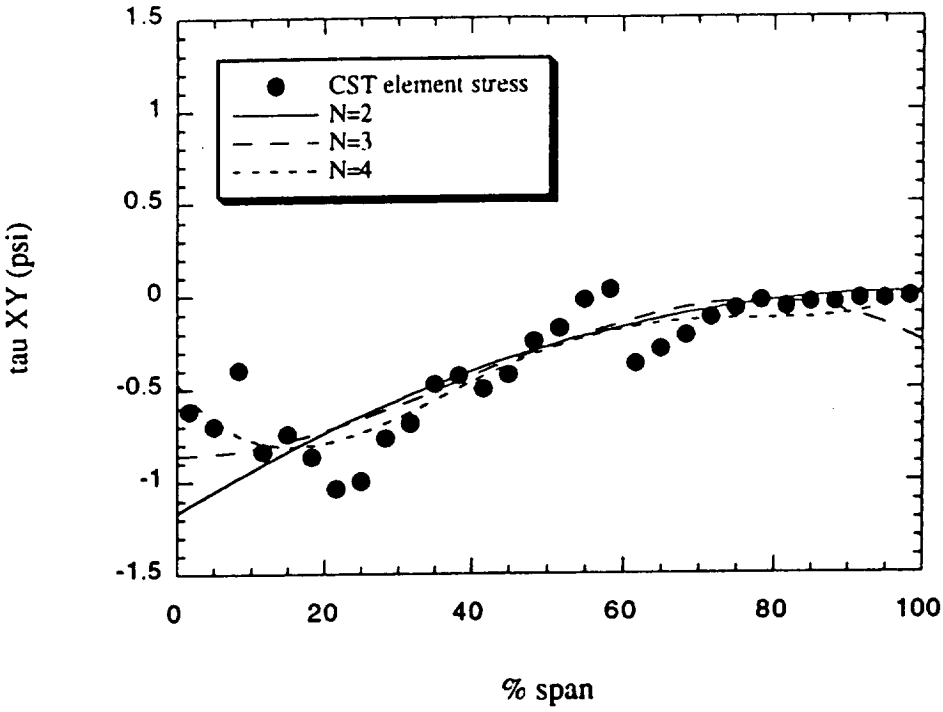


Figure 7.27 - $\sigma_{xy}$ stress smoothing along line B - Denke wing (load case 2)

## 7.4 Turner/Martin/Weikel wing

Figure 7.28 shows both the basic wing skin mesh and the refined wing skin mesh for the Turner wing using CST elements. In this case the mesh includes both spanwise and chordwise refinements, introducing the presence of floating nodes. Chordwise mesh refinement consists of one dummy spar per spar interval, and is employed to allow for more CST elements across the chord. One dummy rib per rib interval is then added within the root region. Figure 7.29 shows the LST element model used for comparison.

The effect on wing deflection of modeling the Turner wing with a refined mesh and pure CST shear webs as compared to the LST model is seen in Figures 7.30 and 7.31. Mesh refinement has only a small effect on the spanwise vertical deflection. Tables 7.6 and 7.7, though, show that refining the mesh in this case leads to greater in-plane deflections (x- and y- axes) for the CST model.

With respect to stresses, nodal stress averaging following the results of Turner (Ref. 21) was performed for each CST wing model. Tables 7.8 and 7.9 contain the nodal averages for each of the three stresses within the wing root area as compared to published results. Close agreement is found for $\sigma_{xx}$ and $\sigma_{yy}$. In the case of the shear stress $\sigma_{xy}$ the correlation is not as good.

Natural frequency results for both finite element models as compared with those available from a commercial finite element package (ELFINI, Ref. 22) can be seen in Table 7.10. Excellent agreement using the original mesh is evident. Natural frequency results using the refined mesh decrease in accuracy as the frequency increases due to localized vibration of lumped masses at floating nodes. An attempt to solve this problem involved studying the choice of dummy element thicknesses (1% of a real element's thickness was the choice in all studies up to this point). The effect of varying the dummy element thickness from 1% to 10% on displacements and natural frequencies is shown in Table 7.11.

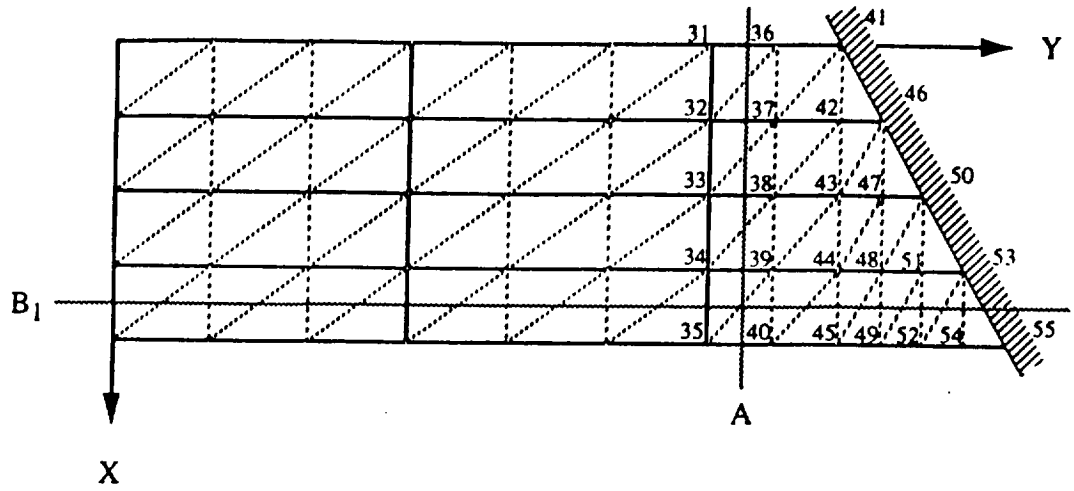


Original CST wingskin mesh

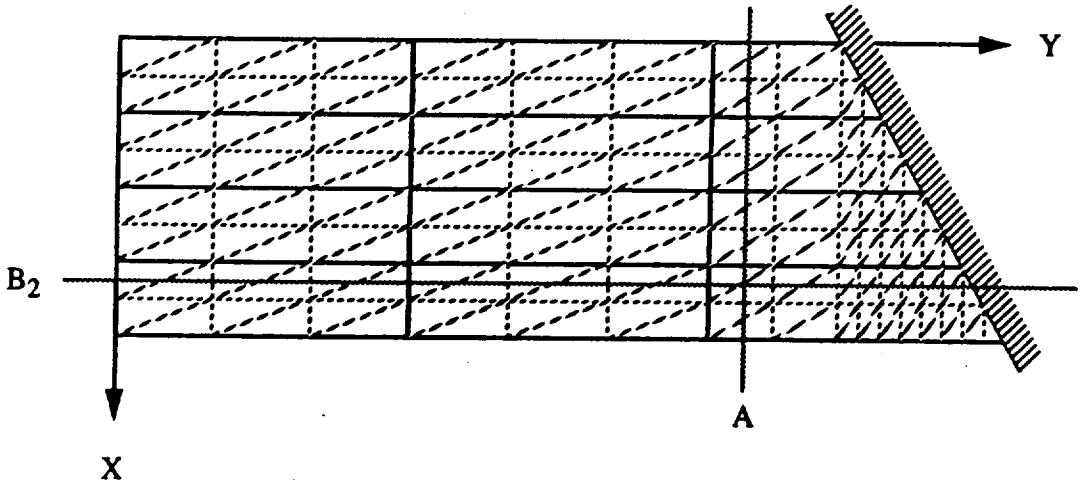


Final CST wingskin mesh (Adspar=1)

Figure 7.28 - Turner wing skin CST meshes

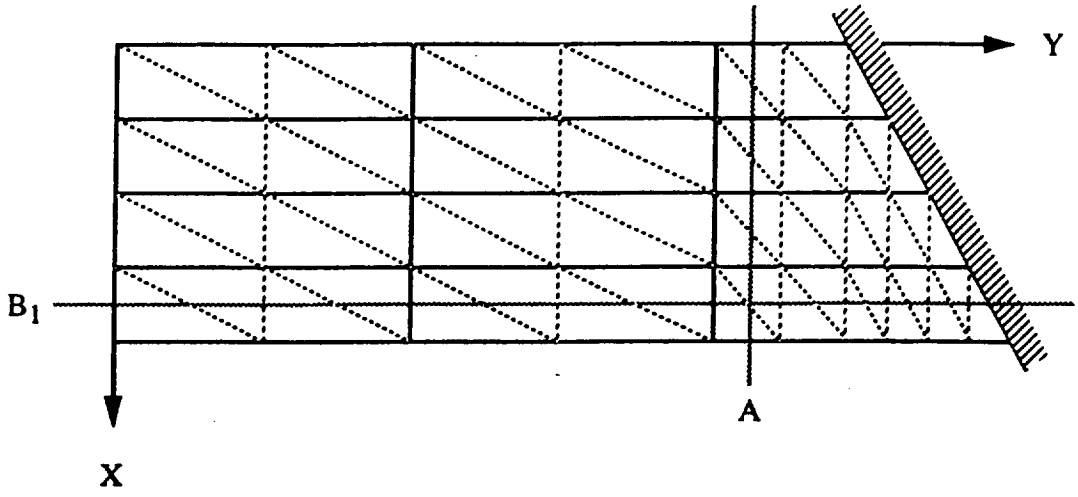


Figure 7.29 - Turner wing skin LST mesh

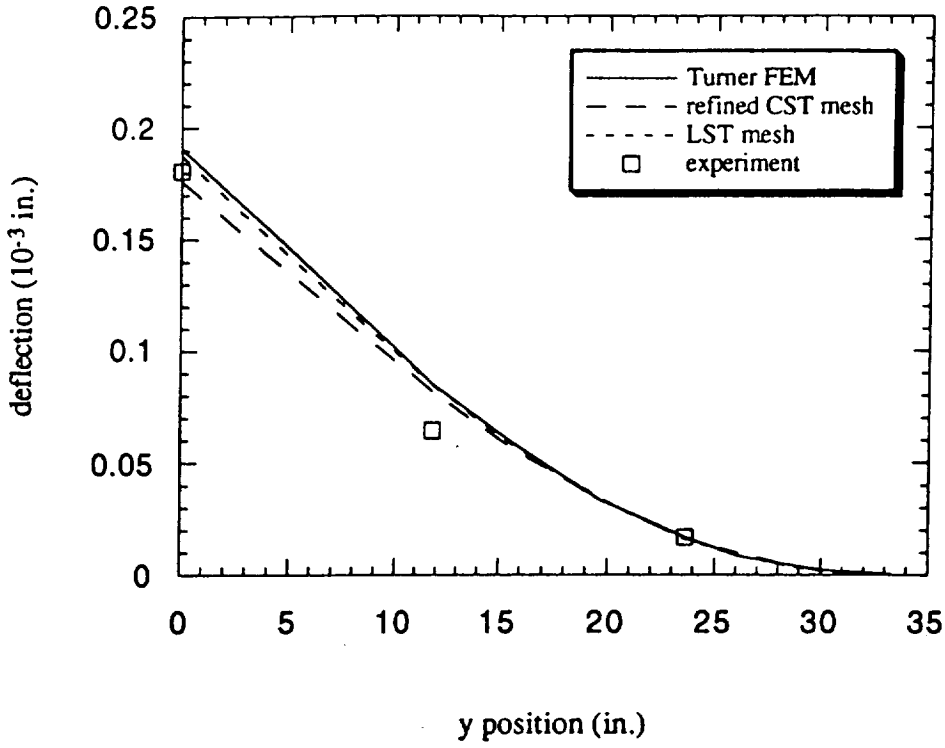


Figure 7.30 - Leading edge deflection - Turner wing

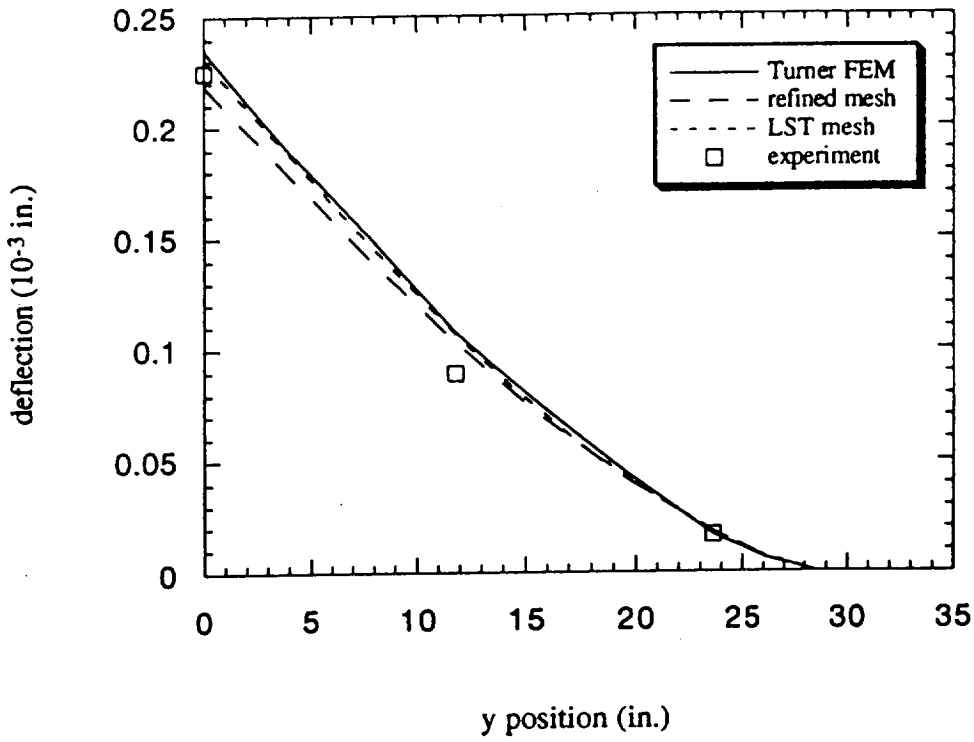


Figure 7.31 - Trailing edge deflection - Turner wing

Table 7.6 - Displacements of the Turner wing (original mesh)

| Node | Turner (x10-6) | | | CST model (x10-6) | | |
|---|---|---|---|---|---|---|
| | u | v | w | u | v | w |
| 31 | 0.008 | -4.491 | -15.910 | 0.009 | -4.874 | -17.444 |
| 32 | -0.443 | -4.333 | -16.690 | -0.422 | -4.747 | -18.447 |
| 33 | -0.850 | -4.251 | -16.939 | -0.820 | -4.650 | -18.818 |
| 34 | -1.225 | -4.142 | -16.069 | -1.180 | -4.530 | -18.053 |
| 35 | -1.585 | -4.060 | -13.669 | -1.532 | -4.473 | -15.740 |
| 36 | -0.030 | -2.666 | -5.695 | 0.009 | -2.878 | -6.302 |
| 37 | -0.660 | -2.840 | -7.797 | -0.616 | -3.104 | -8.534 |
| 38 | -1.014 | -3.043 | -8.947 | -0.983 | -3.329 | -9.882 |
| 39 | -1.327 | -3.069 | -8.933 | -1.299 | -3.368 | -10.022 |
| 40 | -1.682 | -2.991 | -7.463 | -1.662 | -3.311 | -8.586 |
| 41 | 0 | 0 | 0 | 0 | 0 | 0 |
| 42 | -0.480 | -1.252 | -2.004 | -0.393 | -1.315 | -2.103 |
| 43 | -0.858 | -1.801 | -3.421 | -0.798 | -1.960 | -3.669 |
| 44 | -1.184 | -2.029 | -3.923 | -1.141 | -2.231 | -4.319 |
| 45 | -1.511 | -2.098 | -3.232 | -1.478 | -2.328 | -3.660 |
| 46 | 0 | 0 | 0 | 0 | 0 | 0 |
| 47 | -0.513 | -0.940 | -1.091 | -0.440 | -0.981 | -1.154 |
| 48 | -0.904 | -1.341 | -1.689 | -0.850 | -1.455 | -1.831 |
| 49 | -1.226 | -1.548 | -1.333 | -1.191 | -1.688 | -1.486 |
| 50 | 0 | 0 | 0 | 0 | 0 | 0 |
| 51 | -0.483 | -0.679 | -0.384 | -0.429 | -0.708 | -0.398 |
| 52 | -0.836 | -1.016 | -0.178 | -0.788 | -1.076 | -0.175 |
| 53 | 0 | 0 | 0 | 0 | 0 | 0 |
| 54 | -0.383 | -0.506 | 0.260 | -0.338 | -0.504 | 0.299 |
| 55 | 0 | 0 | 0 | 0 | 0 | 0 |

Table 7.7 - Displacements of the Turner wing (refined mesh)

| Node | Turner (x10-6) | | | CST model (x10-6) | | |
|---|---|---|---|---|---|---|
| | u | v | w | u | v | w |
| 31 | 0.008 | -4.491 | -15.910 | 0.103 | -5.074 | -18.053 |
| 32 | -0.443 | -4.333 | -16.690 | -0.425 | -4.857 | -19.000 |
| 33 | -0.850 | -4.251 | -16.939 | -0.828 | -4.744 | -19.312 |
| 34 | -1.225 | -4.142 | -16.069 | -1.198 | -4.616 | -18.458 |
| 35 | -1.585 | -4.060 | -13.669 | -1.562 | -4.562 | -16.005 |
| 36 | -0.030 | -2.666 | -5.695 | 0.048 | -3.066 | -6.520 |
| 37 | -0.660 | -2.840 | -7.797 | -0.629 | -3.227 | -9.634 |
| 38 | -1.014 | -3.043 | -8.947 | -0.993 | -3.410 | -10.190 |
| 39 | -1.327 | -3.069 | -8.933 | -1.304 | -3.429 | -10.259 |
| 40 | -1.682 | -2.991 | -7.463 | -1.658 | -3.363 | -8.665 |
| 41 | 0 | 0 | 0 | 0 | 0 | 0 |
| 42 | -0.480 | -1.252 | -2.004 | -0.444 | -1.426 | -2.133 |
| 43 | -0.858 | -1.801 | -3.421 | -0.821 | -2.054 | -3.772 |
| 44 | -1.184 | -2.029 | -3.923 | -1.144 | -2.300 | -4.400 |
| 45 | -1.511 | -2.098 | -3.232 | -1.476 | -2.379 | -3.588 |
| 46 | 0 | 0 | 0 | 0 | 0 | 0 |
| 47 | -0.513 | -0.940 | -1.091 | -0.485 | -1.039 | -1.196 |
| 48 | -0.904 | -1.341 | -1.689 | -0.874 | -1.502 | -1.877 |
| 49 | -1.226 | -1.548 | -1.333 | -1.208 | -1.713 | -1.398 |
| 50 | 0 | 0 | 0 | 0 | 0 | 0 |
| 51 | -0.483 | -0.679 | -0.384 | -0.467 | -0.733 | -0.406 |
| 52 | -0.836 | -1.016 | -0.178 | -0.822 | -1.089 | -0.089 |
| 53 | 0 | 0 | 0 | 0 | 0 | 0 |
| 54 | -0.383 | -0.506 | 0.260 | -0.377 | -0.503 | 0.349 |
| 55 | 0 | 0 | 0 | 0 | 0 | 0 |

Table 7.8 - Summary of Turner computed nodal stress averages (original mesh)

| Node | Turner stress averages (psi) | | | CST stress averages (psi) | | |
|---|---|---|---|---|---|---|
| | Sigma X | Sigma Y | Sigma XY | Sigma X | Sigma Y | Sigma XY |
| 36 | 0.36 | 8.93 | 0.45 | 0.49 | 8.85 | -0.28 |
| 37 | 0.61 | 6.68 | -0.38 | 0.61 | 7.57 | -0.51 |
| 38 | 0.60 | 5.41 | -0.17 | 0.51 | 5.73 | -0.19 |
| 39 | 0.34 | 4.60 | 0.04 | 0.30 | 4.85 | -0.01 |
| 40 | 0.20 | 4.28 | 0.12 | 0.13 | 4.42 | 0.12 |
| 41 | 0.98 | 9.55 | -0.87 | 1.05 | 9.11 | -0.88 |
| 42 | 0.91 | 7.43 | -0.41 | 0.90 | 7.42 | -0.58 |
| 43 | 0.59 | 5.56 | 0.00 | 0.51 | 5.94 | -0.07 |
| 44 | 0.29 | 4.42 | 0.25 | 0.21 | 4.71 | 0.23 |
| 45 | 0.15 | 3.80 | 0.38 | 0.09 | 4.11 | 0.34 |
| 46 | 0.52 | 7.13 | -0.15 | 0.66 | 6.92 | -0.39 |
| 47 | 0.29 | 5.60 | 0.17 | 0.29 | 5.64 | -0.03 |
| 48 | 0.15 | 4.27 | 0.41 | 0.10 | 4.59 | 0.33 |
| 49 | 0.08 | 3.55 | 0.52 | 0.00 | 3.91 | 0.47 |
| 50 | -0.07 | 5.18 | 0.24 | 0.06 | 5.03 | 0.04 |
| 51 | -0.08 | 4.10 | 0.44 | -0.09 | 4.11 | 0.28 |
| 52 | -0.05 | 3.43 | 0.53 | -0.09 | 3.67 | 0.43 |
| 53 | -0.26 | 3.71 | 0.37 | -0.16 | 3.61 | 0.25 |
| 54 | -0.22 | 3.25 | 0.41 | -0.24 | 3.02 | 0.19 |

Table 7.9 - Summary of Turner computed nodal stress averages (refined mesh)

| Node | Turner stress averages (psi) | | | CST stress averages (psi) | | |
|---|---|---|---|---|---|---|
| | Sigma X | Sigma Y | Sigma XY | Sigma X | Sigma Y | Sigma XY |
| 36 | 0.36 | 8.93 | 0.45 | 0.25 | 9.34 | -0.29 |
| 37 | 0.61 | 6.68 | -0.38 | 0.67 | 7.22 | -0.45 |
| 38 | 0.60 | 5.41 | -0.17 | 0.55 | 5.61 | -0.29 |
| 39 | 0.34 | 4.60 | 0.04 | 0.32 | 4.77 | -0.15 |
| 40 | 0.20 | 4.28 | 0.12 | 0.07 | 4.37 | -0.06 |
| 41 | 0.98 | 9.55 | -0.87 | 1.08 | 10.22 | -0.95 |
| 42 | 0.91 | 7.43 | -0.41 | 0.91 | 7.89 | -0.04 |
| 43 | 0.59 | 5.56 | 0.00 | 0.62 | 5.89 | -0.03 |
| 44 | 0.29 | 4.42 | 0.25 | 0.32 | 4.64 | 0.29 |
| 45 | 0.15 | 3.80 | 0.38 | 0.10 | 4.07 | 0.31 |
| 46 | 0.52 | 7.13 | -0.15 | 0.66 | 7.78 | -0.28 |
| 47 | 0.29 | 5.60 | 0.17 | 0.34 | 6.08 | 0.09 |
| 48 | 0.15 | 4.27 | 0.41 | 0.20 | 4.67 | 0.35 |
| 49 | 0.08 | 3.55 | 0.52 | 0.04 | 3.88 | 0.56 |
| 50 | -0.07 | 5.18 | 0.24 | 0.02 | 5.58 | 0.11 |
| 51 | -0.08 | 4.10 | 0.44 | -0.06 | 4.42 | 0.33 |
| 52 | -0.05 | 3.43 | 0.53 | -0.03 | 3.65 | 0.40 |
| 53 | -0.26 | 3.71 | 0.37 | -0.28 | 3.87 | 0.31 |
| 54 | -0.22 | 3.25 | 0.41 | -0.13 | 3.33 | 0.23 |

Table 7.10 - Natural frequencies of the Turner wing

| | Natural Frequency (Hz) | | |
|---|---|---|---|
| Mode | Original CST model | Refined CST model | ELFINI |
| 1 | 120 | 119 | 116 |
| 2 | 337 | 327 | 318 |
| 3 | 419 | 411 | 418 |
| 4 | 602 | 540 | 577 |
| 5 | 1107 | 687 | 1086 |

Table 7.11 - Dummy thickness effect on Turner displacements and natural frequencies

| | Natural Frequencies (Hz) | | | | |
|---|---|---|---|---|---|
| Mode | Original CST model | Refined CST models (1%) | (5%) | (10%) | ELFINI |
| 1 | 120 | 119 | 119 | 119 | 116 |
| 2 | 337 | 327 | 327 | 326 | 318 |
| 3 | 419 | 411 | 426 | 429 | 418 |
| 4 | 602 | 540 | 593 | 599 | 577 |
| 5 | 1107 | 687 | 1074 | 1130 | 1076 |
| Load point displacement ($10^{-3}$ in.) | 0.216 | 0.219 | 0.218 | 0.217 | N/A |

Increased thicknesses result in increased natural frequency accuracy with an insignificant decrease in tip displacement. The study's effect on element stresses can be seen in Figures 7.32 and 7.33. Figure 7.32 details the change in leading and trailing edge cap stresses for an increase in dummy membrane thickness while Figure 7.33 shows the change in CST element stresses $\sigma_{xx}$ and $\sigma_{yy}$ along line $B_2$. Again, increased dummy element thicknesses have a minimal effect on both cap and membrane stresses. Subsequently, a good rule of thumb is to use dummy elements with a thickness of between 5% and 10% of what the actual structure requires only if accurate natural frequency / mode shape information is desired.

Stress smoothing was again employed for each CST wing model, with finite element stress results available from ELFINI. For each stress, a polynomial was found at each cut A and $B_1/B_2$ (Figures 7.28 and 7.29) for both the basic CST model and the LST model while being compared to ELFINI results and the CST model's smoothed stresses. Numerical details of the various curve fitting polynomials for each wing mesh are in Tables 7.12 and 7.13, but with a polynomial order of N=4 having been previously established, this degree will be used for all subsequent stress comparisons. Plots are shown in Figures 7.34 through 7.39. Note the linear, piecewise continuous nature of the LST model's stresses along each cut. Additionally, the ELFINI stress results can be seen in Figures 7.40 through 7.42 for each stress.

Good agreement with ELFINI for all models can easily be seen for $\sigma_{yy}$ along with excellent curve fits at each cut. Along cut A, reasonable accuracy in both the element stresses and the N=4 stress polynomial is obtained for $\sigma_{xx}$ while poor accuracy between ELFINI and stress smoothing results exist for $\sigma_{xy}$. It is also worth noting the decrease in accuracy as one nears the trailing edge root location (100% chord). Along spanwise cuts $B_1/B_2$, the N=4 curve fit and element stresses are better for $\sigma_{xy}$ but this time $\sigma_{xx}$ ELFINI results and stress results are quite different. In general, good agreement exists between the

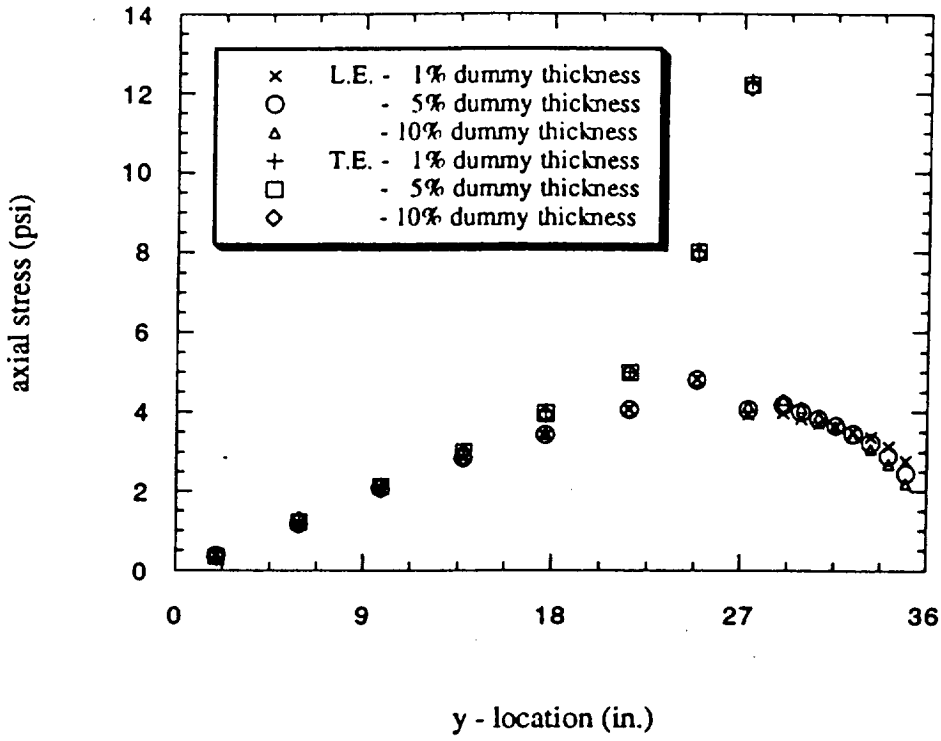


Figure 7.32 - Dummy thickness effect on Turner cap stresses

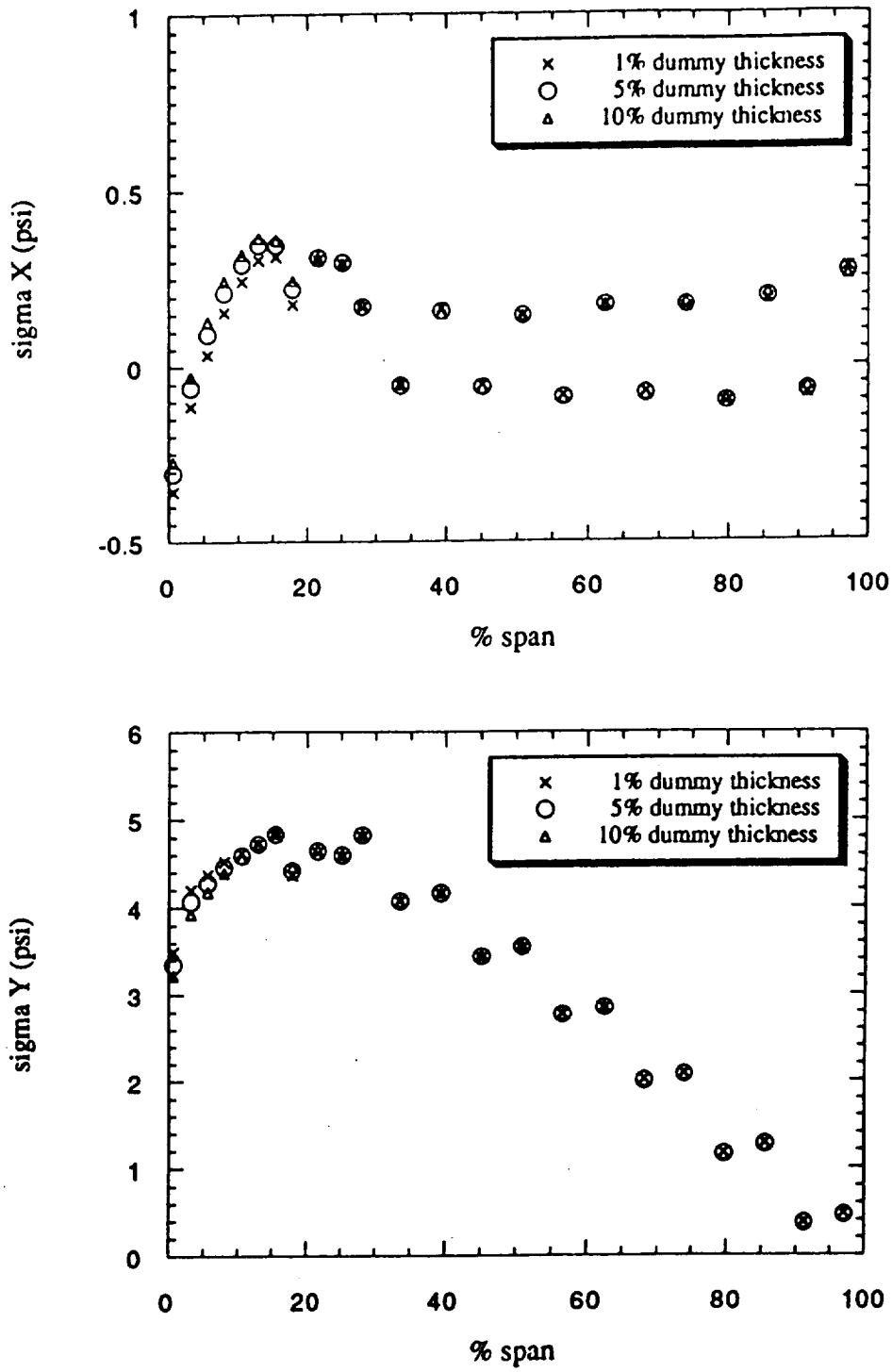


Figure 7.33 - Dummy thickness effect on Turner membrane stresses along line $B_2$

Table 7.12 - Turner stress smoothing polynomials (original CST mesh)

Sigma X:

N=2 $S = 0.04528 + 0.04588x - 0.003832y - 0.0019x^2 - 0.003465xy + 0.0009846y^2$

N=3 $S = 0.6845 - 0.03744x - 0.1511y + 0.00983x^2 + 0.004395xy + 0.008456y^2 - 0.001147x^3 + 0.0006225x^2y - 0.0004522xy^2 - 0.00008472y^3$

N=4 $S = 0.908 - 0.4852x - 0.07524y + 0.1462x^2 + 0.01168xy - 0.000891y^2 - 0.01702x^3 - 0.001019x^2y - 0.0001546xy^2 + 0.0002379y^3 + 0.0006553x^4 + 0.0x^3y + 0.00005336x^2y^2 - 0.0000195xy^3 - 0.000002632y^4$

N=5 $S = 1.534 - 1.709x - 0.08587y + 0.9185x^2 - 0.1164xy + 0.02993y^2 - 0.1907x^3 + 0.01492x^2y + 0.007555xy^2 - 0.002937y^3 + 0.01719x^4 - 0.000755x^3y - 0.000653x^2y^2 - 0.0001503xy^3 + 0.000107y^4 - 0.0005716x^5 + 0.000033x^4y - 0.000004953x^3y^2 + 0.00001668x^2y^3 - 0.000001182xy^4 - 0.000001176y^5$

Sigma Y:

N=2 $S = -1.1 + 0.0166x + 0.4174y + 0.01546x^2 - 0.0238xy - 0.002058y^2$

N=3 $S = 0.6766 - 0.1821x - 0.02451y + 0.06061x^2 - 0.007962xy + 0.02102y^2 - 0.004979x^3 + 0.002886x^2y - 0.001505xy^2 - 0.0002467y^3$

N=4 $S = 0.9147 - 0.979x + 0.2071y + 0.3286x^2 + 0.01566xy - 0.01273y^2 - 0.044x^3 + 0.004483x^2y - 0.002706xy^2 + 0.001263y^3 + 0.001983x^4 - 0.0005238x^3y + 0.0002468x^2y^2 - 0.00003682xy^3 - 0.0000182y^4$

N=5 $S = 1.854 - 3.575x + 0.5373y + 1.824x^2 - 0.1196xy - 0.03281y^2 - 0.388x^3 + 0.02312x^2y + 0.00878xy^2 + 0.0005012y^3 + 0.03721x^4 - 0.004233x^3y + 0.000665x^2y^2 - 0.0005914xy^3 + 0.00006662y^4 - 0.00132x^5 + 0.000253x^4y - 0.00007632x^3y^2 + 0.00001977x^2y^3 + 0.000004684xy^4 - 0.000001425y^5$

Tau XY:

N=2 $S = -1.592 + 0.07176x + 0.0341y + 0.006499x^2 - 0.008611xy + 0.001713y^2$

N=3 $S = -0.9605 + 0.0574x - 0.1024y - 0.01467x^2 + 0.009038xy + 0.006647y^2 + 0.001343x^3 - 0.00002344x^2y - 0.0005146xy^2 - 0.00002641y^3$

N=4 $S = -1.064 - 0.04879x + 0.03493y - 0.03781x^2 + 0.03417xy - 0.01263y^2 + 0.009817x^3 - 0.005126x^2y - 0.0002034xy^2 + 0.0007198y^3 - 0.0004908x^4 + 0.0001609x^3y + 0.00007006x^2y^2 - 0.00002309xy^3 - 0.00000845y^4$

N=5 $S = -2.28 + 0.944x + 0.371y - 0.423x^2 - 0.06124xy - 0.0476y^2 + 0.08784x^3 - 0.00114x^2y + 0.008833xy^2 + 0.001904y^3 - 0.007789x^4 + 0.0003322x^3y - 0.000295x^2y^2 - 0.0003157xy^3 - 0.0000147y^4 + 0.00025x^5 - 0.00000504x^4y - 0.000003095x^3y^2 + 0.000008086x^2y^3 + 0.000002909xy^4 - 0.0000001938y^5$

Table 7.13 - Turner stress smoothing polynomials (refined CST mesh)

Sigma X:

N=2 $S = -0.039 + 0.06141x + 0.002043y - 0.002725x^2 - 0.003556xy + 0.0008221y^2$

N=3 $S = 0.5111 + 0.1366x - 0.1681y - 0.02271x^2 + 0.003742xy + 0.00983y^2 + 0.0006101x^3 + 0.0005858x^2y - 0.0004033xy^2 - 0.0001182y^3$

N=4 $S = 0.501 - 0.02049x - 0.07597y - 0.001607x^2 + 0.01968xy - 0.00351y^2 + 0.000373x^3 - 0.001673x^2y - 0.0005401xy^2 + 0.0004465y^3 - 0.00003432x^4 + 0.00003975x^3y + 0.00004602x^2y^2 - 0.000007925xy^3 - 0.000007251y^4$

N=5 $S = 0.1862 + 0.1011x - 0.06611y + 0.1174x^2 - 0.1133xy + 0.02747y^2 - 0.03218x^3 + 0.008646x^2y + 0.009438xy^2 - 0.0031y^3 + 0.002985x^4 + 0.000123x^3y - 0.0006824x^2y^2 - 0.000238xy^3 + 0.0001248y^4 - 0.0000922x^5 - 0.0000079x^4y + 0.0x^3y^2 + 0.0000145x^2y^3 + 0.00000079xy^4 - 0.00000159y^5$

Sigma Y:

N=2 $S = -1.239 + 0.04716x + 0.4226y + 0.01422x^2 - 0.02482xy - 0.00193y^2$

N=3 $S = 0.4089 + 0.1094x - 0.03197y - 0.005225x^2 - 0.001642xy + 0.01977y^2 - 0.001089x^3 + 0.002496x^2y - 0.001543xy^2 - 0.0002065y^3$

N=4 $S = 0.3438 - 0.1477x + 0.1505y + 0.03614x^2 + 0.03247xy - 0.007506y^2 - 0.005673x^3 - 0.00005743x^2y - 0.002126xy^2 + 0.0009176y^3 + 0.0003089x^4 - 0.0002046x^3y + 0.0001907x^2y^2 - 0.00003542xy^3 - 0.00001229y^4$

N=5 $S = 0.02015 - 0.626x + 0.4174y + 0.395x^2 - 0.04725xy - 0.0265y^2 - 0.088x^3 + 0.00004231x^2y + 0.008073xy^2 + 0.000368y^3 + 0.0086x^4 - 0.0006335x^3y + 0.000297x^2y^2 - 0.00049xy^3 + 0.00005806y^4 - 0.000307x^5 + 0.0000548x^4y - 0.00002804x^3y^2 + 0.000007519x^2y^3 + 0.000005508xy^4 - 0.000001306y^5$

Tau XY:

N=2 $S = -1.782 + 0.122x + 0.0442y + 0.003449x^2 - 0.009177xy + 0.001441y^2$

N=3 $S = -1.092 + 0.1442x - 0.108y - 0.02863x^2 + 0.009283xy + 0.007144y^2 + 0.002026x^3 - 0.00008864x^2y - 0.0004913xy^2 - 0.00004331y^3$

N=4 $S = -1.237 + 0.02735x - 0.02508y - 0.1311x^2 + 0.03314xy - 0.005875y^2 + 0.01912x^3 - 0.003733x^2y - 0.000557xy^2 + 0.0004753y^3 - 0.0007873x^4 + 0.00007442x^3y + 0.00006826x^2y^2 - 0.00001512xy^3 - 0.000005812y^4$

N=5 $S = -2.327 + 0.8856x + 0.4347y - 0.422x^2 - 0.042xy - 0.06231y^2 + 0.0937x^3 - 0.009295x^2y + 0.009168xy^2 + 0.003004y^3 - 0.008746x^4 + 0.00123x^3y - 0.0002126x^2y^2 - 0.0003394xy^3 - 0.0000504y^4 + 0.00029x^5 - 0.0000345x^4y - 0.00001082x^3y^2 + 0.000008993x^2y^3 + 0.000003068xy^4 + 0.0000002293y^5$

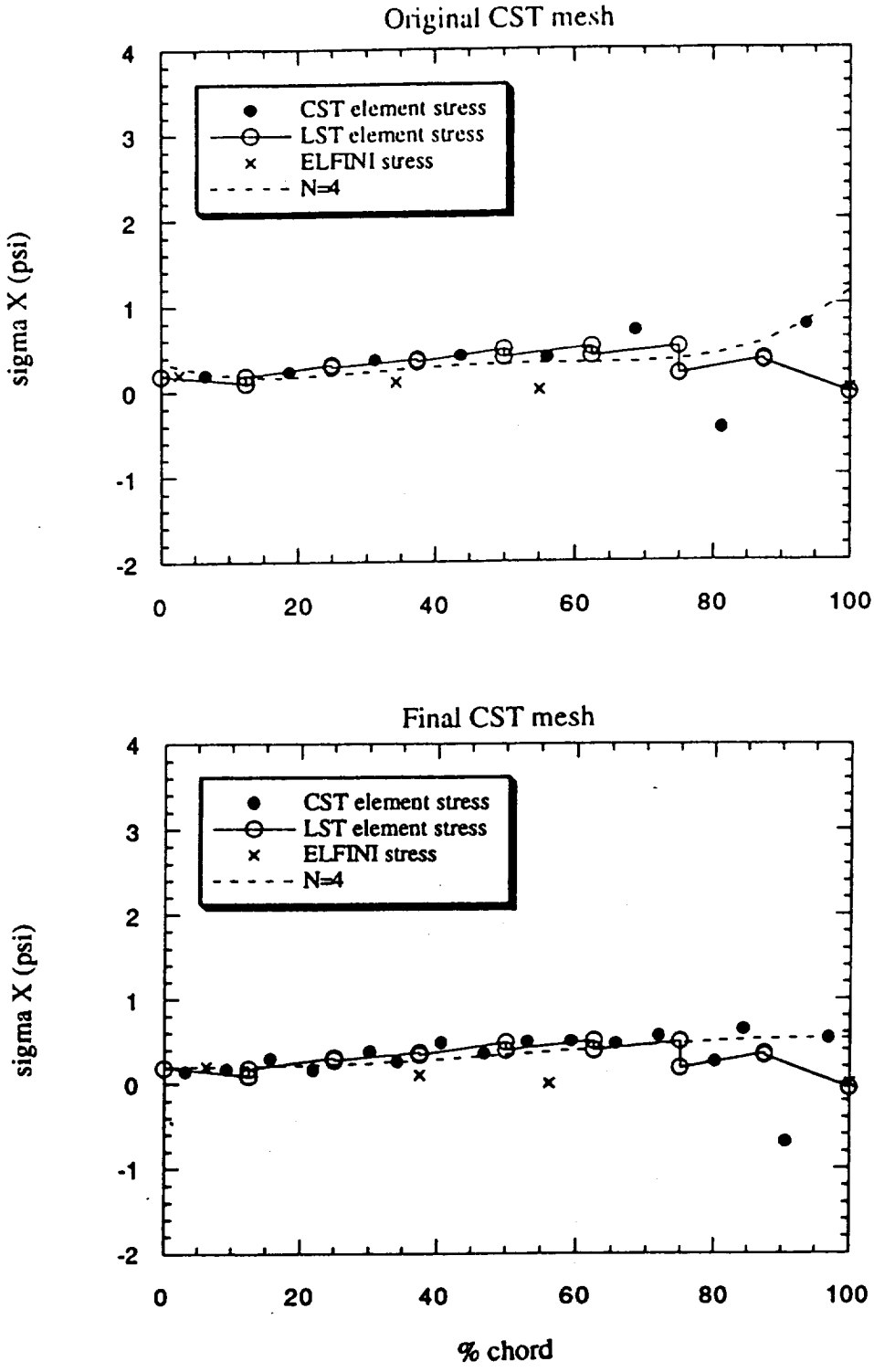


Figure 7.34 - $\sigma_{xx}$ stress smoothing along line A - Turner wing

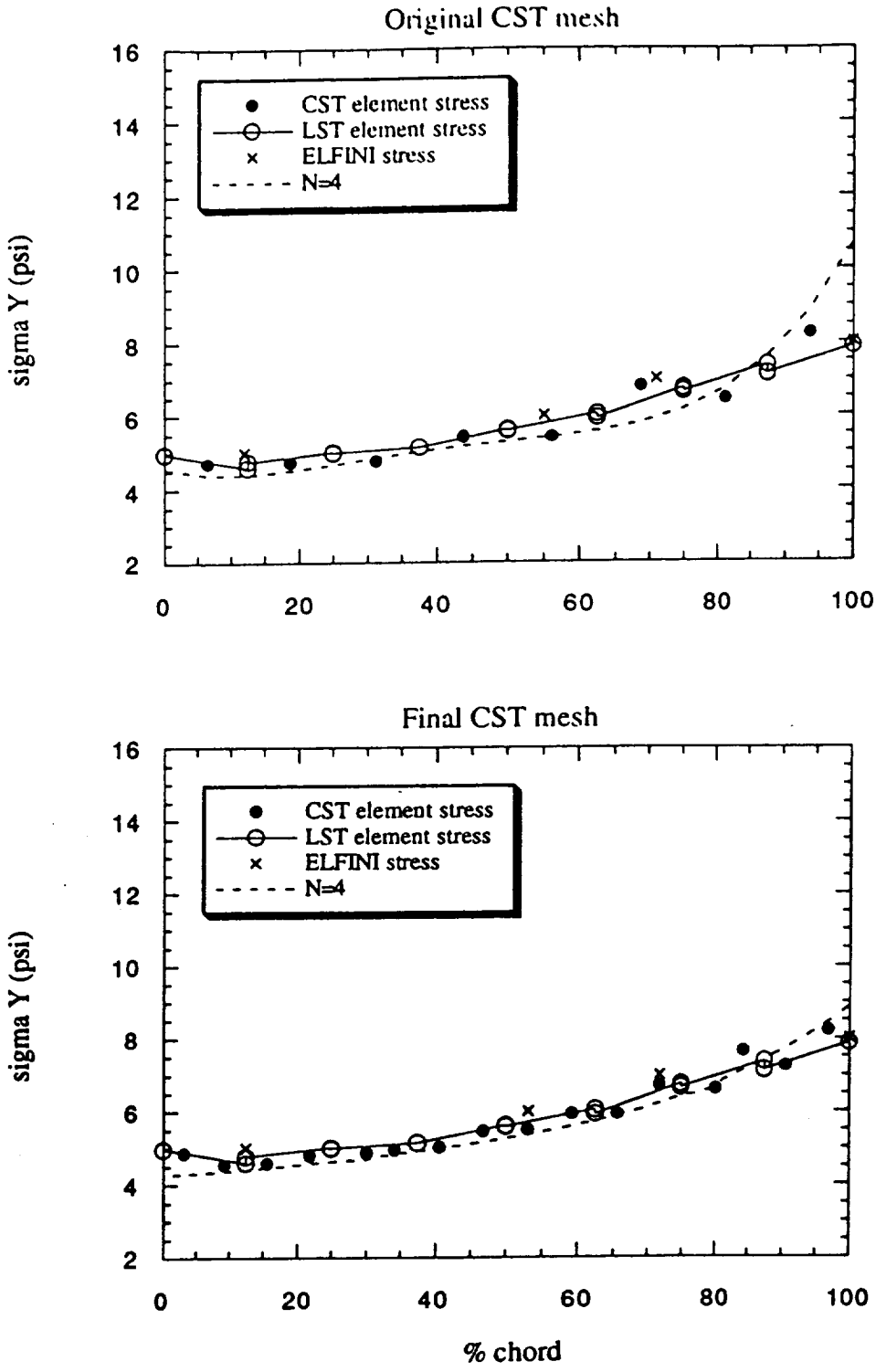


Figure 7.35 - $\sigma_{yy}$ stress smoothing along line A - Turner wing

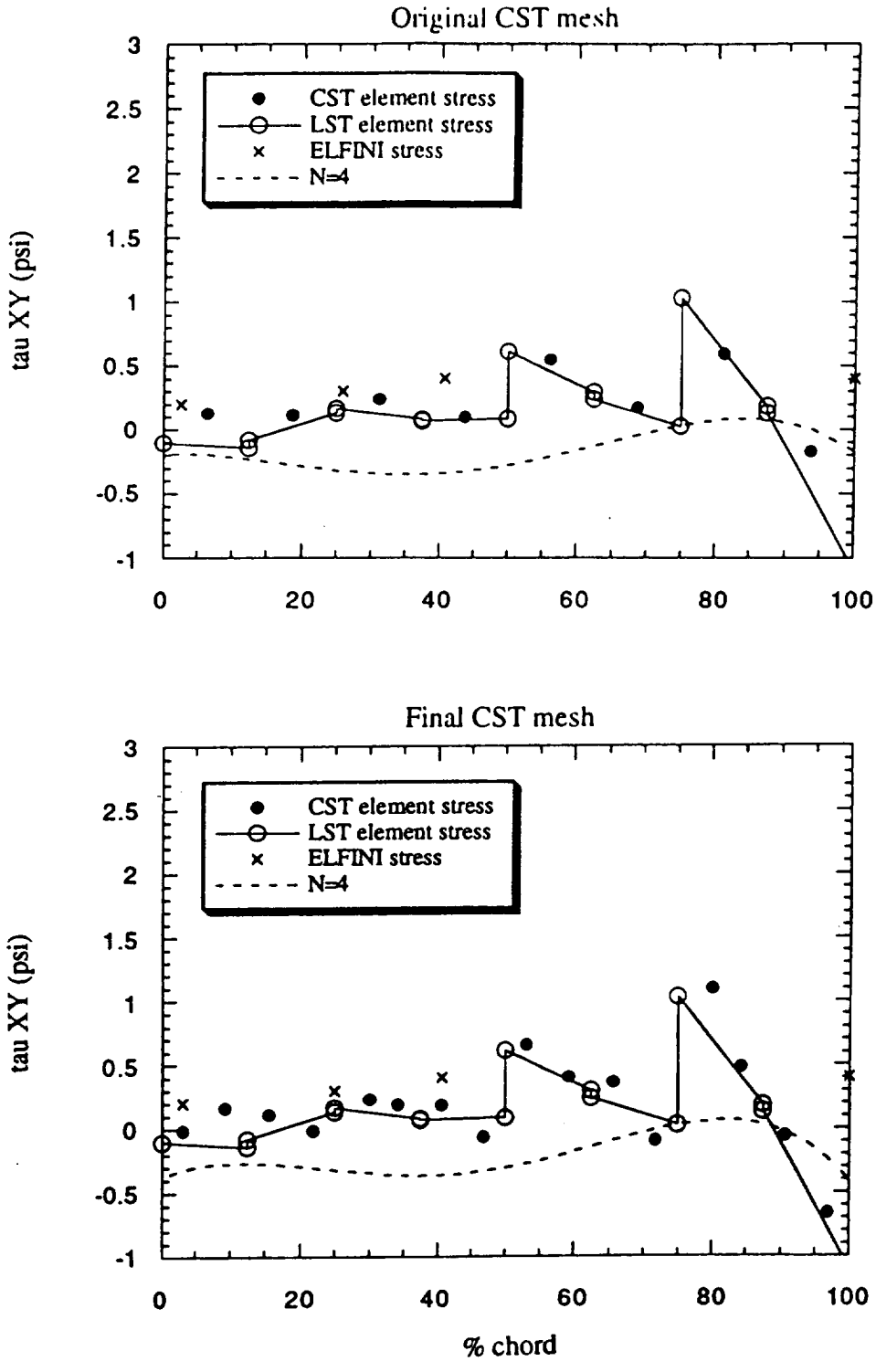


Figure 7.36 - $\sigma_{xy}$ stress smoothing along line A - Turner wing

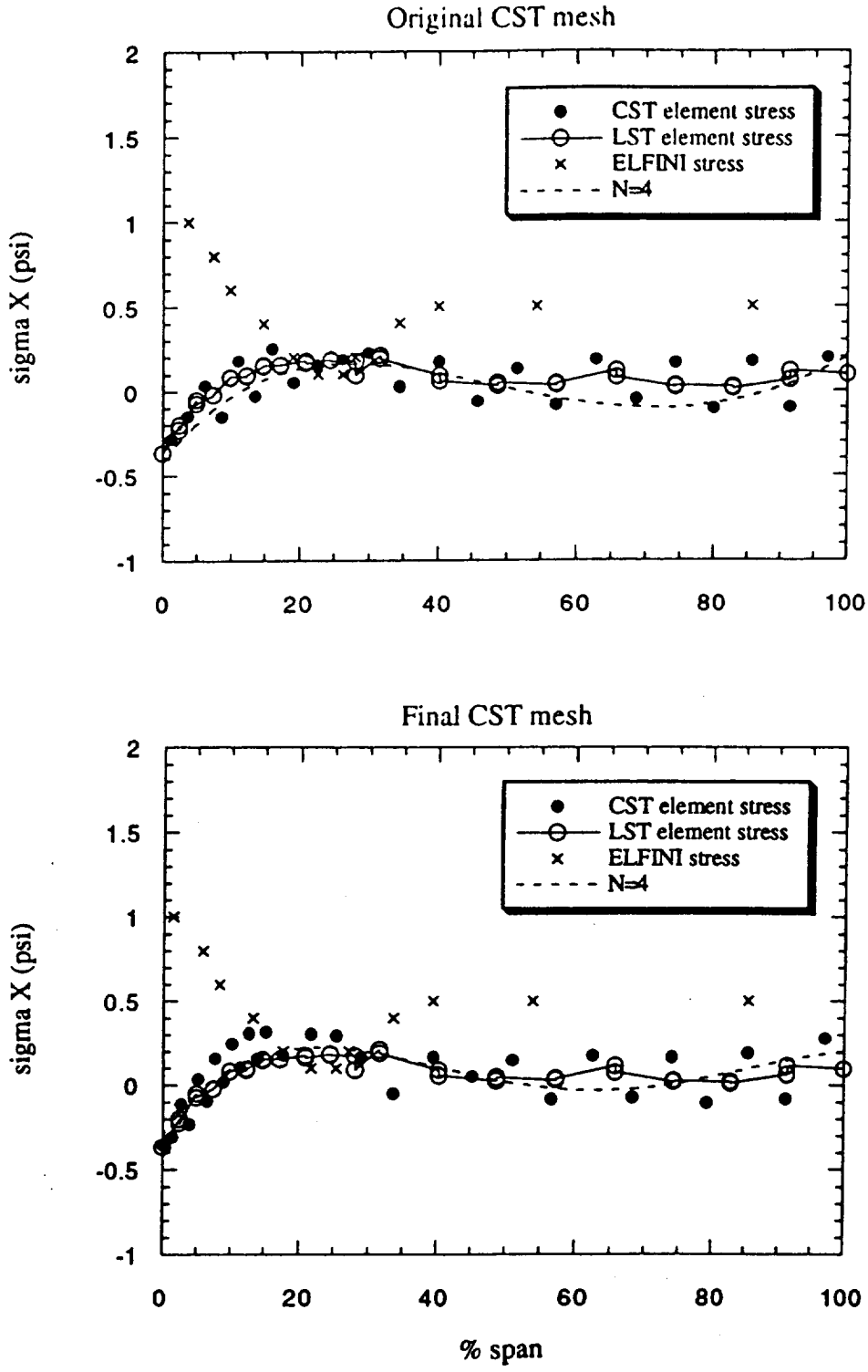


Figure 7.37 - $\sigma_{xx}$ stress smoothing along lines $B_1$ and $B_2$ - Turner wing

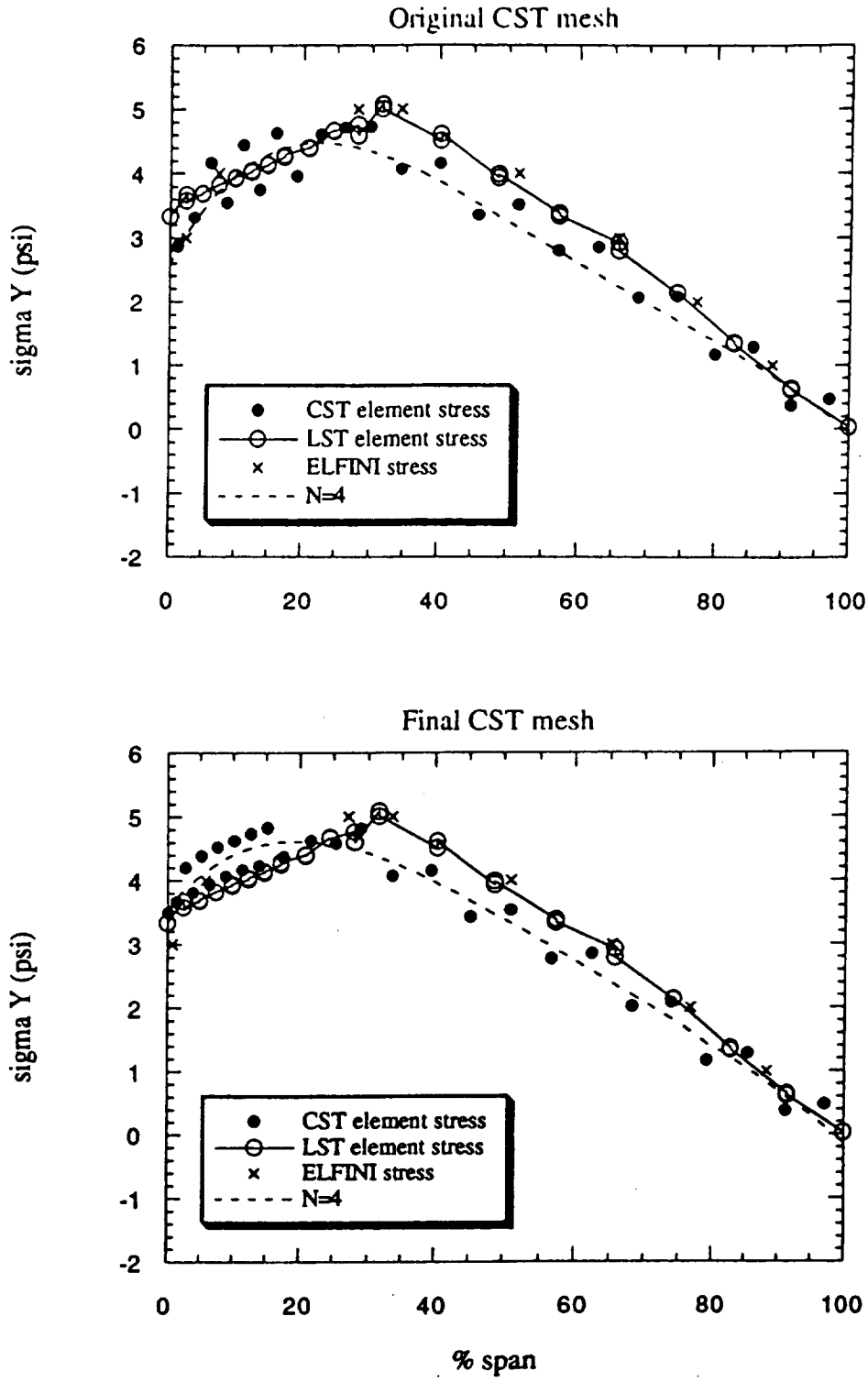


Figure 7.38- $\sigma_{yy}$ stress smoothing along lines $B_1$ and $B_2$ - Turner wing

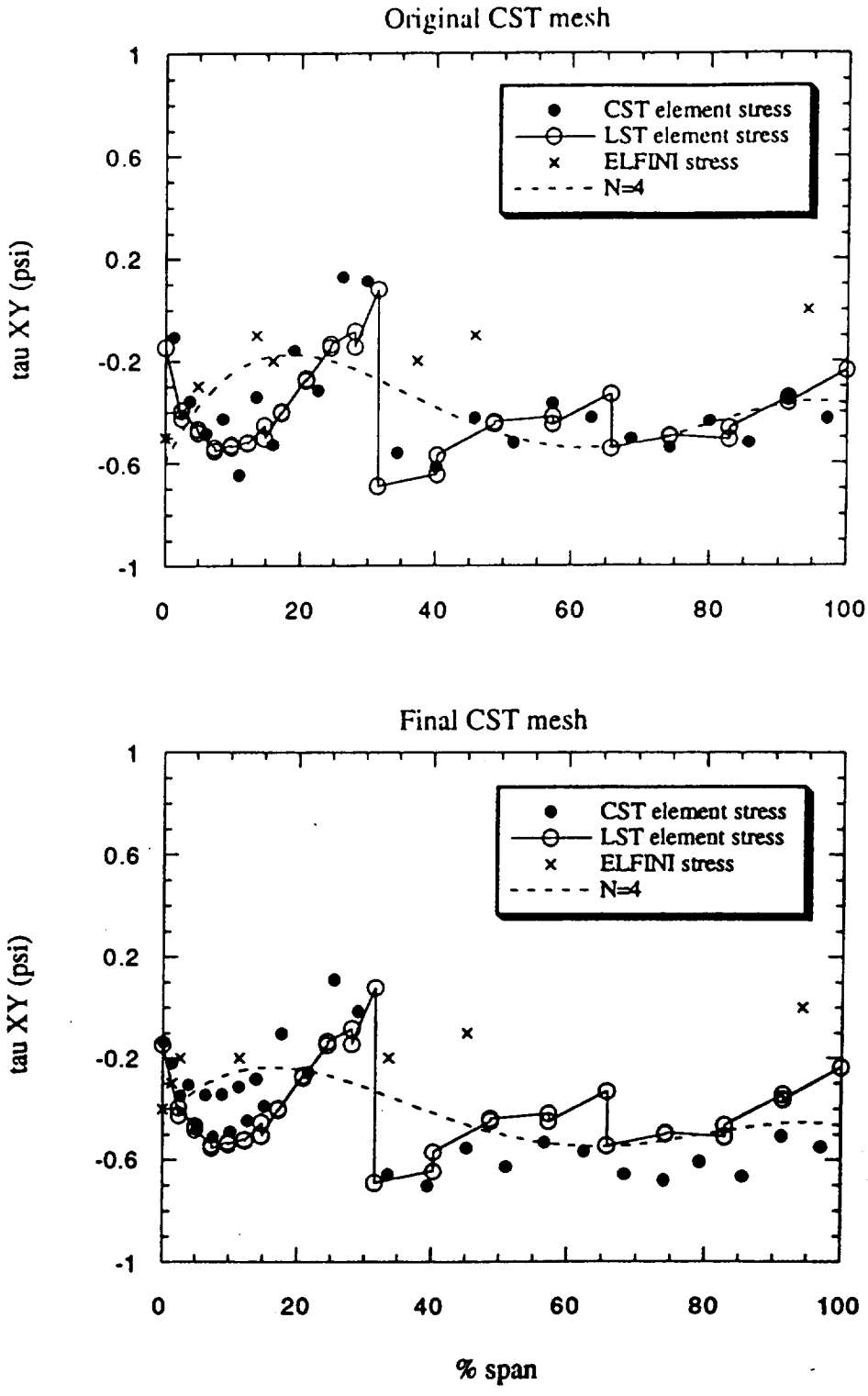


Figure 7.39 - $\sigma_{xy}$ stress smoothing along lines $B_1$ and $B_2$ - Turner wing

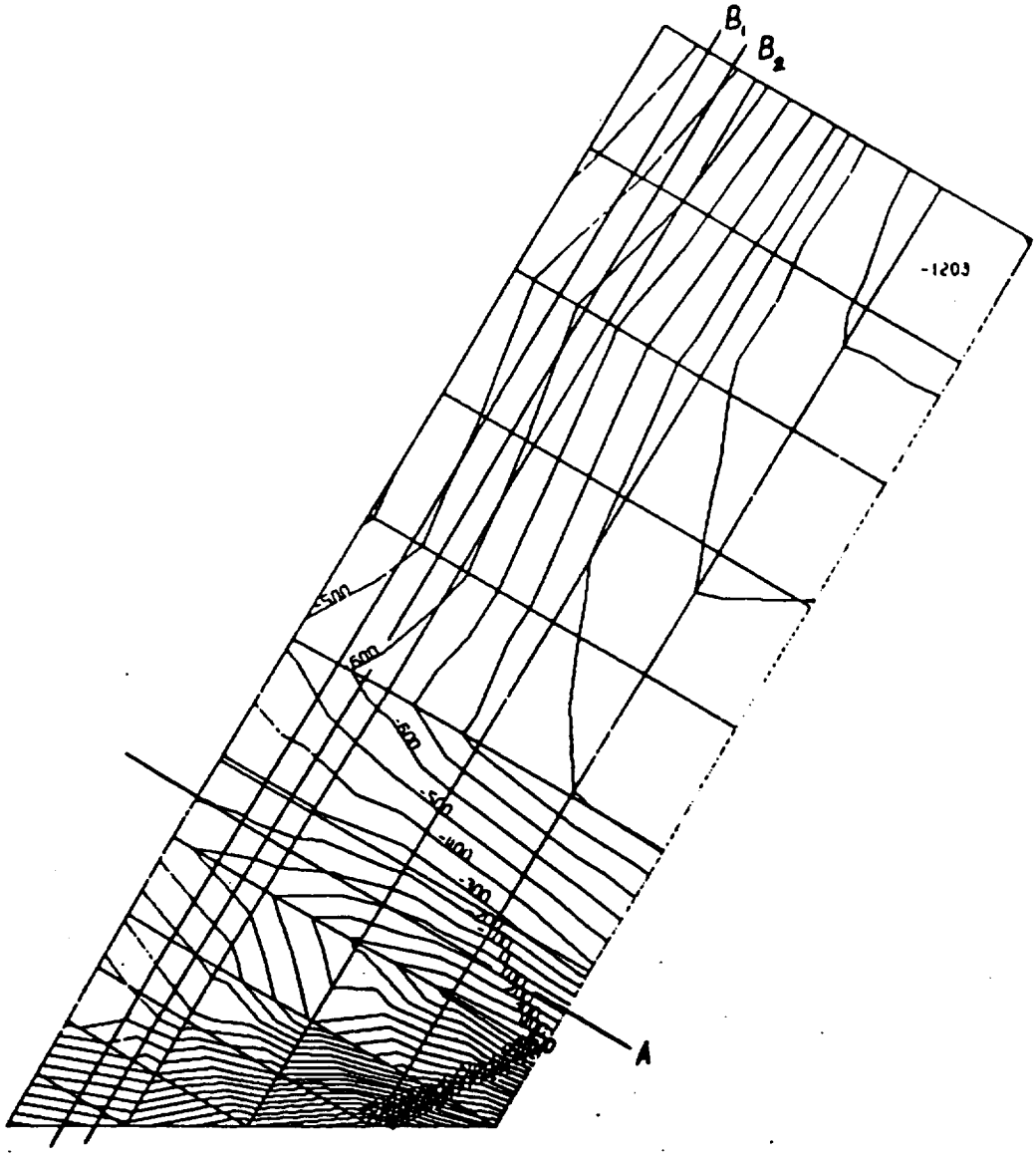


Figure 7.40 - $\sigma_{xx}$ stress contour plot - ELFINI finite element model

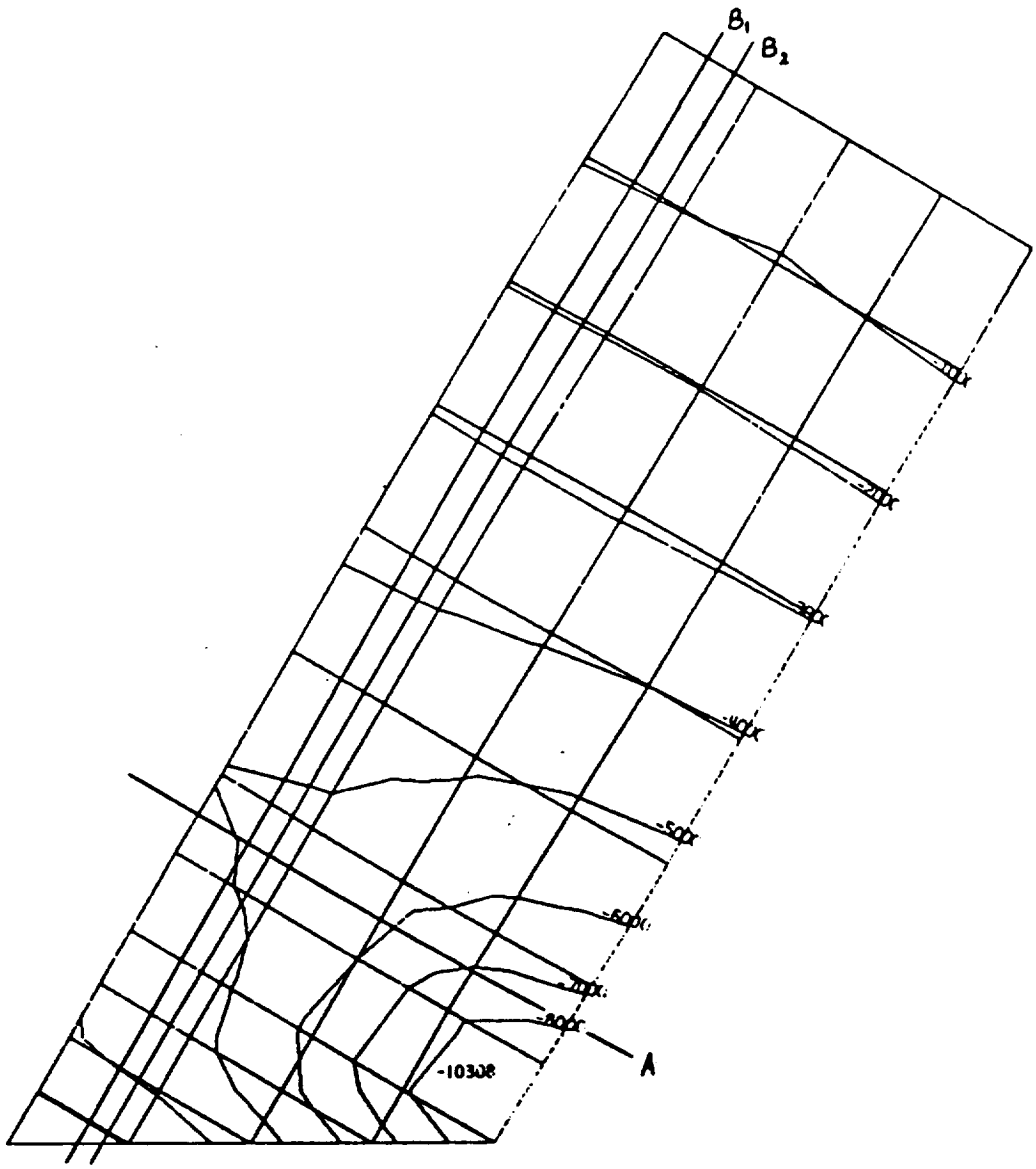


Figure 7.41 - $\sigma_{yy}$ stress contour plot - ELFINI finite element model

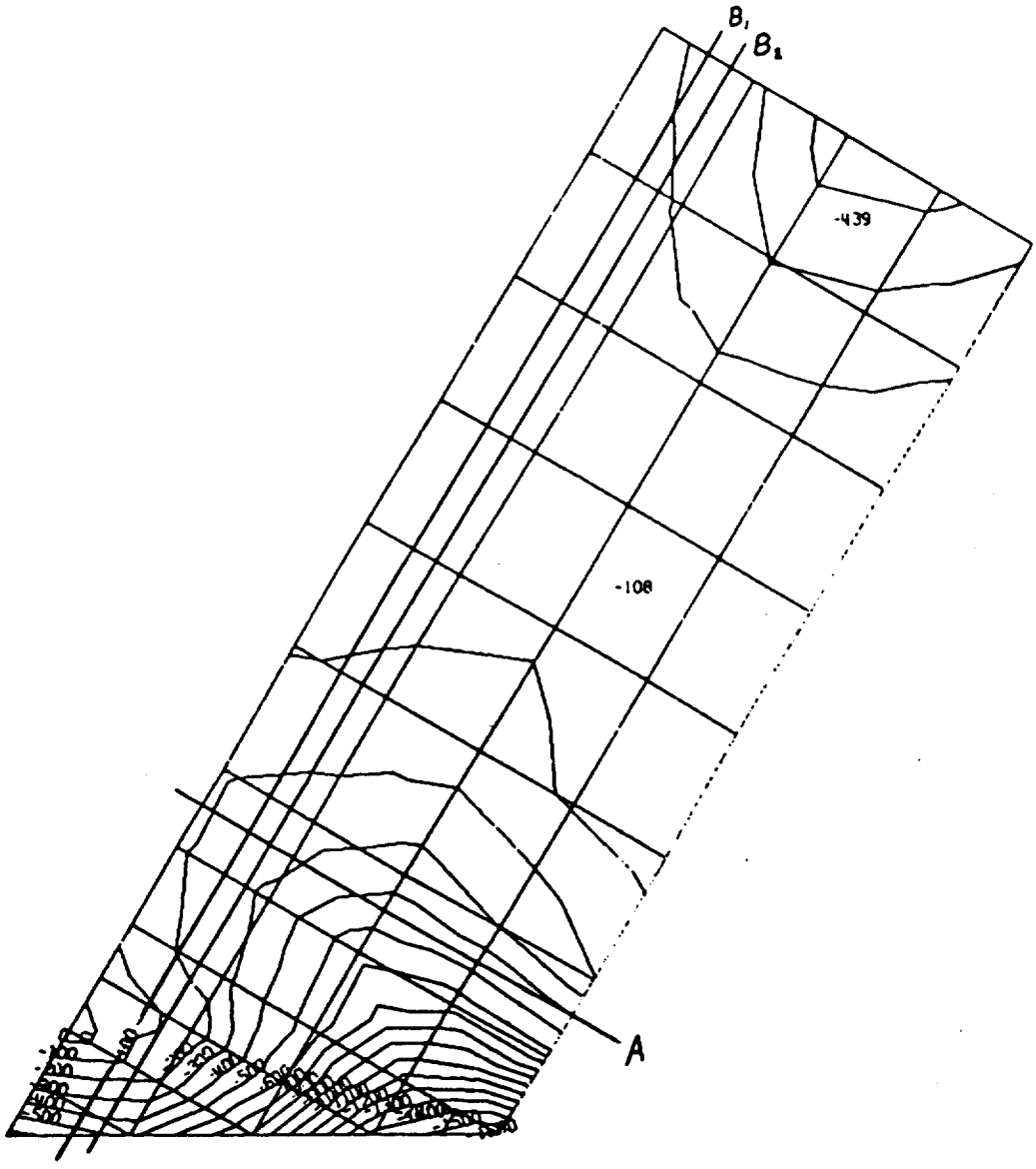


Figure 7.42 - $\sigma_{xy}$ stress contour plot - ELFINI finite element model

point stresses of the CST elements and the linear stresses of the LST elements.

It should be remembered, however, that both $\sigma_{xx}$ and $\sigma_{xy}$ are significantly small as compared with $\sigma_{yy}$. Thus, failure predictions for the Turner wing by the current CST/LST modeling technique and ELFINI as well as test data will all be in good agreement. Also, there is a doubt as to the accuracy of measured $\sigma_{xx}$ and $\sigma_{xy}$ values, and large stress gradients at the root trailing edge are certainly affecting accuracy of these small stresses.

# CHAPTER 8

# ANALYTIC SENSITIVITY RESULTS

## 8.1 Introduction

Analytic sensitivity calculations are checked by corresponding finite difference derivatives. In addition, computational efficiency issues of employing analytic sensitivities versus finite difference sensitivities is evaluated. The wing models of choice for all future discussions are the Gallagher model 1 wing (adrib = 4) and the Denke wing (adrib=2) both having shear web CSTs.

## 8.2 Analytic sensitivities vs. finite difference sensitivities

With respect to finite difference methods, the expression

$$\frac{\partial x}{\partial v} \equiv \frac{\Delta x}{\Delta v} = \frac{x_2 - x_1}{v_2 - v_1} \tag{8-1}$$

describes the derivative of any behavior function 'x' with respect to a change in any variable 'v.' For large perturbations in 'v,' truncation error results in inaccurate derivatives due to it being a first order approximation, while theoretically as $\Delta v$ approaches zero, the approximation becomes exact. Realistically, this process introduces round-off errors due to computer finite length representation of numbers (Ref. 1).

As an example of shape design variable sensitivity, the Gallagher model under a uniform load and it's perturbed version with respect to both $x_{FR}$ and $y_R$ are compared. The analytic sensitivities of the vertical displacement at the trailing edge tip, the first natural frequency, the leading edge root cap stress and the spanwise plane stress $\sigma_{yy}$ in the CST

leading edge wing skin root element are calculated. In using finite differences, perturbations of 0.001% to 0.1% of the characteristic dimension (chord length for $x_{FR}$ and span length for $y_R$) are used. The results are found in Tables 8.1 and 8.2. The Denke wing model under a 100 lb. trailing edge tip load is tested in the exact same fashion as above. Results are shown in Tables 8.3 and 8.4. Since the program is written in double precision, round-off errors in the finite difference scheme for small perturbations do not show for the range analyzed. For larger perturbations, truncation error explains any discrepancies. The analytic sensitivities are seen to be in complete agreement.

As an example of sizing design variable sensitivity, the Gallagher model is used and the same sensitivities are sought, this time with respect to the cross-sectional area of the leading edge spar cap element. Table 8.5 shows the results. Again, the same performance as detailed for the shape sensitivities is achieved.

To further exhibit the accuracy of the Gallagher model's analytic sensitivities, a comparison between those found from the best CST model (adrib = 5) and those from the LST model is shown in Table 8.6. Since the maximum deflections differ by 6.7%, it can be assumed that all sensitivities would yield closer results if each wing model's deflection behavior were more similar.

A parametric study to assess the usefulness of analytic sensitivities for future optimization usage is performed using the Gallagher model 1 wing under a 100 lb. trailing edge tip load. Shape variable $x_{FR}$ is incrementally perturbed to alter the wing planform. The trailing edge tip vertical displacement, the second natural frequency, the trailing edge root cap stress and the spanwise plane stress $\sigma_{yy}$ for a centrally located CST wing skin element are plotted versus $x_{FR}$ in Figure 8.1. First order Taylor series representations for each output are obtained from

Table 8.1 - Analytic vs. finite difference $x_{FR}$ sensitivities - Gallagher CST model 1

Shape design variable: leading edge wing tip x-location ($x_{FR}$)

| Output Parameter | Analytic Sensitivity | Finite Difference Sensitivity | | |
|---|---|---|---|---|
| | | design variable perturbation | | |
| | | .001chord | .01chord | .1chord |
| trailing edge tip displacement (in. / in.) | 0.0206 | 0.0206 | 0.0207 | 0.0213 |
| 1st natural frequency (Hz. / in.) | 0.991 | 0.991 | 0.994 | 1.023 |
| leading edge root cap stress (psi / in.) | -269.69 | -269.33 | -269.87 | -271.61 |
| leading edge root wingskin sigma Y (psi / in.) | -697.16 | -697.33 | -697.13 | -696.03 |

Table 8.2 - Analytic vs. finite difference $y_R$ sensitivities - Gallagher CST model 1

Shape design variable: wing tip y-location ($y_R$)

| Output Parameter | Analytic Sensitivity | Finite Difference Sensitivity | | |
|---|---|---|---|---|
| | | design variable perturbation | | |
| | | .001span | .01span | .1span |
| trailing edge tip displacement (in. / in.) | 0.1082 | 0.1083 | 0.1091 | 0.1173 |
| 1st natural frequency (Hz. / in.) | -3.68 | -3.68 | -3.63 | -3.21 |
| leading edge root cap stress (psi / in.) | 537.16 | 537.12 | 535.49 | 520.00 |
| leading edge root wingskin sigma Y (psi / in.) | 590.29 | 589.99 | 588.44 | 571.43 |

Table 8.3 - Analytic vs. finite difference $x_{FR}$ sensitivities - Denke CST model

Shape design variable: leading edge wing tip x-location ($x_{FR}$)

| Output Parameter | Analytic Sensitivity | Finite Difference Sensitivity | | |
|---|---|---|---|---|
| | | design variable perturbation | | |
| | | .001chord | .01chord | .1chord |
| trailing edge tip displacement (in. / in.) | $7.798 \times 10^{-6}$ | $7.830 \times 10^{-6}$ | $8.250 \times 10^{-6}$ | $9.081 \times 10^{-6}$ |
| 1st natural frequency (Hz. / in.) | $1.617 \times 10^{-3}$ | $1.567 \times 10^{-3}$ | $1.129 \times 10^{-3}$ | $0.253 \times 10^{-3}$ |
| leading edge root cap stress (psi / in.) | 0.180 | 0.180 | 0.176 | 0.139 |
| leading edge root wingskin sigma Y (psi / in.) | 0.667 | 0.667 | 0.660 | 0.616 |

Table 8.4 - Analytic vs. finite difference $y_R$ sensitivities - Denke CST model

Shape design variable: wing tip y-location ($y_R$)

| Output Parameter | Analytic Sensitivity | Finite Difference Sensitivity | | |
|---|---|---|---|---|
| | | design variable perturbation | | |
| | | .001span | .01span | .1span |
| trailing edge tip displacement (in. / in.) | $1.082 \times 10^{-3}$ | $1.083 \times 10^{-3}$ | $1.089 \times 10^{-3}$ | $1.155 \times 10^{-3}$ |
| 1st natural frequency (Hz. / in.) | -1.61 | -1.61 | -1.60 | -1.53 |
| leading edge root cap stress (psi / in.) | 8.32 | 8.32 | 8.33 | 8.40 |
| leading edge root wingskin sigma Y (psi / in.) | 5.63 | 5.64 | 5.65 | 5.85 |

Table 8.5 - Analytic vs. finite difference $A_1$ sensitivities - Gallagher CST model 1

Shape design variable: leading edge root cap area ($A_1$)

| Output Parameter | Analytic Sensitivity | Finite Difference Sensitivity | | |
|---|---|---|---|---|
| | | design variable perturbation | | |
| | | $.001A_1$ | $.01A_1$ | $.1A_1$ |
| trailing edge tip displacement (in. / in.$^2$) | -0.0716 | -0.0716 | -0.0716 | -0.0709 |
| 1st natural frequency (Hz. / in.$^2$) | 2.65 | 2.65 | 2.65 | 2.63 |
| leading edge root cap stress (psi / in.$^2$) | 19152.7 | 19150.7 | 19134.2 | 18970.2 |
| leading edge root wingskin sigma Y (psi / in.$^2$) | 21046.9 | 21044.8 | 21026.6 | 20846.4 |

Table 8.6 - CST vs. LST analytic shape sensitivities - Gallagher CST model 1

Output parameter: trailing edge wing tip z-displacement

CST nodal displacement = 1.253 in.

LST nodal displacement = 1.343 in. (6.7 % difference)

| Design variable | Analytic Sensitivity | | Percent difference |
|---|---|---|---|
| | CST model | LST model | |
| $x_{FL}$ | 0.044846 | 0.049825 | 9.99 |
| $x_{AL}$ | -0.057923 | -0.064331 | 9.96 |
| $x_{FR}$ | 0.022222 | 0.025040 | 11.25 |
| $x_{AR}$ | -0.009145 | -0.010533 | 13.18 |
| $y_R$ | -0.115513 | -.127102 | 9.12 |
| $y_R$ | 0.115513 | 0.127102 | 9.12 |
| $\alpha$ | 0.392320 | 0.399118 | 1.70 |

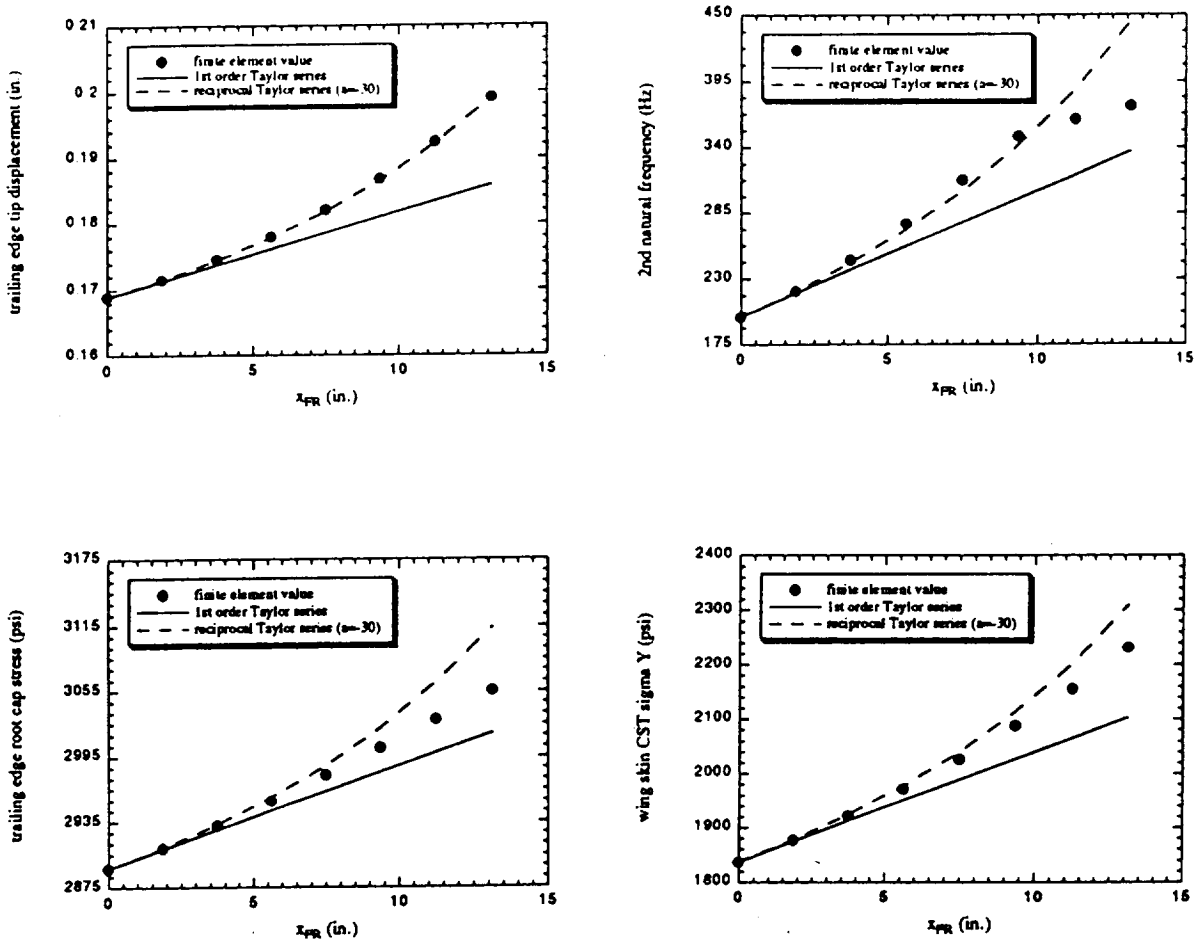


Figure 8.1 - $X_{FR}$ parametric study - Gallagher CST model 1

$$f(x_{FR}) \approx f(x_{FR}|_0) + \left.\frac{\partial f(x_{FR})}{\partial x_{FR}}\right|_0 (x_{FR} - x_{FR}|_0) \tag{8-2}$$

and also plotted. Here, $x_{FR}|_0$ is the original value of $x_{FR}$ and $f(x_{FR}|_0)$ is the value of any parameter. Additionally, reciprocal first order Taylor series approximations (Ref. 1) are calculated from

$$f(x_{FR}) \approx f(x_{FR}|_0) - (x_{FR}|_0 + a)^2 \left.\frac{\partial f(x_{FR})}{\partial x_{FR}}\right|_0 \left(\frac{1}{x_{FR}+a} - \frac{1}{x_{FR}|_0 + a}\right) \tag{8-3}$$

Here, 'a' is an offset variable to allow for our $x_{FR}|_0 = 0$ case. Figure 8.1 shows the reciprocal approximation when a=-30. As can be seen, first order approximations to the non-linear data yield good accuracy for relatively large perturbations in $x_{FR}$.

### 8.3 Computation time assessment

The Gallagher model 1 wing is used for evaluation of CPU time required for analytic sensitivity calculation. A CPU breakdown of each section of the finite element program is shown in Table 8.7 with an explanation as follows. Static solution time includes solving for every degree of freedom's displacements and all finite element stresses. Dynamic solution time includes computing all natural frequencies and mode shapes (equal to the number of degrees of freedom). Design variable sensitivity time includes calculating all displacement, element stress and natural frequency sensitivities with respect to any single shape or size type variable.

In looking at the model with four divisions per section, it can be seen that the total CPU time to compute the model's displacements, stresses, natural frequencies and mode shapes is 271.811 seconds, with either an additional 14.503 seconds to calculate one set of

Table 8.7 - Finite element code CPU breakdown - Gallagher CST model 1

CPU seconds / module

| Program module | Number of dummy ribs per section | | | | |
|---|---|---|---|---|---|
| | 0 | 1 | 2 | 3 | 4 |
| degrees of freedom | 90 | 180 | 270 | 360 | 450 |
| finite elements | 156 | 264 | 420 | 552 | 684 |
| program initialization | 0.100 | 0.152 | 0.227 | 0.316 | 0.363 |
| form global stiffness and mass matrices | 0.098 | 0.176 | 0.316 | 0.426 | 0.496 |
| static solution: | | | | | |
| * displacements | 0.113 | 0.855 | 2.656 | 6.020 | 11.402 |
| * stresses | 0.016 | 0.031 | 0.051 | 0.062 | 0.074 |
| dynamic solution: | | | | | |
| * natural frequencies and mode shapes | 3.527 | 20.065 | 60.336 | 138.784 | 259.476 |
| shape variable sensitivity: | | | | | |
| * w.r.t. one variable | 2.695 | 4.883 | 8.277 | 11.292 | 14.503 |
| * w.r.t. all shape variables | 18.865 | 34.181 | 57.939 | 79.044 | 101.521 |
| sizing variable sensitivity: | | | | | |
| * w.r.t. one variable | 0.046 | 0.098 | 0.177 | 0.263 | 0.361 |
| * w.r.t. all size variables | 7.222 | 25.846 | 74.144 | 145.385 | 246.719 |
| solution time: | | | | | |
| * no sensitivities | 3.854 | 21.279 | 63.586 | 145.608 | 271.811 |
| solution time: | | | | | |
| * all sensitivities | 29.941 | 81.306 | 195.669 | 370.037 | 620.051 |

analytic shape sensitivities or an additional 0.361 seconds to calculate one set of analytic size sensitivities, for a worse case run time of 286.314 seconds. Using finite differences, this same model would have to be analyzed twice (543.622 seconds total) before even proceeding with the differencing calculations, thus showing the huge computational advantage of computing the sensitivities analytically within the program.

Notice the disproportionate amount of time required to calculate the complete set of model natural frequencies and mode shapes. In the future a new eigenproblem solver will be added that will solve for only a user specified number of frequencies which will drastically cut down the run time.

# CHAPTER 9

# CONCLUSION

A fresh examination of wing finite element modeling practices shows that accurate displacements and natural frequencies can be obtained using simple triangular elements (such as the CST and LST) together with rod elements. Smoothing and averaging of resulting stresses lead to globally reliable stress predictors. With automatic mesh generation and dummy elements, finite element models of wings, including their skins, ribs and spars, can be generated efficiently. The elements used make it possible to obtain derivatives of behavior functions such as displacement, stress and natural frequency analytically with respect to shape and sizing design variables.

Extensive numerical tests comparing predictors of the current capability developed with experiments and commercial finite element codes are described. Analytic sensitivity calculations are compared to finite difference results and optimization package usage of these sensitivities is explained. Thus, the optimization of wing structural systems during conceptual or preliminary design phases can be made practical and computationally cost effective.

Future extensions of this work include:

a) composite material capability,

b) efficient computation of low frequency modes,

c) skin buckling predictions,

d) integration with aerodynamic loads,

e) reliable weight estimation for as-built wings.

The work can also be extended to the modeling of whole airplanes.

## LIST OF REFERENCES


1. Haftka, R.T., and Gurdal, Z., "Elements of Structural Optimization", Third Revised and Expanded Edition, Kluwer Academic Publishers, Dordrecht, Boston, New York 1992.

2. Hornlein, H.R.E.M., "Takeoff in Optimum Structural Design", Computer Aided Optimal Design: Structural and Mechanical Systems", edited by C.A. Mota Soares, Springer Verlag, Berlin, 1987.

3. Miura, H., and Neill, D.J., "Applications of Structural Optimization Methods to Fixed Wing Aircraft and Spacecraft in the 1980s", NASA Technical Memorandum 103939, May 1992 (Also paper AIAA 92-4726, in Proceedings of the Fourth AIAA/USAF/NASA/OAI Symposium on Multidisciplinary Analysis and Optimization, Cleveland, OH, September 21-23, 1992, pp. 298-322)

4. Schmit, L.A., "Structural Optimization - Some Key Ideas and Insights", New Directions in Optimum Structural Design", edited by E. Atrek, R.H. Gallagher, K.M., Ragsdell, O.C. Zienkiewicz, John Wiley&Sons, 1984.

5. Bhatia, K.G., and Wertheimer, J., "Aeroelastic Challenges for a High Speed Civil Transport", AIAA 93-1478, in proceedings of the 34th AIAA/ASME/ASCE/AHS/ASC Structures, Structural Dynamics and Materials Conference, La Jolla, CA, April 1993.

6. Giles, G.L., "Equivalent Plate Analysis of Wing Box Structures with General Planform Geometry", Journal of Aircraft, Vol. 23, No. 11, November 1986, pp. 859-864.

7. Bil, C., Van Dalen, F., Rothwell, A., Arendsen, P. and Wiggenraad, J.F.M., "Structural Optimization in Preliminary Aircraft Design: a Finite Element Approach", ICAS-92-6.7R2, Proceedings of ICAS, 1992, pp. 1505-1515.

8. Adelman, H.M., and Haftka, R.T., "Sensitivity Analysis of Discrete Structural Systems", AIAA Journal, Vol. 24, No. 5, May 1986, pp. 823-832.

9. Barthelemy, J-F.,M., and Haftka, R.T., "Recent Advances in Approximation Concepts for Optimum Structural Design", NASA TM-104032, March 1991.

10. Schmit, L.A., and Miura, H.,"Approximation Concepts for Efficient Structural Analysis", NASA CR-2552, March 1976.

11. Felippa, C.A., "Refined Finite Element Analysis of Linear and Non Linear Two Dimensional Structures", Department of Civil Engineering, University of California, Berkeley, October 1966, (NTIS No. PB 178419).

12. Wang, B.P. , Babu, D., Nambiar, R.V., and Lawrence, K.L., "Shape Design Sensitivity Analysis Using Closed Form Stiffness Matrix for Hierarchic Triangular Elements", Computers & Structures, Vol. 43., No. 1, 1992, pp. 69-75.

13. Botkin, M.E., "Three Dimensional Shape Optimization Using Fully Automatic Mesh Generation", AIAA Journal, Vol. 30, No. 7, July 1992, pp. 1932-1934.

14. Daryl L. Logan, A First Course in the Finite Element Method, PWS Engineering, 1986.

15. Cook, R., Malkus, D., and Plesha, M., "Concepts and Applications of Finite Element Analysis", John Wiley & Sons, 1989.

16. Felippa, C.A., "Solution of Linear Equations with Skyline-Stored Symmetric Matrix", Computers & Structures, Vol. 5, No. 1, 1975, pp. 13-29.

17. C. A. Felippa, "Refined Finite Element Analysis of Linear and Nonlinear Two-Dimensional Structures," Report No. 66-22, PB-178 418, National Science Foundation Grant GK-75, October 1966.

18. Leon, S.J., "Linear Algebra with Applications", McMillan Publishing Co., 2nd edition, 1986, pp. 188-195.

19. Gallagher, R.H., and Rattinger, I., "The Deformational Behavior of Low Aspect Ratio Multi-Web Wings", in three parts: Part I, The Aeronautical Quarterly, November 1961, pp. 361-372, Part II, The Aeronautical Quarterly, February 1962, pp. 77-88.

20. Denke, P.H., "Digital Analysis of Non-Linear Structures", Matrix Methods of Structural Analysis, Fraijs De Veubeuke, editor, Pergamon Press, 1964, pp. 323-326.

21. Turner, M.J., Martin, H.C., and Weikel, R.C., "Further Developments and Applications of the Stiffness Method", in Matrix Methods of Structural Analysis, Fraijs De Veubeuke, editor, Pergamon Press, 1964, pp. 203-266.

22. Lecina, G., and Petiau, C., "Advances in Optimal Design with Composite Materials", in Computer Aided Optimal Design: Structural and Mechanical Systems", C.A. Mota

Soares, editor, Springer Verlag, 1987.

23. J. N. Reddy, An Introduction to the Finite Element Method, McGraw-Hill, 1985.

24. R. M. Pickett, M. F. Rubenstein and R. B. Nelson, "Automated Structural Synthesis Using a Reduced Number of Design Coordinates," AIAA Journal, Vol. 11, No. 4, April 1973, pp. 489-494.

# APPENDIX A

# ELEMENT STIFFNESS, STRESS AND MASS MATRICES

## A.1 Rod element

### A.1.1 Stiffness matrix

The stiffness matrix for a linear, three dimensional rod in its local coordinates (Ref. 14) is given by

$$[k_L] = \frac{AE}{L}\begin{bmatrix} 1 & -1 \\ -1 & 1 \end{bmatrix} \tag{A-1}$$

where A is the cross-sectional area, E is the Modulus of Elasticity, L is the element length and the two degrees of freedom are the axial displacements $\bar{u}_1$ and $\bar{u}_2$ only. To transform this to the global system, the equation [kglobal] = $[T]^T$x [klocal] x [T] is used with

$$[T] = \begin{bmatrix} cx & cy & cz & 0 & 0 & 0 \\ 0 & 0 & 0 & cx & cy & cz \end{bmatrix} \tag{A-2}$$

where $cx = {}^{(x_2-x_1)}/_L$, $cy = {}^{(y_2-y_1)}/_L$, $cz = {}^{(z_2-z_1)}/_L$ (directional cosines) and

$$L = \sqrt{(x_2-x_1)^2 + (y_2-y_1)^2 + (z_2-z_1)^2} \tag{A-3}$$

to arrive at the symmetric 6x6 global stiffness matrix

$$[k_G] = \frac{AE}{L}\begin{bmatrix} cx^2 & cxcy & cxcz & -cx^2 & -cxcy & -cxcz \\ cxcy & cy^2 & cycz & -cxcy & -cy^2 & -cycz \\ cxcz & cycz & cz^2 & -cxcz & -cycz & -cz^2 \\ -cx^2 & -cxcy & -cxcz & cx^2 & cxcy & cxcz \\ -cxcy & -cy^2 & -cycz & cxcy & cy^2 & cycz \\ -cxcz & -cycz & -cz^2 & cxcz & cycz & cz^2 \end{bmatrix}$$

### A.1.2 Stress matrix

The axial stress is a scalar and is found through Hooke's stress/strain law $\sigma = E\varepsilon$ . To find the local strain in the rod, this is simply the change in length divided by the original length in matrix form as

$$\varepsilon_{local} = \frac{1}{L}(\overline{u_2} - \overline{u_1}) = \frac{1}{L}[-1 \;\; 1]\{U_L\} \tag{A-4}$$

with $\{U_L\}^T = \{\bar{u}_1, \bar{u}_2\}$. Global strain is found using the previous transformation $[T]\{U_G\}$ in place of $\{U_L\}$:

$$\varepsilon_{global} = \frac{1}{L}[-1 \;\; 1][T]\{U_G\} \tag{A-5}$$

where $\{U_G\}^T = \{u_1, v_1, w_1, u_2, v_2, w_2\}$. In matrix form the stress can now be given as a scalar using known global displacements as

$$\sigma = \frac{E}{L}[1 \; -1][T]\{U_G\} \tag{A-6}$$

or in explicit form as

$$\sigma = \frac{E\left[(x_2 - x_1)(u_2 - u_1) + (y_2 - y_1)(v_2 - v_1) + (z_2 - z_1)(w_2 - w_1)\right]}{(x_2 - x_1)^2 + (y_2 - y_1)^2 + (z_2 - z_1)^2} \tag{A-7}$$

### A.1.3 Mass matrix

The mass of a rod element is equal to $\rho AL$ where $\rho$ is the mass density with A and L defined previously. To form the 6x6 lumped mass matrix in the global system, the mass is allocated evenly to each degree of freedom by dividing by the number of nodes. Thus

$$m_{rod} = \frac{\rho AL}{2}\begin{bmatrix} 1&0&0&0&0&0 \\ 0&1&0&0&0&0 \\ 0&0&1&0&0&0 \\ 0&0&0&1&0&0 \\ 0&0&0&0&1&0 \\ 0&0&0&0&0&1 \end{bmatrix} \tag{A-8}$$

## A.2 CST element

### A.2.1 Stiffness matrix

The derivation of a constant strain or constant stress triangular element is taken

directly from Ref. 23 and Figure A.1. Its basic assumptions are:

1. isotropic material
2. uniform thickness 't'
3. plane stress state
4. constant strain in field

Based on element geometry, the displacement state in local coordinates is

$$\begin{bmatrix} \bar{u}(x,y) \\ \bar{v}(x,y) \end{bmatrix} = \begin{bmatrix} (-(b-s)x-hy)\bar{u}_P + (-s(x-s)+h(y-s))\bar{u}_Q + xb\bar{u}_R \\ (-(b-s)x-hy)\bar{v}_P + (-s(x-s)+h(y-s))\bar{v}_Q + xb\bar{v}_R \end{bmatrix} \tag{A-9}$$

where b, s, h and a are local geometric variables (b is the major base, s is the minor base, h is the element height and a is the total area). The strain-displacement relation obtained by differentiating the above with respect to x, y and z is then

$$\begin{Bmatrix} \varepsilon_{xx} \\ \varepsilon_{yy} \\ \varepsilon_{xy} \end{Bmatrix} = \frac{1}{bh}\begin{bmatrix} -(b-s) & 0 & -s & 0 & b & 0 \\ 0 & -h & 0 & h & 0 & 0 \\ -h & -(b-s) & h & -s & 0 & b \end{bmatrix} \begin{Bmatrix} \bar{u}_P \\ \bar{v}_P \\ \bar{u}_Q \\ \bar{v}_Q \\ \bar{u}_R \\ \bar{v}_R \end{Bmatrix} = [B]\{U_L\} \tag{A-10}$$

and the displacement transformation law from global coordinates is

$$\begin{Bmatrix} \bar{u}_P \\ \bar{v}_P \\ \bar{u}_Q \\ \bar{v}_Q \\ \bar{u}_R \\ \bar{v}_R \end{Bmatrix} = \begin{bmatrix} [\lambda] & [0] & [0] \\ [0] & [\lambda] & [0] \\ [0] & [0] & [\lambda] \end{bmatrix} \begin{Bmatrix} u_P \\ v_P \\ w_P \\ u_Q \\ v_Q \\ w_Q \\ u_R \\ v_R \\ w_R \end{Bmatrix} = [\Lambda] \{U_G\} \tag{A-11}$$

where

$$[\lambda] = \begin{bmatrix} l_1 & m_1 & n_1 \\ l_2 & m_2 & n_2 \end{bmatrix} \tag{A-12}$$

and

$$[0] = \begin{bmatrix} 0 & 0 & 0 \\ 0 & 0 & 0 \end{bmatrix} \tag{A-13}$$

The l, m and n terms are direction cosines of the local axes with respect to the global axes with

$$l_1 = \frac{1}{h}(x_R - (\frac{s}{b})(x_Q - x_P) - x_P) \tag{A-14}$$

$$m_1 = \frac{1}{h}\left(y_R - \left(\frac{s}{b}\right)(y_Q - y_P) - y_P\right) \tag{A-15}$$

$$n_1 = \frac{1}{h}\left(z_R - \left(\frac{s}{b}\right)(z_Q - z_P) - z_P\right) \tag{A-16}$$

$$l_2 = \frac{1}{b}(x_Q - x_P) \tag{A-17}$$

$$m_2 = \frac{1}{b}(y_Q - y_P) \tag{A-18}$$

$$n_2 = \frac{1}{b}(z_Q - z_P) \tag{A-19}$$

Due to the plane stress assumption, Hooke's Law gives

$$\begin{Bmatrix} \sigma_{xx} \\ \sigma_{yy} \\ \sigma_{xy} \end{Bmatrix} = \frac{E}{1-\nu^2}\begin{bmatrix} 1 & \nu & 0 \\ \nu & 1 & 0 \\ 0 & 0 & \frac{1-\nu}{2} \end{bmatrix}\begin{Bmatrix} \varepsilon_{xx} \\ \varepsilon_{yy} \\ \varepsilon_{xy} \end{Bmatrix} = [D]\begin{Bmatrix} \varepsilon_{xx} \\ \varepsilon_{yy} \\ \varepsilon_{xy} \end{Bmatrix} \tag{A-20}$$

where E is the Modulus of Elasticity and $\upsilon$ is poisson's ratio. To find the stiffness matrix in local coordinates, integrating over the area via

$$[k_L] = \int_V [B]^T [D][B]\,dV = t\int_S [B]^T [D][B]\,dS = [\bar{k}_n] + [\bar{k}_s] \tag{A-21}$$

assuming a constant thickness 't' results in

$$\left[\bar{k}_n\right] = \frac{Et}{4a(1-\nu^2)}\begin{bmatrix} (b-s)^2 & \nu(b-s)h & (b-s)s & -\nu(b-s)h & -(b-s)b & 0 \\ \nu(b-s)h & h^2 & \nu hs & -h^2 & -\nu bh & 0 \\ (b-s)s & \nu hs & s^2 & -\nu hs & -bs & 0 \\ -\nu(b-s)h & -h^2 & -\nu hs & h^2 & \nu hb & 0 \\ -(b-s)b & -\nu bh & -bs & \nu hb & b^2 & 0 \\ 0 & 0 & 0 & 0 & 0 & 0 \end{bmatrix} \tag{A-22}$$

and

$$\left[\bar{k}_s\right] = \frac{Et}{8a(1+\nu)}\begin{bmatrix} h^2 & (b-s)h & -h^2 & hs & 0 & -bh \\ (b-s)h & (b-s)^2 & -(b-s)h & (b-s)s & 0 & -(b-s)b \\ -h^2 & -(b-s)h & h^2 & -hs & 0 & bh \\ hs & (b-s)s & -hs & s^2 & 0 & -bs \\ 0 & 0 & 0 & 0 & 0 & 0 \\ -bh & -(b-s)b & bh & -bs & 0 & b^2 \end{bmatrix} \tag{A-23}$$

The 9x9 global stiffness matrix for the CST is then

$$\left[k_G\right] = \left[\Lambda\right]^T\left[k_L\right]\left[\Lambda\right] \tag{A-24}$$

### A.2.2 Stress matrix

Using Hooke's Law again, the 3x1 CST stress vector is given by

$$\begin{Bmatrix} \sigma_{xx} \\ \sigma_{yy} \\ \sigma_{xy} \end{Bmatrix} = \left[D\right]\begin{Bmatrix} \varepsilon_{xx} \\ \varepsilon_{yy} \\ \varepsilon_{xy} \end{Bmatrix} = \left[D\right]\left[B\right]\{U_L\} = \left[D\right]\left[B\right]\left[\Lambda\right]\{U_G\} \tag{A-25}$$

### A.2.3 Mass matrix

The mass of a CST element is equal to $\rho A t$ where $\rho$ is the mass density with A and t defined previously. To form the 9x9 lumped mass matrix in the global system, the mass is allocated evenly to each degree of freedom by dividing by the number of nodes. Thus

$$m_{CST} = \frac{\rho A t}{3}\begin{bmatrix} 1&0&0&0&0&0 \\ 0&1&0&0&0&0 \\ 0&0&1&0&0&0 \\ 0&0&0&1&0&0 \\ 0&0&0&0&1&0 \\ 0&0&0&0&0&1 \end{bmatrix} \tag{A-26}$$

## A.3 LST element

### A.3.1 Stiffness matrix

The derivation of a linear strain triangular element is taken directly from Ref. 17 and Figure A.1. It's basic assumptions are:

1. isotropic material
2. uniform thickness
3. plane stress state
4. linear strain in field

The local 12x12 stiffness matrix is given by

$$[k_L] = [M]^T[N][M] \tag{A-27}$$

with

$$[M] = \frac{1}{2a}\begin{bmatrix} 3b_1 & 0 & -b_2 & 0 & -b_3 & 0 & 4b_2 & 0 & 0 & 0 & 4b_3 & 0 \\ -b_1 & 0 & 3b_2 & 0 & -b_3 & 0 & 4b_1 & 0 & 4b_3 & 0 & 0 & 0 \\ -b_1 & 0 & -b_2 & 0 & 3b_3 & 0 & 0 & 0 & 4b_2 & 0 & 4b_1 & 0 \\ 0 & 3a_1 & 0 & -a_2 & 0 & -a_3 & 0 & 4a_2 & 0 & 0 & 0 & 4a_3 \\ 0 & -a_1 & 0 & 3a_2 & 0 & -a_3 & 0 & 4a_1 & 0 & 4a_3 & 0 & 0 \\ 0 & -a_1 & 0 & -a_2 & 0 & 3a_3 & 0 & 0 & 0 & 4a_2 & 0 & 4a_1 \\ 3a_1 & 3b_1 & -a_2 & -b_2 & -a_3 & -b_3 & 4a_2 & 4b_2 & 0 & 0 & 4a_3 & 4b_3 \\ -a_1 & -b_1 & 3a_2 & 3b_2 & -a_3 & -b_3 & 4a_1 & 4b_1 & 4a_3 & 4b_3 & 0 & 0 \\ -a_1 & -b_1 & -a_2 & -b_2 & 3a_3 & 3b_3 & 0 & 0 & 4a_2 & 4b_2 & 4a_1 & 4b_1 \end{bmatrix} \tag{A-28}$$

and

$$[N] = \frac{at}{12}\begin{bmatrix} 2c_{11} & c_{11} & c_{11} & 2c_{12} & c_{12} & c_{12} & 0 & 0 & 0 \\ c_{11} & 2c_{11} & c_{11} & c_{12} & 2c_{12} & c_{12} & 0 & 0 & 0 \\ c_{11} & c_{11} & 2c_{11} & c_{12} & c_{12} & 2c_{12} & 0 & 0 & 0 \\ 2c_{12} & c_{12} & c_{12} & 2c_2 & c_{22} & c_{22} & 0 & 0 & 0 \\ c_{12} & 2c_{12} & c_{12} & c_{22} & 2c_{22} & c_{22} & 0 & 0 & 0 \\ c_{12} & c_{12} & c_{12} & c_{22} & c_{22} & 2c_{22} & 0 & 0 & 0 \\ 0 & 0 & 0 & 0 & 0 & 0 & 2c_{33} & c_{33} & c_{33} \\ 0 & 0 & 0 & 0 & 0 & 0 & c_{33} & 2c_{33} & c_{33} \\ 0 & 0 & 0 & 0 & 0 & 0 & c_{33} & c_{33} & 2c_{33} \end{bmatrix} \tag{A-29}$$

where $c_{11} = c_{22} = {}^{E}/_{(1 - \nu^2)}$, $c_{12} = {}^{\nu E}/_{(1- \nu^2)}$ and $c_{33} = {}^{E(1 - \nu)}/_{2(1 - \nu^2)} = {}^{E}/_{2(1 + \nu)}$. The global geometry variables $\{B\} = \{a_1, a_2, a_3, b_1, b_2, b_3\}$ are linked to the local geometry variables $\{G\} = \{b, s, h, a\}$ by

$$a_1 = -h \qquad a_2 = h \qquad a_3 = 0$$

$$b_1 = s - b \qquad b_2 = -s \qquad b_3 = b$$

To find the 18x18 global stiffness matrix, transformation is the same as for the CST in section A.2.1 using

$$\left[k_G\right] = \begin{bmatrix} [\Lambda] & [0] \\ [0] & [\Lambda] \end{bmatrix}^T \left[k_L\right] \begin{bmatrix} [\Lambda] & [0] \\ [0] & [\Lambda] \end{bmatrix} = \left[\tilde{\Lambda}\right]^T \left[k_L\right] \left[\tilde{\Lambda}\right] \tag{A-30}$$

### A.3.2 Stress matrix

Using Hooke's Law, the 9x1 stress vector consisting of $\sigma_{xx}$, $\sigma_{yy}$ and $\sigma_{xy}$ for each of the three end nodes P, Q and R is

$$\begin{Bmatrix} \begin{Bmatrix} \sigma_{xx} \\ \sigma_{yy} \\ \sigma_{xy} \end{Bmatrix}_P \\ \begin{Bmatrix} \sigma_{xx} \\ \sigma_{yy} \\ \sigma_{xy} \end{Bmatrix}_Q \\ \begin{Bmatrix} \sigma_{xx} \\ \sigma_{yy} \\ \sigma_{xy} \end{Bmatrix}_R \end{Bmatrix} = \begin{bmatrix} [C] & [0] & [0] \\ [0] & [C] & [0] \\ [0] & [0] & [C] \end{bmatrix} \begin{Bmatrix} \begin{Bmatrix} \varepsilon_{xx} \\ \varepsilon_{yy} \\ \varepsilon_{xy} \end{Bmatrix}_P \\ \begin{Bmatrix} \varepsilon_{xx} \\ \varepsilon_{yy} \\ \varepsilon_{xy} \end{Bmatrix}_Q \\ \begin{Bmatrix} \varepsilon_{xx} \\ \varepsilon_{yy} \\ \varepsilon_{xy} \end{Bmatrix}_R \end{Bmatrix} = [\tilde{C}]\,\{\tilde{\varepsilon}\} \tag{A-31}$$

where

$$[C] = \frac{E}{1-\nu^2}\begin{bmatrix} 1 & \nu & 0 \\ \nu & 1 & 0 \\ 0 & 0 & \dfrac{1-\nu}{2} \end{bmatrix} \tag{A-32}$$

and

$$\{\tilde{\varepsilon}\} = [M]\{U_L\} = [M][\tilde{\Lambda}]\{U_G\} \tag{A-33}$$

Therefore,

$$\begin{Bmatrix} \begin{Bmatrix} \sigma_{xx} \\ \sigma_{yy} \\ \sigma_{xy} \end{Bmatrix}_P \\ \begin{Bmatrix} \sigma_{xx} \\ \sigma_{yy} \\ \sigma_{xy} \end{Bmatrix}_Q \\ \begin{Bmatrix} \sigma_{xx} \\ \sigma_{yy} \\ \sigma_{xy} \end{Bmatrix}_R \end{Bmatrix} = [\tilde{C}][M][\tilde{\Lambda}]\{U_G\} \tag{A-34}$$

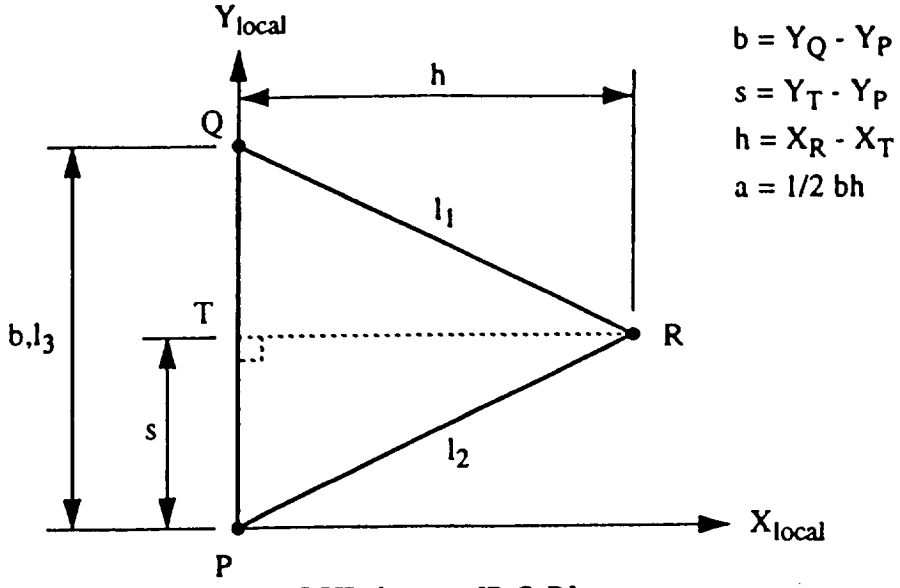


CST element [P Q R]

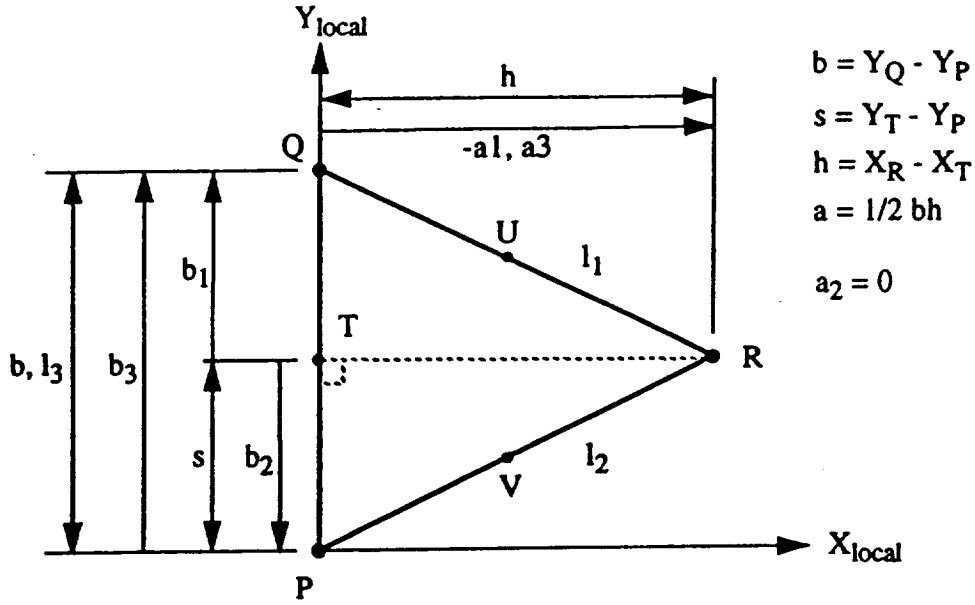


LST element [P Q R T U V]

Figure A.1 - Triangular membrane elements used

# APPENDIX B

## ELEMENT COORDINATE SHAPE VARIABLE DERIVATIVES

### B.1 $d\{X\}/d(x_{FL}, x_{AL}, x_{FR}, x_{AR}, y_L, y_R)$

Based on the geometry in Figure 3.1, it can be seen that every 'y' value at point 'i' is a linear combination of $y_L$ and $y_R$ such that

$$y_i = y_L + p_s(y_R - y_L) = (1 - p_s)y_L + p_s y_R \tag{B-1}$$

where $p_s$ = percent span ratio in the y-direction and is given by

$$p_s = \frac{y_i - y_L}{y_R - y_L} \tag{B-2}$$

Now, differentiating $y_i$ with respect to the six shape variables yields

$$dy_i/dx_{FL} = 0$$

$$dy_i/dx_{AL} = 0$$

$$dy_i/dx_{FR} = 0$$

$$dy_i/dx_{AR} = 0$$

$$dy_i/dy_L = 1 - p_s$$

$$dy_i/dy_R = p_s$$

For the 'x' values at point 'i,' if 'i' is along either the wing root or wing tip, the situation is the same as for the 'y' values above. Along the root, 'x' is given by

$$x_i = x_{FL} + p_{rc}(x_{AL} - x_{FL}) = (1 - p_{rc})x_{FL} + p_{rc}x_{AL} \quad \text{(B-3)}$$

while along the tip, 'x' is given by

$$x_i = x_{FR} + p_{tc}(x_{AR} - x_{FR}) = (1 - p_{tc})x_{FR} + p_{tc}x_{AR} \quad \text{(B-4)}$$

where $p_{rc}$ = percent chord ratio along the root and $p_{tc}$ = percent chord ratio along the tip and are given by

$$p_{rc} = \frac{x_i - x_{FL}}{x_{AL} - x_{FL}} \quad \text{(B-5)}$$

and

$$p_{tc} = \frac{x_i - x_{FR}}{x_{AR} - x_{FR}} \quad \text{(B-6)}$$

Therefore, differentiating $x_i$ along the root with respect to each shape variable gives

$$dx_i/dx_{FL} = 1 - p_{rc}$$

$$dx_i/dx_{AL} = p_{rc}$$

$$dx_i/dx_{FR} = 0$$

$$dx_i/dx_{AR} = 0$$

$$dx_i/dy_L = 0$$

$$dx_i/dy_R = 0$$

while doing the same along the wing tip yields

$$dx_i/dx_{FL} = 0$$

$$dx_i/dx_{AL} = 0$$

$$dx_i/dx_{FR} = 1 - p_{tc}$$

$$dx_i/dx_{AR} = p_{tc}$$

$$dx_i/dy_L = 0$$

$$dx_i/dy_R = 0$$

For all remaining nodes, the 'x' values are a linear combination of all four 'x' -valued shape variables. Fortunately, due to the nature of the wing geometry, since we know the 'x' derivatives along both the root and tip, it is a straightforward process to interpolate what they should be for any point 'i' across the span. In other words

$$x_i = (x_i)_{root} + p_s [(x_i)_{tip} - (x_i)_{root}] \tag{B-7}$$

or

$$x_i = [(1 - p_{rc}) x_{FL} + p_{rc} x_{AL}] (1 - p_s) + [(1 - p_{tc}) x_{FR} + p_{tc} x_{AR}] p_s \tag{B-8}$$

where $p_s$ has been defined above (eqn. B-2). Differentiating with respect to each shape variable then yields the more general and final form of

$$dx_i/dx_{FL} = (1 - p_{rc})(1 - p_s)$$

$$dx_i/dx_{AL} = p_{rc}(1 - p_s)$$

$$dx_i/dx_{FR} = (1 - p_{tc})p_s$$

$$dx_i/dx_{AR} = p_{tc}p_s$$

$$dx_i/dy_L = 0$$

$$dx_i/dy_R = 0$$

As one can see, this reduces to the simplified forms along the root and tip above when $p_s$ equals 0 and 1, respectively. When the depth distribution is given in global coordinates, then all 'z' values at point 'i' are independent of these shape variables so that their derivatives are equal to zero. If the depth distribution is dependant on the wing trapezoid shape, sensitivities with respect to shape variables must be included.

In summary,

$$\frac{\partial}{\partial x_{FL}} \begin{Bmatrix} x_i \\ y_i \\ z_i \end{Bmatrix} = \begin{Bmatrix} (1-p_{rc})\,(1-p_s) \\ 0 \\ 0 \end{Bmatrix} \tag{B-9}$$

$$\frac{\partial}{\partial x_{AL}} \begin{Bmatrix} x_i \\ y_i \\ z_i \end{Bmatrix} = \begin{Bmatrix} p_{rc}\,(1-p_s) \\ 0 \\ 0 \end{Bmatrix} \tag{B-10}$$

$$\frac{\partial}{\partial x_{FR}} \begin{Bmatrix} x_i \\ y_i \\ z_i \end{Bmatrix} = \begin{Bmatrix} (1-p_{tc})\,p_s \\ 0 \\ 0 \end{Bmatrix} \tag{B-11}$$

$$\frac{\partial}{\partial x_{AR}} \begin{Bmatrix} x_i \\ y_i \\ z_i \end{Bmatrix} = \begin{Bmatrix} p_{tc}p_s \\ 0 \\ 0 \end{Bmatrix} \tag{B-12}$$

$$\frac{\partial}{\partial y_L}\begin{Bmatrix} x_i \\ y_i \\ z_i \end{Bmatrix} = \begin{Bmatrix} 0 \\ 1-p_s \\ 0 \end{Bmatrix} \tag{B-13}$$

$$\frac{\partial}{\partial y_R}\begin{Bmatrix} x_i \\ y_i \\ z_i \end{Bmatrix} = \begin{Bmatrix} 0 \\ p_s \\ 0 \end{Bmatrix} \tag{B-14}$$

**B.2 d{X}/d(α)**

Based on the geometry in Figure 3.1, it can also be seen that for any nodal point 'i', if given a 'y' value, then the corresponding 'x' value is given by

$$x_i = y_i \tan\alpha + C \tag{B-15}$$

where C is any constant. If all 'y' and 'z' coordinates are assumed to be independent of the sweep angle, differentiating with respect to the design variable α gives

$$\frac{\partial}{\partial \alpha}\begin{Bmatrix} x_i \\ y_i \\ z_i \end{Bmatrix} = \begin{Bmatrix} y_i(\sec(\alpha))^2 \\ 0 \\ 0 \end{Bmatrix} \tag{B-16}$$

# APPENDIX C

# SHAPE VARIABLE SENSITIVITIES

## C.1 Global displacement sensitivity with respect to any shape variable

From the basic static equation [K]{U} = {F}, one can differentiate with respect to any shape design variable β to get

$$[K]\frac{\partial\{U\}}{\partial\beta} + \frac{\partial[K]}{\partial\beta}\{U\} = \frac{\partial\{F\}}{\partial\beta} \tag{C-1}$$

where [K] is the global stiffness matrix, {U} is the global displacement vector and {F} is the global load vector.

For any loading case in which the applied loads are independent of model geometry,

$$\frac{\partial\{U\}}{\partial\beta} = -[K]^{-1}\frac{\partial[K]}{\partial\beta}\{U\} \tag{C-2}$$

With [K] and {U} having already been computed, and the partial derivative of displacement with respect to any shape design variable desired, it is only necessary to compute the global stiffness matrix derivative. This is done on an element by element basis and the individual results are then merged as done when forming [K] previously.

### C.1.1 Rod element stiffness sensitivity

Using chain rule differentiation, the derivative of a rod element stiffness matrix with respect to any shape design variable is

$$\frac{\partial[k_G]}{\partial\beta} = \frac{\partial[k_G]}{\partial\{X\}}\frac{\partial\{X\}}{\partial\beta} \tag{C-3}$$

where $\{X\} = \{x_1, y_1, z_1, x_2, y_2, z_2\}$. The partial differentiation of $\{X\}$ with respect to any design variable has previously been calculated in Appendix B. To find the partial derivative of $[k_G]$ with respect to the rod element's nodal coordinates $\{X\}$, straight-forward chain rule differentiation is carried out (with the following simplifications: $\Delta x = x_2 - x_1$, $\Delta y = y_2 - y_1$, $\Delta z = z_2 - z_1$) with 'i' ranging from 1 to 6:

$$\frac{\partial[k_G]}{\partial X_i} = \begin{bmatrix} [AA]_i & -[AA]_i \\ -[AA]_i & [AA]_i \end{bmatrix} \tag{C-4}$$

where

$$[AA]_1 = \frac{3AE}{L^5}\begin{bmatrix} (\Delta x)^3 & (\Delta x)^2\Delta y & (\Delta x)^2\Delta z \\ (\Delta x)^2\Delta y & (\Delta y)^2\Delta x & \Delta x\Delta y\Delta z \\ (\Delta x)^2\Delta z & \Delta x\Delta y\Delta z & (\Delta z)^2\Delta x \end{bmatrix} - \frac{AE}{L^3}\begin{bmatrix} 2\Delta x & \Delta y & \Delta z \\ \Delta y & 0 & 0 \\ \Delta z & 0 & 0 \end{bmatrix} \tag{C-5}$$

$$[AA]_2 = -\frac{3AE}{L^5}\begin{bmatrix} (\Delta x)^3 & (\Delta x)^2\Delta y & (\Delta x)^2\Delta z \\ (\Delta x)^2\Delta y & (\Delta y)^2\Delta x & \Delta x\Delta y\Delta z \\ (\Delta x)^2\Delta z & \Delta x\Delta y\Delta z & (\Delta z)^2\Delta x \end{bmatrix} + \frac{AE}{L^3}\begin{bmatrix} 2\Delta x & \Delta y & \Delta z \\ \Delta y & 0 & 0 \\ \Delta z & 0 & 0 \end{bmatrix} \tag{C-6}$$

$$[AA]_3 = \frac{3AE}{L^5}\begin{bmatrix} (\Delta x)^2\Delta y & (\Delta y)^2\Delta x & \Delta x\Delta y\Delta z \\ (\Delta y)^2\Delta x & (\Delta y)^3 & (\Delta y)^2\Delta x \\ \Delta x\Delta y\Delta z & (\Delta y)^2\Delta x & (\Delta z)^2\Delta y \end{bmatrix} - \frac{AE}{L^3}\begin{bmatrix} 0 & \Delta x & 0 \\ \Delta x & 2\Delta y & \Delta z \\ 0 & \Delta z & 0 \end{bmatrix} \tag{C-7}$$

$$[AA]_4 = -\frac{3AE}{L^5}\begin{bmatrix}(\Delta x)^2\Delta y & (\Delta y)^2\Delta x & \Delta x\Delta y\Delta z\\ (\Delta y)^2\Delta x & (\Delta y)^3 & (\Delta y)^2\Delta x\\ \Delta x\Delta y\Delta z & (\Delta y)^2\Delta x & (\Delta z)^2\Delta y\end{bmatrix} + \frac{AE}{L^3}\begin{bmatrix}0 & \Delta x & 0\\ \Delta x & 2\Delta y & \Delta z\\ 0 & \Delta z & 0\end{bmatrix} \tag{C-8}$$

$$[AA]_5 = \frac{3AE}{L^5}\begin{bmatrix}(\Delta x)^2\Delta z & \Delta x\Delta y\Delta z & (\Delta z)^2\Delta x\\ \Delta x\Delta y\Delta z & (\Delta y)^2\Delta z & (\Delta z)^2\Delta y\\ (\Delta z)^2\Delta x & (\Delta z)^2\Delta y & (\Delta z)^3\end{bmatrix} - \frac{AE}{L^3}\begin{bmatrix}0 & 0 & \Delta x\\ 0 & 0 & \Delta y\\ \Delta x & \Delta y & 2\Delta z\end{bmatrix} \tag{C-9}$$

$$[AA]_6 = -\frac{3AE}{L^5}\begin{bmatrix}(\Delta x)^2\Delta z & \Delta x\Delta y\Delta z & (\Delta z)^2\Delta x\\ \Delta x\Delta y\Delta z & (\Delta y)^2\Delta z & (\Delta z)^2\Delta y\\ (\Delta z)^2\Delta x & (\Delta z)^2\Delta y & (\Delta z)^3\end{bmatrix} + \frac{AE}{L^3}\begin{bmatrix}0 & 0 & \Delta x\\ 0 & 0 & \Delta y\\ \Delta x & \Delta y & 2\Delta z\end{bmatrix} \tag{C-10}$$

Then, the 6x6 rod element global stiffness matrix sensitivity with respect to shape design variable $\beta$ is

$$\frac{\partial[k_G]}{\partial\beta} = \frac{\partial[k_G]}{\partial X_1}\frac{\partial X_1}{\partial\beta} + \frac{\partial[k_G]}{\partial X_2}\frac{\partial X_2}{\partial\beta} + \ldots + \frac{\partial[k_G]}{\partial X_6}\frac{\partial X_6}{\partial\beta} \tag{C-11}$$

### C.1.2 CST element stiffness sensitivity

Chain-rule differentiation of 9x9 CST stiffness matrix $[k_G]$ with respect to any shape design variable gives

$$\frac{\partial[k_G]}{\partial\beta} = \frac{\partial[k_G]}{\partial\{X\}}\frac{\partial\{X\}}{\partial\beta} \tag{C-12}$$

so that only the partial derivative of $[k_G]$ with respect to $\{X\}$ needs to be found. To calculate this, differentiation of the matrix expression for $[k_G]$ yields

$$\frac{\partial[k_G]}{\partial\{X\}} = [\Lambda]^T[k_L]\frac{\partial[\Lambda]}{\partial\{X\}} + [\Lambda]^T\frac{\partial[k_L]}{\partial\{X\}}[\Lambda] + \frac{\partial[\Lambda]}{\partial\{X\}}^T[k_L][\Lambda] \qquad \text{(C-13)}$$

where $\{X\} = \{x_1, y_1, z_1, x_2, y_2, z_2, x_3, y_3, z_3\}$. All undifferentiated matrices are known so that the only unknowns are the transformation matrix derivatives and the local stiffness matrix derivatives each with respect to nodal coordinates.

Before proceeding, all geometric variables will be linked to each other through Figure A.1 and the following equations:

$\{L\} = \{l_1, l_2, l_3\}$ = function of $\{X\}$ only where

$l_1 = [(x_3 - x_2)^2 + (y_3 - y_2)^2 + (z_3 - z_2)^2]^{1/2}$

$l_2 = [(x_3 - x_1)^2 + (y_3 - y_1)^2 + (z_3 - z_1)^2]^{1/2}$

$l_3 = [(x_2 - x_1)^2 + (y_2 - y_1)^2 + (z_2 - z_1)^2]^{1/2}$

$\{G\} = \{b, s, h, a\}$ = function of $\{L\}$ only where

$b = l_3$

$s = (l_2^2 + l_3^2 - l_1^2)/(2l_3)$

$h = [l_2^2 - (l_2^2 + l_3^2 - l_1^2)^2/(4l_3^2)]^{1/2}$

$a = (^1/_2)\, l_3[l_2^2 - (l_2^2 + l_3^2 - l_1^2)/(4l_3^2)]^{1/2}$

$[k_L]$ = function of Young's Modulus, thickness and $\{G\}$ only

$[\Lambda]$ = function of $\{G\}$ and $\{X\}$ only

### C.1.2.1 d[$k_L$]/d{X}:

Chain rule differentiation of the 6x6 [klocal] with respect to vector {X} gives

$$\frac{\partial[k_L]}{\partial\{X\}} = \frac{\partial[k_L]}{\partial\{G\}}\frac{\partial\{G\}}{\partial\{L\}}\frac{\partial\{L\}}{\partial\{X\}} \tag{C-14}$$

where

$$\frac{\partial[k_L]}{\partial\{G\}} = \frac{\partial[\bar{k}_N]}{\partial\{G\}} + \frac{\partial[\bar{k}_S]}{\partial\{G\}} \tag{C-15}$$

and the following derivatives are used:

$$\frac{\partial[\bar{k}_N]}{\partial G_1} = \frac{Et}{4a(1-\nu^2)}\begin{bmatrix} 2(b-s) & \nu h & s & -\nu h & s-2b & 0 \\ \nu h & 0 & 0 & 0 & -\nu h & 0 \\ s & 0 & 0 & 0 & -s & 0 \\ -\nu h & 0 & 0 & 0 & \nu h & 0 \\ s-2b & -\nu h & -s & \nu h & 2b & 0 \\ 0 & 0 & 0 & 0 & 0 & 0 \end{bmatrix} \tag{C-16}$$

$$\frac{\partial[\bar{k}_N]}{\partial G_2} = \frac{Et}{4a(1-\nu^2)}\begin{bmatrix} 2(s-b) & -\nu h & s & -\nu h & s-2b & 0 \\ \nu h & 0 & 0 & 0 & -\nu h & 0 \\ s & 0 & 0 & 0 & -s & 0 \\ -\nu h & 0 & 0 & 0 & \nu h & 0 \\ s-2b & -\nu h & -s & \nu h & 2b & 0 \\ 0 & 0 & 0 & 0 & 0 & 0 \end{bmatrix} \tag{C-17}$$

$$\frac{\partial[\bar{k}_N]}{\partial G_3} = \frac{Et}{4a(1-\nu^2)}\begin{bmatrix} 0 & (b-s)\nu & 0 & -(b-s)\nu & 0 & 0 \\ (b-s)\nu & 2h & s\nu & -2h & -b\nu & 0 \\ 0 & s\nu & 0 & -s\nu & 0 & 0 \\ -(b-s)\nu & -2h & -s\nu & 2h & b\nu & 0 \\ 0 & -b\nu & 0 & b\nu & 0 & 0 \\ 0 & 0 & 0 & 0 & 0 & 0 \end{bmatrix} \qquad \text{(C-18)}$$

$$\frac{\partial[\bar{k}_N]}{\partial G_4} = \frac{Et}{4a^2(1-\nu^2)}\begin{bmatrix} -(b-s)^2 & -(b-s)\nu h & -(b-s)s & (b-s)\nu h & (b-s)b & 0 \\ -(b-s)\nu h & -h^2 & s\nu & h^2 & \nu bh & 0 \\ -(b-s)s & s\nu & -s^2 & \nu sh & bs & 0 \\ (b-s)\nu h & h^2 & \nu sh & -h^2 & -\nu bh & 0 \\ (b-s)b & \nu bh & bs & -\nu bh & -b^2 & 0 \\ 0 & 0 & 0 & 0 & 0 & 0 \end{bmatrix}$$

(C-19)

$$\frac{\partial[\bar{k}_S]}{\partial G_1} = \frac{Et}{8a(1+\nu)}\begin{bmatrix} 0 & h & 0 & 0 & 0 & -h \\ h & 2(b-s) & -h & s & 0 & s-2b \\ 0 & -h & 0 & 0 & 0 & h \\ 0 & s & 0 & 0 & 0 & -s \\ 0 & 0 & 0 & 0 & 0 & 0 \\ -h & s-2b & h & -s & 0 & 2b \end{bmatrix} \qquad \text{(C-20)}$$

$$\frac{\partial[\bar{k}_S]}{\partial G_2} = \frac{Et}{8a(1+\nu)}\begin{bmatrix} 0 & -h & 0 & h & 0 & 0 \\ -h & -2(b-s) & h & b-2s & 0 & b \\ 0 & h & 0 & -h & 0 & 0 \\ h & b-2s & -h & 2s & 0 & -b \\ 0 & 0 & 0 & 0 & 0 & 0 \\ 0 & b & 0 & -b & 0 & 0 \end{bmatrix} \qquad \text{(C-21)}$$

$$\frac{\partial\left[\bar{k}_S\right]}{\partial G_3} = \frac{Et}{8a(1+\nu)}\begin{bmatrix} 2h & (b-s) & -2h & s & 0 & -b \\ (b-s) & 0 & -(b-s) & 0 & 0 & 0 \\ -2h & -(b-s) & 2h & -s & 0 & b \\ s & 0 & -s & 0 & 0 & 0 \\ 0 & 0 & 0 & 0 & 0 & 0 \\ -b & 0 & b & 0 & 0 & 0 \end{bmatrix} \tag{C-22}$$

$$\frac{\partial\left[\bar{k}_S\right]}{\partial G_4} = \frac{Et}{8a(1+\nu)}\begin{bmatrix} -h^2 & -(b-s)h & -2h & -sh & 0 & bh \\ -(b-s)h & -(b-s)^2 & (b-s)h & -(b-s)s & 0 & (b-s)b \\ -2h & (b-s)h & -h^2 & sh & 0 & -bh \\ -sh & -(b-s)s & sh & -s^2 & 0 & bs \\ 0 & 0 & 0 & 0 & 0 & 0 \\ bh & (b-s)b & -bh & bs & 0 & -b^2 \end{bmatrix} \left(\frac{1}{a}\right) \tag{C-23}$$

along with

$$\frac{\partial\{G\}}{\partial\{L\}} = \begin{bmatrix} 0 & 0 & 1 \\ -\dfrac{l_1}{l_3} & \dfrac{l_2}{l_3} & \dfrac{l_1^2+l_3^2-l_2^2}{2l_3^2} \\ \dfrac{l_1(l_2^2+l_3^2-l_1^2)}{2hl_3^2} & \dfrac{l_2(l_1^2+l_3^2-l_2^2)}{2hl_3^2} & (l_2^2+l_3^2-l_1^2)\dfrac{(l_2^2-l_1^2-l_3^2)}{4hl_3^3} \\ \dfrac{l_1(l_2^2+l_3^2-l_1^2)}{8a} & \dfrac{l_2(l_1^2+l_3^2-l_2^2)}{8a} & \dfrac{l_3(l_1^2+l_2^2-l_3^2)}{8a} \end{bmatrix} \tag{C-24}$$

and

$$\frac{\partial\{L\}}{\partial\{X\}} = \begin{bmatrix} 0 & 0 & 0 & \frac{x_2-x_3}{l_1} & \frac{y_2-y_3}{l_1} & \frac{z_2-z_3}{l_1} & \frac{x_3-x_2}{l_1} & \frac{y_3-y_2}{l_1} & \frac{z_3-z_2}{l_1} \\ \frac{x_1-x_3}{l_2} & \frac{y_1-y_3}{l_2} & \frac{z_1-z_3}{l_2} & 0 & 0 & 0 & \frac{x_3-x_1}{l_2} & \frac{y_3-y_1}{l_2} & \frac{z_3-z_1}{l_2} \\ \frac{x_1-x_2}{l_3} & \frac{x_1-x_2}{l_3} & \frac{z_1-z_2}{l_3} & \frac{x_2-x_1}{l_3} & \frac{y_2-y_1}{l_3} & \frac{z_2-z_1}{l_3} & 0 & 0 & 0 \end{bmatrix} \tag{C-25}$$

Thus, to find the derivative of $[k_L]$ with respect to any $X_i$, chain rule summation yields

$$\frac{\partial[k_L]}{\partial X_i} = \frac{\partial[k_L]}{\partial G_1}\frac{\partial G_1}{\partial\{L\}}\frac{\partial\{L\}}{\partial X_i} + \ldots + \frac{\partial[k_L]}{\partial G_4}\frac{\partial G_4}{\partial\{L\}}\frac{\partial\{L\}}{\partial X_i} \tag{C-26}$$

where $\frac{\partial G_j}{\partial\{L\}}$ is the 1x3 row 'j' of $\frac{\partial\{G\}}{\partial\{L\}}$ and $\frac{\partial\{L\}}{\partial X_i}$ is the 3x1 column 'i' of $\frac{\partial\{L\}}{\partial\{X\}}$.

**d [Λ] /d[X]:**

Chain rule differentiation of the 6x9 transformation matrix [Λ] with respect to {X} gives

$$\frac{D[\Lambda]}{D\{X\}} = \frac{\partial[\Lambda]}{\partial\{G\}}\frac{\partial\{G\}}{\partial\{L\}}\frac{\partial\{L\}}{\partial\{X\}} + \frac{\partial[\Lambda]}{\partial\{X\}} \tag{C-27}$$

where $\frac{D[\Lambda]}{D\{X\}}$ is the total derivative since there is explicit dependance of $[\Lambda]$ on $\{X\}$.

The following new derivatives are used:

$$\frac{\partial[\Lambda]}{\partial G_i} = \begin{bmatrix} [AA]_i & [0] & [0] \\ [0] & [AA]_i & [0] \\ [0] & [0] & [AA]_i \end{bmatrix} \qquad (i = 1 \text{ to } 4) \tag{C-28}$$

with

$$[AA]_1 = \begin{bmatrix} \frac{s(x_2-x_1)}{b^2h} & \frac{s(y_2-y_1)}{b^2h} & \frac{s(z_2-z_1)}{b^2h} \\ -\frac{(x_2-x_1)}{b^2} & -\frac{(y_2-y_1)}{b^2} & -\frac{(z_2-z_1)}{b^2} \end{bmatrix} \tag{C-29}$$

$$[AA]_2 = \begin{bmatrix} -\frac{(x_2-x_1)}{bh} & -\frac{(y_2-y_1)}{bh} & -\frac{(z_2-z_1)}{bh} \\ 0 & 0 & 0 \end{bmatrix} \tag{C-30}$$

$$[AA]_3 = \begin{bmatrix} -\frac{x_3-\frac{s}{b}(x_2-x_1)-x_1}{h^2} & -\frac{y_3-\frac{s}{b}(y_2-y_1)-y_1}{h^2} & -\frac{z_3-\frac{s}{b}(z_2-z_1)-z_1}{h^2} \\ 0 & 0 & 0 \end{bmatrix} \tag{C-31}$$

$$[AA]_4 = \begin{bmatrix} 0 & 0 & 0 \\ 0 & 0 & 0 \end{bmatrix} \tag{C-32}$$

and

$$\frac{\partial[\Lambda]}{\partial X_i} = \begin{bmatrix} [BB]_i & [0] & [0] \\ [0] & [BB]_i & [0] \\ [0] & [0] & [BB]_i \end{bmatrix} \qquad (i = 1 \text{ to } 9): \tag{C-33}$$

with

$$[BB]_1 = \begin{bmatrix} \frac{1}{h}(\frac{s}{b} - 1) & 0 & 0 \\ -\frac{1}{b} & 0 & 0 \end{bmatrix} \tag{C-34}$$

$$[BB]_2 = \begin{bmatrix} 0 & \frac{1}{h}(\frac{s}{b} - 1) & 0 \\ 0 & -\frac{1}{b} & 0 \end{bmatrix} \tag{C-35}$$

$$[BB]_3 = \begin{bmatrix} 0 & 0 & \frac{1}{h}(\frac{s}{b} - 1) \\ 0 & 0 & -\frac{1}{b} \end{bmatrix} \tag{C-36}$$

$$[BB]_4 = \begin{bmatrix} -\frac{s}{bh} & 0 & 0 \\ \frac{1}{b} & 0 & 0 \end{bmatrix} \tag{C-37}$$

$$[BB]_5 = \begin{bmatrix} 0 & -\frac{s}{bh} & 0 \\ 0 & \frac{1}{b} & 0 \end{bmatrix} \tag{C-38}$$

$$[BB]_6 = \begin{bmatrix} 0 & 0 & -\frac{s}{bh} \\ 0 & 0 & \frac{1}{b} \end{bmatrix} \tag{C-39}$$

$$[BB]_7 = \begin{bmatrix} \frac{1}{h} & 0 & 0 \\ 0 & 0 & 0 \end{bmatrix} \tag{C-40}$$

$$[BB]_8 = \begin{bmatrix} 0 & \frac{1}{h} & 0 \\ 0 & 0 & 0 \end{bmatrix} \tag{C-41}$$

$$[BB]_9 = \begin{bmatrix} 0 & \frac{1}{h} & 0 \\ 0 & 0 & 0 \end{bmatrix} \tag{C-42}$$

### C.1.3 LST element stiffness sensitivity

Chain-rule differentiation of $[k_G]$ with respect any shape design variable gives

$$\frac{\partial [k_G]}{\partial \beta} = \frac{\partial [k_G]}{\partial \{X\}} \frac{\partial \{X\}}{\partial \beta} \tag{C-43}$$

so that only the partial derivative of $[k_G]$ with respect to $\{X\}$ needs to be found. To calculate this, differentiation of the LST matrix expression for $[k_G]$ yields

$$\frac{\partial[k_G]}{\partial\{X\}} = [\tilde{\Lambda}]^T [k_L] \frac{\partial[\tilde{\Lambda}]}{\partial\{X\}} + [\tilde{\Lambda}]^T \frac{\partial[k_L]}{\partial\{X\}} [\tilde{\Lambda}] + \frac{\partial[\tilde{\Lambda}]^T}{\partial\{X\}} [k_L] [\tilde{\Lambda}] \qquad \text{(C-44)}$$

where $\{X\} = \{x_1, y_1, z_1, x_2, y_2, z_2, x_3, y_3\}$ even though the LST has twice the number of nodes of the CST element. The reasoning is that since the side nodes are assumed to be placed at the mid-point of each side, their location depends on the corner nodes. All undifferentiated matrices are known so that the only unknowns are the transformation matrix derivatives and the local stiffness matrix derivatives with respect to nodal coordinates.

Like the CST element, all geometric variables will be linked to each other through Figure A.1 and the following equations and vectors:

$\{L\} = \{l_1\ l_2\ l_3\}$ = function of $\{X\}$ only where

$l_1 = [(x_3 - x_2)^2 + (y_3 - y_2)^2 + (z_3 - z_2)^2]^{1/2}$

$l_2 = [(x_3 - x_1)^2 + (y_3 - y_1)^2 + (z_3 - z_1)^2]^{1/2}$

$l_3 = [(x_2 - x_1)^2 + (y_2 - y_1)^2 + (z_2 - z_1)^2]^{1/2}$

$\{G\} = \{b\ s\ h\ a\}$ = function of $\{L\}$ only where

$b = l_3$

$s = (l_2^2 + l_3^2 - l_1^2)/(2l_3)$

$h = [l_2^2 - (l_2^2 + l_3^2 - l_1^2)^2/(4l_3^2)]^{1/2}$

$a = (^1/_2)\, l_3[l_2^2 - (l_2^2 + l_3^2 - l_1^2)/(4l_3^2)]^{1/2}$

$\{B\} = \{a1\ a2\ a3\ b1\ b2\ b3\}$ = function of $\{G\}$ only where

$a1 = -h$

$a2 = h$

$a3 = 0$

$b1 = s - b$

$b2 = -s$

b3 = b

$[k_L]$ = function of Young's Modulus, thickness, {G} and {B} only

$[\Lambda]$ = function of {G} and {X} only

**$d[k_L]/d\{X\}$:**

Chain rule differentiation of 12x12 $[k_L]$ with respect to {X} gives

$$\frac{\partial[k_L]}{\partial\{X\}} = \frac{\partial[k_L]}{\partial\{B\}}\frac{\partial\{B\}}{\partial\{G\}}\frac{\partial\{G\}}{\partial\{X\}} + \frac{\partial[k_L]}{\partial\{G\}}\frac{\partial\{G\}}{\partial\{X\}} \tag{C-45}$$

From the CST element in Appendix C.1.2 we have the 4x9 derivative matrix $^{d\{G\}}/_{d\{X\}}$ already. Differentiating each component of {B} with respect to each component of {G} gives the 6x4 matrix

$$\frac{\partial\{B\}}{\partial\{G\}} = \begin{bmatrix} 0 & 0 & -1 & 0 \\ 0 & 0 & 1 & 0 \\ 0 & 0 & 0 & 0 \\ -1 & 1 & 0 & 0 \\ 0 & -1 & 0 & 0 \\ 1 & 0 & 0 & 0 \end{bmatrix} \tag{C-46}$$

All that remains is the single derivative of $[k_L]$ with respect to both {B} and {G} where $[k_L] = [M]^T[N][M]$ from Appendix A.3.1. Differentiation of the 12x12 local stiffness matrix against the six components of vector {B} yields

$$\frac{\partial[k_L]}{\partial\{B\}} = [M]^T[N]\frac{\partial[M]}{\partial\{B\}} + \frac{\partial[M]}{\partial\{B\}}^T[N][M] \tag{C-47}$$

with all undifferentiated matrices previously known ([N] is not a function of {B}).

Straightforward differentiation of 9x12 [M] with respect to {B} yields

$$\frac{\partial[M]}{\partial B_1} = \frac{1}{2a}\begin{bmatrix} 0 & 0 & 0 & 0 & 0 & 0 & 0 & 0 & 0 & 0 & 0 & 0 \\ 0 & 0 & 0 & 0 & 0 & 0 & 0 & 0 & 0 & 0 & 0 & 0 \\ 0 & 0 & 0 & 0 & 0 & 0 & 0 & 0 & 0 & 0 & 0 & 0 \\ 0 & 3 & 0 & 0 & 0 & 0 & 0 & 0 & 0 & 0 & 0 & 0 \\ 0 & -1 & 0 & 0 & 0 & 0 & 0 & 4 & 0 & 0 & 0 & 0 \\ 0 & -1 & 0 & 0 & 0 & 0 & 0 & 0 & 0 & 0 & 0 & 4 \\ 3 & 0 & 0 & 0 & 0 & 0 & 0 & 0 & 0 & 0 & 0 & 0 \\ -1 & 0 & 0 & 0 & 0 & 0 & 4 & 0 & 0 & 0 & 0 & 0 \\ -1 & 0 & 0 & 0 & 0 & 0 & 0 & 0 & 0 & 0 & 4 & 0 \end{bmatrix} \tag{C-48}$$

$$\frac{\partial[M]}{\partial B_2} = \frac{1}{2a}\begin{bmatrix} 0 & 0 & 0 & 0 & 0 & 0 & 0 & 0 & 0 & 0 & 0 & 0 \\ 0 & 0 & 0 & 0 & 0 & 0 & 0 & 0 & 0 & 0 & 0 & 0 \\ 0 & 0 & 0 & 0 & 0 & 0 & 0 & 0 & 0 & 0 & 0 & 0 \\ 0 & 0 & 0 & -1 & 0 & 0 & 0 & 4 & 0 & 0 & 0 & 0 \\ 0 & 0 & 0 & 3 & 0 & 0 & 0 & 0 & 0 & 0 & 0 & 0 \\ 0 & 0 & 0 & -1 & 0 & 0 & 0 & 0 & 0 & 4 & 0 & 0 \\ 0 & 0 & -1 & 0 & 0 & 0 & 4 & 0 & 0 & 0 & 0 & 0 \\ 0 & 0 & 3 & 0 & 0 & 0 & 0 & 0 & 0 & 0 & 0 & 0 \\ 0 & 0 & -1 & 0 & 0 & 0 & 0 & 4 & 0 & 0 & 0 & 0 \end{bmatrix} \tag{C-49}$$

$$\frac{\partial[M]}{\partial B_3} = \frac{1}{2a}\begin{bmatrix} 0 & 0 & 0 & 0 & 0 & 0 & 0 & 0 & 0 & 0 & 0 & 0 \\ 0 & 0 & 0 & 0 & 0 & 0 & 0 & 0 & 0 & 0 & 0 & 0 \\ 0 & 0 & 0 & 0 & 0 & 0 & 0 & 0 & 0 & 0 & 0 & 0 \\ 0 & 0 & 0 & 0 & 0 & -1 & 0 & 0 & 0 & 0 & 0 & 4 \\ 0 & 0 & 0 & 0 & 0 & -1 & 0 & 0 & 0 & 4 & 0 & 0 \\ 0 & 0 & 0 & 0 & 0 & 3 & 0 & 0 & 0 & 0 & 0 & 0 \\ 0 & 0 & 0 & 0 & -1 & 0 & 0 & 0 & 0 & 4 & 0 & 0 \\ 0 & 0 & 0 & 0 & -1 & 0 & 0 & 0 & 4 & 0 & 0 & 0 \\ 0 & 0 & 0 & 0 & 3 & 0 & 0 & 0 & 0 & 0 & 0 & 0 \end{bmatrix} \tag{C-50}$$

$$\frac{\partial[M]}{\partial B_4} = \frac{1}{2a}\begin{bmatrix} 3 & 0 & 0 & 0 & 0 & 0 & 0 & 0 & 0 & 0 & 0 & 0 \\ -1 & 0 & 0 & 0 & 0 & 0 & 4 & 0 & 0 & 0 & 0 & 0 \\ -1 & 0 & 0 & 0 & 0 & 0 & 0 & 0 & 0 & 0 & 4 & 0 \\ 0 & 0 & 0 & 0 & 0 & 0 & 0 & 0 & 0 & 0 & 0 & 0 \\ 0 & 0 & 0 & 0 & 0 & 0 & 0 & 0 & 0 & 0 & 0 & 0 \\ 0 & 0 & 0 & 0 & 0 & 0 & 0 & 0 & 0 & 0 & 0 & 0 \\ 0 & 3 & 0 & 0 & 0 & 0 & 0 & 0 & 0 & 0 & 0 & 0 \\ 0 & -1 & 0 & 0 & 0 & 0 & 0 & 4 & 0 & 0 & 0 & 0 \\ 0 & -1 & 0 & 0 & 0 & 0 & 0 & 0 & 0 & 0 & 0 & 4 \end{bmatrix} \tag{C-51}$$

$$\frac{\partial[M]}{\partial B_5} = \frac{1}{2a}\begin{bmatrix} 0 & 0 & -1 & 0 & 0 & 0 & 4 & 0 & 0 & 0 & 0 & 0 \\ 0 & 0 & 3 & 0 & 0 & 0 & 0 & 0 & 0 & 0 & 0 & 0 \\ 0 & 0 & -1 & 0 & 0 & 0 & 0 & 0 & 4 & 0 & 0 & 0 \\ 0 & 0 & 0 & 0 & 0 & 0 & 0 & 0 & 0 & 0 & 0 & 0 \\ 0 & 0 & 0 & 0 & 0 & 0 & 0 & 0 & 0 & 0 & 0 & 0 \\ 0 & 0 & 0 & 0 & 0 & 0 & 0 & 0 & 0 & 0 & 0 & 0 \\ 0 & 0 & 0 & -1 & 0 & 0 & 0 & 4 & 0 & 0 & 0 & 0 \\ 0 & 0 & 0 & 3 & 0 & 0 & 0 & 0 & 0 & 0 & 0 & 0 \\ 0 & 0 & 0 & -1 & 0 & 0 & 0 & 0 & 0 & 4 & 0 & 0 \end{bmatrix} \tag{C-52}$$

$$\frac{\partial[M]}{\partial B_6} = \frac{1}{2a}\begin{bmatrix} 0 & 0 & 0 & 0 & -1 & 0 & 0 & 0 & 0 & 0 & 4 & 0 \\ 0 & 0 & 0 & 0 & -1 & 0 & 0 & 0 & 4 & 0 & 0 & 0 \\ 0 & 0 & 0 & 0 & 3 & 0 & 0 & 0 & 0 & 0 & 0 & 0 \\ 0 & 0 & 0 & 0 & 0 & 0 & 0 & 0 & 0 & 0 & 0 & 0 \\ 0 & 0 & 0 & 0 & 0 & 0 & 0 & 0 & 0 & 0 & 0 & 0 \\ 0 & 0 & 0 & 0 & 0 & 0 & 0 & 0 & 0 & 0 & 0 & 0 \\ 0 & 0 & 0 & 0 & 0 & -1 & 0 & 0 & 0 & 0 & 0 & 4 \\ 0 & 0 & 0 & 0 & 0 & -1 & 0 & 0 & 0 & 0 & 0 & 0 \\ 0 & 0 & 0 & 0 & 0 & 3 & 0 & 0 & 0 & 4 & 0 & 0 \end{bmatrix} \tag{C-53}$$

Differentiation of the 12x12 local stiffness matrix against the four components of vector {G} gives

$$\frac{\partial[k_L]}{\partial\{G\}} = [M]^T[N]\frac{\partial[M]}{\partial\{G\}} + \frac{\partial[M]}{\partial\{G\}}^T[N][M] \tag{C-54}$$

with all undifferentiated matrices previously known ([N] is not a function of {G}). Straightforward differentiation of 9x12 [M] with respect to {G} is simplified since [M] is not a function of $G_1$, $G_2$ or $G_3$. Therefore,

$$\frac{\partial[M]}{\partial G_1} = \frac{\partial[M]}{\partial G_2} = \frac{\partial[M]}{\partial G_3} = 0 \tag{C-55}$$

and

$$\frac{\partial[M]}{\partial G_4} = -\frac{1}{2a^2}\begin{bmatrix} 3b_1 & 0 & -b_2 & 0 & -b_3 & 0 & 4b_2 & 0 & 0 & 0 & 4b_3 & 0 \\ -b_1 & 0 & 3b_2 & 0 & -b_3 & 0 & 4b_1 & 0 & 4b_3 & 0 & 0 & 0 \\ -b_1 & 0 & -b_2 & 0 & 3b_3 & 0 & 0 & 0 & 4b_2 & 0 & 4b_1 & 0 \\ 0 & 3a_1 & 0 & -a_2 & 0 & -a_3 & 0 & 4a_2 & 0 & 0 & 0 & 4a_3 \\ 0 & -a_1 & 0 & 3a_2 & 0 & -a_3 & 0 & 4a_1 & 0 & 4a_3 & 0 & 0 \\ 0 & -a_1 & 0 & -a_2 & 0 & 3a_3 & 0 & 0 & 0 & 4a_2 & 0 & 4a_1 \\ 3a_1 & 3b_1 & -a_2 & -b_2 & -a_3 & -b_3 & 4a_2 & 4b_2 & 0 & 0 & 4a_3 & 4b_3 \\ -a_1 & -b_1 & 3a_2 & 3b_2 & -a_3 & -b_3 & 4a_1 & 4b_1 & 4a_3 & 4b_3 & 0 & 0 \\ -a_1 & -b_1 & -a_2 & -b_2 & 3a_3 & 3b_3 & 0 & 0 & 4a_2 & 4b_2 & 4a_1 & 4b_1 \end{bmatrix} \tag{C-56}$$

Thus, all necessary derivative matrices are known and $^{d[k_L]}/_{d\{X\}}$ can be calculated.

**d [$\tilde{\Lambda}$] /d[X]:**

Since the 12x18 LST transformation matrix is formed from two 6x9 CST transformation matrices, the derivative with respect to {X} is simply the CST's transformation derivative with respect to {X} (Appendix C.1.2) used twice as

$$\frac{\partial[\tilde{\Lambda}]}{\partial\{X\}} = \begin{bmatrix} \frac{\partial[\Lambda]}{\partial\{X\}} & [0] \\ [0] & \frac{\partial[\Lambda]}{\partial\{X\}} \end{bmatrix} \tag{C-57}$$

## C.2 Global stress sensitivity with respect to any shape variable

Unlike displacement sensitivities, stress sensitivities can be calculated on an element by element basis.

### C.2.1 Rod element stress sensitivity

The derivative of the rod element's scalar axial stress is

$$\frac{\partial\sigma}{\partial\beta} = \frac{\partial\sigma}{\partial\{X\}}\frac{\partial\{X\}}{\partial\beta} + \frac{\partial\sigma}{\partial\{U_G\}}\frac{\partial\{U_G\}}{\partial\beta} \tag{C-58}$$

where $\{X\} = \{x_1, y_1, z_1, x_2, y_2, z_2\}$ and $U_G = \{u_1, v_1, w_1, u_2, v_2, w_2\}$.With the design variable displacement and coordinate derivatives having been previously calculated, all that is necessary is the derivative of the stress equation with respect to {X} and $\{U_G\}$. For completeness, this results in

$$\frac{\partial \sigma}{\partial x_1} = \frac{E}{L^4}\left[L^2(u_2-u_1) - 2\left[(x_2-x_1)(u_2-u_1) + (y_2-y_1)(v_2-v_1) + (z_2-z_1)(w_2-w_1)\right](x_2-x_1)\right] \quad \text{(C-59)}$$

$$\frac{\partial \sigma}{\partial y_1} = \frac{E}{L^4}\left[L^2(v_2-v_1) - 2\left[(x_2-x_1)(u_2-u_1) + (y_2-y_1)(v_2-v_1) + (z_2-z_1)(w_2-w_1)\right](y_2-y_1)\right] \quad \text{(C-60)}$$

$$\frac{\partial \sigma}{\partial z_1} = \frac{E}{L^4}\left[L^2(w_2-w_1) - 2\left[(x_2-x_1)(u_2-u_1) + (y_2-y_1)(v_2-v_1) + (z_2-z_1)(w_2-w_1)\right](z_2-z_1)\right] \quad \text{(C-61)}$$

$$\frac{\partial \sigma}{\partial x_2} = -\frac{\partial \sigma}{\partial x_1} \quad \text{(C-62)}$$

$$\frac{\partial \sigma}{\partial y_2} = -\frac{\partial \sigma}{\partial y_1} \quad \text{(C-63)}$$

$$\frac{\partial \sigma}{\partial z_2} = -\frac{\partial \sigma}{\partial z_1} \quad \text{(C-64)}$$

and

$$\frac{\partial \sigma}{\partial u_1} = -\frac{E}{L^2}(x_2-x_1) \quad \text{(C-65)}$$

$$\frac{\partial \sigma}{\partial v_1} = -\frac{E}{L^2}(y_2-y_1) \quad \text{(C-66)}$$

$$\frac{\partial \sigma}{\partial w_1} = -\frac{E}{L^2}(z_2-z_1) \quad \text{(C-67)}$$

$$\frac{\partial \sigma}{\partial u_2} = -\frac{\partial \sigma}{\partial u_1} \quad \text{(C-68)}$$

$$\frac{\partial \sigma}{\partial v_2} = -\frac{\partial \sigma}{\partial v_1} \quad \text{(C-69)}$$

$$\frac{\partial \sigma}{\partial w_2} = -\frac{\partial \sigma}{\partial w_1} \quad \text{(C-70)}$$

### C.2.2 CST element stress sensitivity

Using chain-rule differentiation on the CST stress equation yields

$$\frac{\partial}{\partial\beta}\begin{Bmatrix}\sigma_{xx}\\ \sigma_{yy}\\ \sigma_{xy}\end{Bmatrix}^{T} = [D][B][\Lambda]\frac{\partial\{U_G\}}{\partial\beta} + [D][B]\frac{\partial[\Lambda]}{\partial\beta}\{U_G\} + [D]\frac{\partial[B]}{\partial\beta}[\Lambda]\{U_G\} \tag{C-71}$$

where $\{U_G\} = \{u_1, v_1, w_1, u_2, v_2, w_2, u_3, v_3, w_3\}$ and all undifferentiated matrices are previously known. The displacement sensitivity vector is also known as it was calculated above. Therefore, to find the CST stress sensitivities with respect to shape, only the transformation matrix derivative and [B] matrix derivative are needed. Fortunately, the transformation derivative has already been found to be

$$\frac{\partial[\Lambda]}{\partial\beta} = \left[\frac{\partial[\Lambda]}{\partial\{G\}}\frac{\partial\{G\}}{\partial\{L\}}\frac{\partial\{L\}}{\partial\{X\}} + \frac{\partial[\Lambda]}{\partial\{X\}}\right]\frac{\partial\{X\}}{\partial\beta} \tag{C-72}$$

Thus, to find $^{d[B]}/_{d(\beta)}$, use the chain rule to get

$$\frac{\partial[B]}{\partial\beta} = \frac{\partial[B]}{\partial\{G\}}\frac{\partial\{G\}}{\partial\{L\}}\frac{\partial\{L\}}{\partial\{X\}}\frac{\partial\{X\}}{\partial\beta} \tag{C-73}$$

Here, the only unknown is $^{d[B]}/_{d\{G\}}$ which can be explicitly found as

$$\frac{\partial [B]}{\partial G_1} = \begin{bmatrix} -\frac{s}{b^2 h} & 0 & \frac{s}{b^2 h} & 0 & 0 & 0 \\ 0 & \frac{1}{b^2} & 0 & -\frac{1}{b^2} & 0 & 0 \\ \frac{1}{b^2} & -\frac{s}{b^2 h} & -\frac{1}{b^2} & \frac{s}{b^2 h} & 0 & 0 \end{bmatrix} \tag{C-74}$$

$$\frac{\partial [B]}{\partial G_2} = \begin{bmatrix} \frac{1}{bh} & 0 & -\frac{1}{bh} & 0 & 0 & 0 \\ 0 & 0 & 0 & 0 & 0 & 0 \\ 0 & \frac{1}{bh} & 0 & -\frac{1}{bh} & 0 & 0 \end{bmatrix} \tag{C-75}$$

$$\frac{\partial [B]}{\partial G_3} = \begin{bmatrix} \frac{(b-s)}{bh^2} & 0 & \frac{s}{bh^2} & 0 & -\frac{1}{h^2} & 0 \\ 0 & 0 & 0 & 0 & 0 & 0 \\ 0 & \frac{(b-s)}{bh^2} & 0 & \frac{s}{bh^2} & 0 & -\frac{1}{h^2} \end{bmatrix} \tag{C-76}$$

$$\frac{\partial [B]}{\partial G_4} = \begin{bmatrix} 0 & 0 & 0 & 0 & 0 & 0 \\ 0 & 0 & 0 & 0 & 0 & 0 \\ 0 & 0 & 0 & 0 & 0 & 0 \end{bmatrix} \tag{C-77}$$

### C.2.3 LST element stress sensitivity

Using chain-rule differentiation on the LST stress equation yields the 9x1 stress derivative vector with respect to any shape design variable β as

$$\frac{\partial}{\partial\beta}\left\{\begin{Bmatrix}\sigma_{xx}\\ \sigma_{yy}\\ \sigma_{xy}\end{Bmatrix}_1 \begin{Bmatrix}\sigma_{xx}\\ \sigma_{yy}\\ \sigma_{xy}\end{Bmatrix}_2 \begin{Bmatrix}\sigma_{xx}\\ \sigma_{yy}\\ \sigma_{xy}\end{Bmatrix}_3\right\} = [\bar{C}][M][\bar{\Lambda}]\frac{\partial\{U_G\}}{\partial\beta} + [\bar{C}][M]\frac{\partial[\bar{\Lambda}]}{\partial\beta}\{U_G\} + [\bar{C}]\frac{\partial[M]}{\partial\beta}[\bar{\Lambda}]\{U_G\} \tag{C-78}$$

where all undifferentiated matrices are previously known. The displacement sensitivity vector is also known as it was calculated in Appendix C.1. Therefore, to find the LST stress sensitivities with respect to shape, only the transformation matrix derivative and [M] matrix derivative are needed. Fortunately, the transformation derivative matrix has already been found above to be

$$\frac{\partial[\bar{\Lambda}]}{\partial\beta} = \begin{bmatrix}\frac{\partial[\Lambda]}{\partial\{X\}} & [0]\\ [0] & \frac{\partial[\Lambda]}{\partial\{X\}}\end{bmatrix}\frac{\partial\{X\}}{\partial\beta} \tag{C-79}$$

Thus, to find d[M]/d($\beta$), use the chain rule as before to get

$$\frac{\partial[M]}{\partial\beta} = \left(\frac{\partial[M]}{\partial\{B\}}\frac{\partial\{B\}}{\partial\{G\}}\frac{\partial\{G\}}{\partial\{L\}}\frac{\partial\{L\}}{\partial\{X\}} + \frac{\partial[M]}{\partial\{G\}}\frac{\partial\{G\}}{\partial\{L\}}\frac{\partial\{L\}}{\partial\{X\}}\right)\frac{\partial\{X\}}{\partial\beta} \tag{C-80}$$

All of these derivative matrices have been previously calculated in Appendix C.

## C.3 Natural frequency sensitivity with respect to any shape variable

Differentiating the eigenvalue equation

$$[K - \omega^2 M]\ \{\Phi\} = \{0\} \tag{C-81}$$

with respect to any shape design variable $\beta$ yields

$$\frac{\partial \omega_i^2}{\partial \beta} = \frac{\phi_i^T \left[ \frac{\partial [K]}{\partial \beta} - \omega_i^2 \frac{\partial [M]}{\partial \beta} \right] \phi_i}{\phi_i^T [M] \phi_i} \tag{C-82}$$

which is actually the sensitivity of the eigenvalue $\lambda = \omega^2$. The global mass sensitivity matrix $\frac{\partial [M]}{\partial \beta}$ is the only new entry. To calculate this, individual element mass sensitivity matrices are calculated and then merged similar to what is done for the global stiffness matrix.

### C.3.1 Rod element mass matrix sensitivity

Differentiating the 6x6 global rod mass matrix (Appendix A.1.3) yields

$$\frac{\partial [M_{rod}]}{\partial \beta} = \frac{\partial [M_{rod}]}{\partial \{X\}} \frac{\partial \{X\}}{\partial \beta} \tag{C-83}$$

where $\frac{\partial \{X\}}{\partial \beta}$ has been derived previously and $\{X\} = \{x_1, y_1, z_1, x_2, y_2, z_2\}$. Explicit differentiation of $M_{rod}$ with respect to $\{X\}$ yields (since it's length L is a function of $\{X\}$)

$$\frac{\partial [M_{rod}]}{\partial X_1} = -\frac{\rho A}{2L}(x_2 - x_1)\,[I] \tag{C-84}$$

$$\frac{\partial [M_{rod}]}{\partial X_2} = -\frac{\rho A}{2L}(y_2 - y_1)\,[I] \tag{C-85}$$

$$\frac{\partial [M_{rod}]}{\partial X_3} = -\frac{\rho A}{2L}(z_2 - z_1)\,[I] \tag{C-86}$$

$$\frac{\partial [M_{rod}]}{\partial X_4} = \frac{\rho A}{2L}(x_2 - x_1)\,[I] \tag{C-87}$$

$$\frac{\partial [M_{rod}]}{\partial X_5} = \frac{\rho A}{2L}(y_2 - y_1)\,[I] \tag{C-88}$$

$$\frac{\partial [M_{rod}]}{\partial X_6} = \frac{\rho A}{2L}(z_2 - z_1)\,[I] \tag{C-89}$$

where ρ is the density, A is the cross-sectional area, L is the length and I is a 6x6 identity matrix.

### C.3.2 CST element mass matrix sensitivity

Differentiating the 9x9 global CST mass matrix (Appendix A.2.3) yields

$$\frac{\partial [M_{CST}]}{\partial \beta} = \frac{\partial [M_{CST}]}{\partial \{X\}} \frac{\partial \{X\}}{\partial \beta} \tag{C-90}$$

where $\frac{\partial \{X\}}{\partial \beta}$ has been derived previously and $\{X\} = \{x_1, y_1, z_1, x_2, y_2, z_2, x_3, y_3, z_3\}$. Chain rule differentiation of $M_{CST}$ with respect to $\{X\}$ yields (since it's area 'a' is entry #4 in the geometry vector $\{G\} = \{b, s, h, a\}$)

$$\frac{\partial [M_{CST}]}{\partial \{X\}} = \frac{\partial [M_{CST}]}{\partial \{G\}} \frac{\partial \{G\}}{\partial \{L\}} \frac{\partial \{L\}}{\partial \{X\}} \tag{C-91}$$

where $\{G\} = \{b, s, h, a\}$ and $\{L\} = \{l_1, l_2, l_3\}$. Since $M_{CST}$ is not a function of b, s or h, a more exact form gives

$$\frac{\partial [M_{CST}]}{\partial \{X\}} = \frac{\partial [M_{CST}]}{\partial a} \frac{\partial a}{\partial \{L\}} \frac{\partial \{L\}}{\partial \{X\}} \tag{C-92}$$

with 3x9 matrix $\frac{\partial \{L\}}{\partial \{X\}}$ already having been calculated. Thus

$$\frac{\partial [M_{CST}]}{\partial X_i} = \frac{\rho t}{3} \frac{\partial G_4}{\partial \{L\}} \frac{\partial \{L\}}{\partial X_i} [I] \tag{C-93}$$

where $\rho$ is the density, t is the cross-sectional thickness and I is a 9x9 identity matrix.

# APPENDIX D

# SIZE VARIABLE SENSITIVITIES

## D.1 Global displacement sensitivity with respect to any size variable

From the basic static equation [K]{U} = {F}, one can differentiate with respect to any size design variable $\kappa$ to get

$$[K]\frac{\partial\{U\}}{\partial\kappa} + \frac{\partial[K]}{\partial\kappa}\{U\} = \frac{\partial\{F\}}{\partial\kappa} \tag{D-1}$$

where [K] is the global stiffness matrix, {U} is the global displacement vector and {F} is the global load vector.

For any conservative loading case in which the applied loads are independent of model geometry,

$$\frac{\partial\{U\}}{\partial\kappa} = -[K]^{-1}\frac{\partial[K]}{\partial\kappa}\{U\} \tag{D-2}$$

Again, [K] and {U} are known and the stiffness matrix derivative must be formed via merging element by element. But, since a sizing variable exists for each finite element, the derivative of the global stiffness matrix of the system with respect to any one size variable reduces $^{d[K]}/_{d(\kappa)}$ to a matrix whose only entries are that of the element's stiffness matrix derivative with respect to it's own size variable. When this extremely sparse matrix is multiplied by the corresponding entries in {U}, the global displacement derivative is easily calculated.

### D.1.1 Rod element stiffness matrix derivative with respect to it's area

Since $[k_G]$ for rod element 'i' is a linear function of it's area,

$$\frac{\partial [k_G]_i}{\partial A_i} = \frac{E}{L}\begin{bmatrix} cx^2 & cxcy & cxcz & -cx^2 & -cxcy & -cxcz \\ cxcy & cy^2 & cycz & -cxcy & -cy^2 & -cycz \\ cxcz & cycz & cz^2 & -cxcz & -cycz & -cz^2 \\ -cx^2 & -cxcy & -cxcz & cx^2 & cxcy & cxcz \\ -cxcy & -cy^2 & -cycz & cxcy & cy^2 & cycz \\ -cxcz & -cycz & -cz^2 & cxcz & cycz & cz^2 \end{bmatrix} \tag{D-3}$$

where E is the Modulus of Elasticity, L is the element length and cx, cy and cz are the direction cosines given in Appendix A.1.1.

### D.1.2 CST element stiffness matrix derivative with respect to it's thickness

Since $[k_G]$ for CST element 'i' is a linear function of its thickness,

$$\frac{\partial [k_G]_i}{\partial t_i} = [\Lambda]_i^T \frac{\partial [k_L]_i}{\partial t_i} [\Lambda]_i = [\Lambda]_i^T \frac{\partial [\bar{k}_N + \bar{k}_S]_i}{\partial t_i} [\Lambda]_i \tag{D-4}$$

where

$$\frac{\partial\left[\bar{k}_n\right]_i}{\partial t_i} = \frac{E}{4a(1-\nu^2)}\begin{bmatrix} (b-s)^2 & \nu(b-s)h & (b-s)s & -\nu(b-s)h & -(b-s)b & 0 \\ \nu(b-s)h & h^2 & \nu hs & -h^2 & -\nu bh & 0 \\ (b-s)s & \nu hs & s^2 & -\nu hs & -bs & 0 \\ -\nu(b-s)h & -h^2 & -\nu hs & h^2 & \nu hb & 0 \\ -(b-s)b & -\nu bh & -bs & \nu hb & b^2 & 0 \\ 0 & 0 & 0 & 0 & 0 & 0 \end{bmatrix} \tag{D-5}$$

and

$$\frac{\partial\left[\bar{k}_s\right]_i}{\partial t_i} = \frac{E}{8a(1+\nu)}\begin{bmatrix} h^2 & (b-s)h & -h^2 & hs & 0 & -bh \\ (b-s)h & (b-s)^2 & -(b-s)h & (b-s)s & 0 & -(b-s)b \\ -h^2 & -(b-s)h & h^2 & -hs & 0 & bh \\ hs & (b-s)s & -hs & s^2 & 0 & -bs \\ 0 & 0 & 0 & 0 & 0 & 0 \\ -bh & -(b-s)b & bh & -bs & 0 & b^2 \end{bmatrix} \tag{D-6}$$

$\bar{k}_N$ and $\bar{k}_S$ are the normal and shear stiffness matrices.

### D.1.3 LST element stiffness matrix derivative with respect to it's thickness

Since $[k_G]$ for LST element 'i' is a linear function of its thickness,

$$\frac{\partial\left[k_G\right]_i}{\partial t_i} = \left[\tilde{\Lambda}\right]_i^T \frac{\partial\left[k_L\right]_i}{\partial t_i}\left[\tilde{\Lambda}\right]_i \tag{D-7}$$

where

$$\frac{\partial\left[k_L\right]_i}{\partial t_i} = \left[M\right]_i^T \frac{\partial\left[N\right]_i}{\partial t_i}\left[M\right]_i \tag{D-8}$$

and

$$\frac{\partial [N]_i}{\partial t_i} = \frac{a}{12}\begin{bmatrix} 2c_{11} & c_{11} & c_{11} & 2c_{12} & c_{12} & c_{12} & 0 & 0 & 0 \\ c_{11} & 2c_{11} & c_{11} & c_{12} & 2c_{12} & c_{12} & 0 & 0 & 0 \\ c_{11} & c_{11} & 2c_{11} & c_{12} & c_{12} & 2c_{12} & 0 & 0 & 0 \\ 2c_{12} & c_{12} & c_{12} & 2c_2 & c_{22} & c_{22} & 0 & 0 & 0 \\ c_{12} & 2c_{12} & c_{12} & c_{22} & 2c_{22} & c_{22} & 0 & 0 & 0 \\ c_{12} & c_{12} & c_{12} & c_{22} & c_{22} & 2c_{22} & 0 & 0 & 0 \\ 0 & 0 & 0 & 0 & 0 & 0 & 2c_{33} & c_{33} & c_{33} \\ 0 & 0 & 0 & 0 & 0 & 0 & c_{33} & 2c_{33} & c_{33} \\ 0 & 0 & 0 & 0 & 0 & 0 & c_{33} & c_{33} & 2c_{33} \end{bmatrix} \quad \text{(D-9)}$$

## D.2 Global stress sensitivity with respect to any size variable

As with the stress shape variable sensitivities, the stress sizing variable sensitivities are done on an element by element basis as follows:

### D.2.1 Rod 'i' stress sensitivity with respect to rod 'j' area

Differentiating the rod element stress equation with respect to any rod element area gives

$$\frac{\partial \sigma_i}{\partial A_j} = \frac{\partial \sigma_i}{\partial \{U_G\}} \frac{\partial \{U_G\}}{\partial A_j} \quad \text{(D-10)}$$

where the displacement derivative with respect to area 'j' has been found previously. To find the stress derivative with respect to its nodal coordinates, employ straightforward differentiation. This result has been calculated in Appendix C.2.1.

### D.2.2 Rod 'i' stress sensitivity with respect to CST or LST 'j' thickness

Differentiating the rod element stress equation with respect to any CST or LST element thickness gives

$$\frac{\partial \sigma_i}{\partial t_j} = \frac{\partial \sigma_i}{\partial \{U_G\}} \frac{\partial \{U_G\}}{\partial t_j} \tag{D-11}$$

where the displacement derivative with respect to thickness 'j' has been found previously. The stress derivative with respect to its nodal coordinates, has been calculated in Appendix C.2.1.

### D.2.3 CST 'i' stress sensitivity with respect to rod 'j' area

Differentiating the CST element stress equation with respect to any rod element area gives

$$\frac{\partial}{\partial A_j} \begin{Bmatrix} \sigma_{xx} \\ \sigma_{yy} \\ \sigma_{xy} \end{Bmatrix}_i = [D][B][\Lambda] \frac{\partial \{U_G\}}{\partial A_j} \tag{D-12}$$

where the displacement derivative with respect to area 'j' has been found previously. Since [D], [B] and [$\Lambda$] are known, the derivative is easily found.

### D.2.4 CST 'i' stress sensitivity with respect to CST 'j' thickness

Differentiating the CST element stress equation with respect to any CST or LST ele-

ment thickness gives

$$\frac{\partial}{\partial t_j}\begin{Bmatrix}\sigma_{xx}\\ \sigma_{yy}\\ \sigma_{xy}\end{Bmatrix}_i = [D][B][\Lambda]\frac{\partial\{U_G\}}{\partial t_j} \tag{D-13}$$

where the displacement derivative with respect to thickness 'j' has been found previously. Since [D], [B] and [Λ] are previously known, the derivative is easily found.

### D.2.5 LST 'i' stress sensitivity with respect to rod 'j' area

Differentiating the LST element stress equation with respect to any rod element area gives

$$\frac{\partial}{\partial A_j}\left\{\begin{Bmatrix}\sigma_{xx}\\ \sigma_{yy}\\ \sigma_{xy}\end{Bmatrix}_P \begin{Bmatrix}\sigma_{xx}\\ \sigma_{yy}\\ \sigma_{xy}\end{Bmatrix}_Q \begin{Bmatrix}\sigma_{xx}\\ \sigma_{yy}\\ \sigma_{xy}\end{Bmatrix}_R\right\}_i = [\tilde{C}][M][\tilde{\Lambda}]\frac{\partial\{U_G\}}{\partial A_j} \tag{D-14}$$

where the displacement derivative with respect to area 'j' has been found previously. Since $[\tilde{C}]$, [M] and $[\tilde{\Lambda}]$ are previously known, the derivative is easily found.

### D.2.6 LST 'i' stress sensitivity with respect to LST 'j' thickness

Differentiating the LST element stress equation with respect to any CST or LST element thickness gives

$$\frac{\partial}{\partial t_j}\left\{\begin{array}{l}\left\{\begin{array}{l}\sigma_{xx}\\ \sigma_{yy}\\ \sigma_{xy}\end{array}\right\}_P\\ \left\{\begin{array}{l}\sigma_{xx}\\ \sigma_{yy}\\ \sigma_{xy}\end{array}\right\}_Q\\ \left\{\begin{array}{l}\sigma_{xx}\\ \sigma_{yy}\\ \sigma_{xy}\end{array}\right\}_R\end{array}\right\}_i = [\tilde{C}][M][\tilde{\Lambda}]\frac{\partial\{U_G\}}{\partial t_j} \qquad \text{(D-15)}$$

where the displacement derivative with respect to thickness 'j' has been found previously. Since $[\tilde{C}]$, [M] and $[\tilde{\Lambda}]$ are previously known, the derivative is easily found.

## D.3 Natural frequency sensitivity with respect to any size variable

Differentiating the eigenvalue equation

$$[K - \omega^2 M]\ \{\Phi\} = \{0\} \tag{D-16}$$

with respect to any size design variable $\kappa$ yields

$$\frac{\partial \omega_i^2}{\partial \kappa} = \frac{\phi_i^T \left[ \frac{\partial [K]}{\partial \kappa} - \omega_i^2 \frac{\partial [M]}{\partial \kappa} \right] \phi_i}{\phi_i^T [M] \phi_i} \tag{D-17}$$

which is actually the sensitivity of the eigenvalue $\lambda = \omega^2$. The global mass sensitivity matrix $\frac{\partial [M]}{\partial \kappa}$ is the only new entry. The global stiffness sensitivity matrix has been detailed in Appendix D.1 and the global mass sensitivity matrix has the same properties in that it's derivative with respect to any i'th size variable is just the i'th individual mass matrix derivative with all other entries equal to zero.

### D.3.1 Rod element mass matrix sensitivity with respect to it's area

Since $M_{rod}$ for rod element 'i' is a linear function of it's area, differentiating the 6x6 global rod mass matrix (Appendix A.1.3) yields

$$\frac{\partial [M_{rod}]}{\partial A_i} = \frac{\rho L}{2} [I] \tag{D-18}$$

where $\rho$ is the density, L is the length and I is a 6x6 identity matrix.

### D.3.2 CST element mass matrix sensitivity with respect to it's thickness

Since $M_{CST}$ for CST element 'i' is a linear function of it's thickness, differentiating the 9x9 global CST mass matrix (Appendix A.2.3) yields

$$\frac{\partial [M_{CST}]}{\partial t_i} = \frac{\rho A}{3} [I] \tag{D-19}$$

where $\rho$ is the density, A is the area and I is a 9x9 identity matrix